NOVEL CARRIER PROTEIN AND ITS APPLICATION TO A RESPIRATORY SYNCYTIAL VIRUS ANTIVIRAL PEPTIDE

DEVELOPMENT OF AN ALBUMIN-BINDING DOMAIN CARRIER AND A NOVEL PEPTIDE MIMETIC ANTIVIRAL FOR RESPIRATORY SYNCYTIAL VIRUS

By SAMANTHA P. MIHALCO, B.Sc.

A Thesis Submitted to the School of Graduate Studies in Partial Fulfillment of the Requirements for the Degree Master of Science

DESCRIPTIVE NOTE

McMaster University MASTER OF SCIENCE (2017) Hamilton, Ontario (Medical Sciences)

TITLE: Development of an Albumin-Binding Domain Carrier and a Novel Peptide Mimetic Antiviral for Respiratory Syncytial Virus

AUTHOR: Samantha P. Mihalco, B.Sc. (Queen's University)

SUPERVISOR: Dr. James Mahony

NUMBER OF PAGES: xxiv, 133

LAY ABSTRACT

Worldwide, respiratory syncytial virus is a leading cause of lower respiratory infection and hospitalization in children. Nearly all children are infected with the virus by the young age of two. However, respiratory syncytial virus also causes a significant amount of illness and death in the elderly and in immunocompromised individuals. Furthermore, repeated infections by the virus are common throughout life in all populations. With the lack of a vaccine or treatment for this viral infection, an effective antiviral against RSV is required. In this thesis, we developed and evaluated a novel RSV antiviral therapeutic peptide that targets proteins of the viral replication machinery. Since the replication machinery is required for respiratory syncytial virus survival, we hypothesized that infection could be attenuated by preventing formation of the replication machinery. Furthermore, since small protein therapeutics are often cleared quickly from the human body, we investigated human carrier molecules that could be attached to the antiviral protein for stabilization within the body.

ABSTRACT

Background: Respiratory syncytial virus (RSV) is the leading cause of acute lower respiratory tract infection and hospitalization in children worldwide. With no vaccine or antivirals available for the routine prevention or treatment of RSV, an effective RSV antiviral is required. Previous studies have shown that the RSV nucleocapsid complex (NC), phosphoprotein (P), and large polymerase (L) are essential for the replication and survival of RSV since they form the core of the RNA-dependent RNA polymerase (RdRp) complex. Thus, these proteins are viable targets for novel RSV antivirals.

Objective: The Mahony laboratory has previously shown that 20 μM of a peptide mimetic composed of the 21 terminal amino acids of the RSV phosphoprotein ($RSVP_{220-241}$) fused to an HIV-1 Tat cell penetrating peptide (CPP), a hexa-histidine (His) tag, and the *Escherichia coli* (*E. coli*) maltose binding protein carrier (MBP) molecule was sufficient to attenuate RSV A and B replication *in vitro* by approximately 90 and 80%, respectively. We evaluated the fusion of this His-MBP-Tat-$RSVP_{220-241}$ mimetic to a more suitable carrier molecule, an albumin-binding domain (ABD), for future use *in vivo*. In addition, we designed a novel antiviral mimetic composed of the 30 terminal amino acids of the RSV A P protein ($RSVP_{212-241}$), which are involved in binding both L polymerase and NC complexes, fused to a CPP consisting of Tat or nine arginine residues (Arg9), a His-tag, and the MBP carrier. We evaluated the activity of His-MBP-Tat-$RSVP_{212-241,}$ Tat-His-MBP-Tat-$RSVP_{212-241,}$ and His-Arg9-MBP-$RSVP_{212-241}$ mimetics *in vitro* and

hypothesized that a mimetic designed to target both L and NC interactions would be a more effective RSV antiviral than the original His-MBP-Tat-RSVP$_{220-241}$ mimetic.

Methods and Results: The Gateway® Cloning System was used to create expression vectors containing His-, GST-, or His-MBP-ABD-Tat-RSVP$_{220-241}$ and His-MBP-Tat-RSVP$_{212-241}$, whereas inverse PCR and both the In-Fusion® and Gateway® Cloning systems were used to generate expression vectors containing Tat-His-MBP-Tat-RSVP$_{212-241}$ and His-Arg9-MBP-RSVP$_{212-241}$. The fusion proteins were expressed, purified by affinity chromatography, and evaluated *in vitro*. No soluble protein was obtained for the ABD constructs. His-MBP-Tat-RSVP$_{212-241}$ was toxic and not internalized by LLC-MK2 cells, whereas only 0.26 mg of Tat-His-MBP-Tat-RSVP$_{212-241}$ was purified. We were able to show that His-Arg9-MBP-RSVP$_{212-241}$ was non-toxic, internalized, and interacted with the RSV nucleoprotein (N) in a GST pull-down experiment. Furthermore, His-Arg9-MBP-RSVP$_{212-241}$ attenuated RSV A replication and progeny production by 94.8 and 93.33% at 200 μM, respectively. We demonstrated 50.7 and 49% inhibition of RSV A replication and progeny production at 20 μM, respectively. We showed that inhibition of viral replication by 25 μM His-Arg9-MBP-RSVP$_{212-241}$ was not significantly different from inhibition by 20 μM His-MBP-Tat-RSVP$_{220-241}$. Thus, in this thesis we were unable to show that His-Arg9-MBP-RSVP$_{212-241}$ was a more effective RSV antiviral.

Conclusion: The ABD was not a suitable carrier molecule for use with our fusion protein mimetics. However, RSV P protein mimetics that target interactions with the NC complexes and L polymerase are a novel and viable antiviral strategy. We showed that a His-Arg9-MBP-RSVP$_{212-241}$ mimetic was non-toxic, internalized, and interacted with the

RSV N protein *in vitro*. Furthermore, we showed that at 200 μM this novel mimetic could attenuate RSV A replication and progeny production *in vitro* by 94.8 and 93.3%, respectively. Further studies are required to characterize the construct, increase its bioactivity, and identify a suitable human carrier molecule for future evaluation *in vivo*.

Acknowledgments

Firstly, I would like to thank my supervisor Dr. Mahony for being a wonderful mentor over the past few years. You have taught me the importance of the scientific process and how to plan experiments to gain as much information as possible. Furthermore, you have helped me to critically evaluate my own, as well as others' research. I also could not thank you enough for the lab book talk the first week in the lab; because of that talk I kept very detailed lab books, which made writing my thesis a much easier process. Thank you Dr. Mahony for the supportive guidance during my time in your lab. I would also like to thank my committee members, Dr. Marie Elliot and Dr. Brian Lichty. You have supported me throughout my degree and have provided me with excellent guidance and advice.

I would also like to thank all members of the Mahony lab, as each member has helped me along the way, whether it be with science or life. I was lucky to be surrounded by a great group of smart, fun, caring, and humorous guys. You made my time at the lab extremely enjoyable and most definitely entertaining! I would like to thank Dr. David Bulir for the constant support and guidance throughout my project, as well as the extreme couponing that never failed to make me laugh. I would like to thank Sylvia Chong for not only being a wonderful mentor, but also the only other person in the lab that could not stand how messy the guys could be. I would also like to thank Dr. Christopher Stone for the guidance and life advice, as well as making it clear that no matter how personal a question is, it is never too personal to answer. A special thank you to Zachariah Scinocca,

Christopher Chiang, Steven Liang, and Jordan Nelson for the unlimited entertainment and scientific support. We have shared many memories in and out of the lab that I will always cherish. I would also like to thank all the other members of the lab who have made my experience enjoyable: Jodi Gilchrist, Dan Jang, Kathy Luinstra, Lucas Penny, Steven Zhang, and Karanbir Brar.

Lastly, I would like to thank my family who has supported me at every step of my life. My mother and father, Scott and Shelley, have always supported me and encouraged me with any goal in life. I would like to thank my grandmother, Diane Soucie, for being my biggest supporter and shoulder to cry on. You have taught me that positivity, perseverance, determination, and sometimes a good cry is key to achieving your goals. Thank you for being such a loving and supportive role model. I would like to thank my siblings, Shai and Spencer, for the constant support and encouragement even when I am far away from home. Additionally, I would like to thank my nephew, Luke, for being my constant source of happiness.

This thesis is dedicated to my grandmother, Diane Soucie

TABLE OF CONTENTS

ABBREVIATIONS

APS – Ammonium Persulfate

ARG9 – Nine Arginine

BSA – Bovine Serum Albumin

BEAS-2B – Human Lung Bronchus Epithelial Cells

CPP – Cell Penetrating Peptide

DNA – Deoxyribonucleic Acid

DMEM – Dulbecco's Modified Eagle Medium

EDTA – Ethylenediaminetetraacetic Acid

F_1 – Active Subunit of Fusion Protein

F_2 – Active Subunit of Fusion Protein

FBS – Fetal Bovine Serum

FDA – Food and Drug Administration

FITC – Fluorescein Isothiocyanate

FPLC – Fast Protein Liquid Chromatography

F protein – Fusion Protein

GAGs – Glycosaminoglycans

GE – Gene-end

GLP-1 – Glucagon-like Peptide 1

GS – Gene-start

GST – Glutathione S-transferase

GTP – Guanosine-5'-triphosphate

G protein – Attachment Protein

HEp-2 – Human HeLa Contaminant Carcinoma Cells

HIV – Human Immunodeficiency Virus

HSA – Human Serum Albumin

hTrx – Human Thioredoxin

IPTG – Isopropyl β-D-1-thiogalactopyranoside

kDa – Kilodalton

LB – Luria-Bertani Broth

Le – Leader

LLC-MK2 – Rhesus Monkey Kidney Epithelial Cells

L protein – Large Polymerase Protein

LRTI – Lower Respiratory Tract Infection

MBP – Maltose Binding Protein

mRNA – Messenger RNA

M protein – Matrix Protein

M2 protein – Matrix Protein 2

N° – Wildtype Monomeric, RNA-free Nucleoprotein

NS1 – Non-Structural Protein 1

NS2 – Non-Structural Protein 2

N protein – Nucleoprotein

OD – Optical Density

PAMP - Pattern-associated Molecular Pattern

PBS – Phosphate Buffered Saline

PBST – Phosphate Buffered Saline + 0.1% Tween-20

PCR – Polymerase Chain Reaction

PICU – Pediatric Intensive Care Unit

PMSF – Phenylmethylsulfonyl Fluoride

P protein – Phosphoprotein

PRR – Pattern Recognition Receptor

RdRp – RNA-dependent RNA Polymerase

RIPA – Radioimmunoprecipitation Assay

RNA – Ribonucleic Acid

RPM – Revolutions Per Minute

RSV – Respiratory Syncytial Virus

$RSVP_{212-241}$– Last 30 C-terminal Amino Acids of the RSV Phosphoprotein

$RSVP_{220-241}$ – Last 21 C-terminal Amino Acids of RSV Phosphoprotein

SDS – Sodium Dodecyl Sulfate

SDS-PAGE – Sodium Dodecyl Sulfate Polyacrylamide Gel Electrophoresis

SH – Small Hydrophobic Protein

SOC – Super Optimal Broth

TAE – Tris, Acetic Acid, EDTA buffer

TBS – Tris-Buffered Saline

TEMED – Tetramethylethylenediamine

TLR – Toll-like Receptor

x *g* – Centrifugal Force

LIST OF FIGURES

LIST OF TABLES

DECLARATION OF ACADEMIC ACHIEVEMENT

Samantha P. Mihalco performed all experiments described in this thesis except for the following:

1. Cloning of His-MBP-Tat-RSVP$_{220-241}$ and GST-N was performed by Dr. David Bulir.
2. Sylvia Chong provided the clinical stock of RSV A long strain used in this thesis.
3. Steven Liang prepared the chemically competent *E. coli* cells.

Chapter 1 – Background and Objectives

1.1 History of Human Respiratory Syncytial Virus

Human respiratory syncytial virus (RSV) is a serious viral pathogen of infants and children and the leading cause of acute lower respiratory tract infection (LRTI) in this population (Nair et al., 2011). In addition, RSV significantly contributes to mortality and morbidity in the elderly and immunocompromised (Wyde, 1998). RSV was first identified in 1956 as the coryza agent responsible for the coughing, sneezing, and nasal discharge experienced by a population of chimpanzees (Blount et al., 1956). In the same year, an agent related to the chimpanzee coryza agent was isolated from infants with lower respiratory tract infection (Chanock et al., 1962). The isolated agent was later named RSV since infection of human tissue culture cells with the agent resulted in the formation of syncytia (Chanock et al., 1962).

1.2 Global Burden of Respiratory Syncytial Virus

Worldwide, acute LRTIs are the leading cause of child mortality (Rodriguez & Ramilo, 2014). Bronchiolitis and pneumonia are among the most common manifestations of LRTI caused by RSV (Nair et al., 2011; Munywoki et al., 2015). RSV infects nearly all children by the age of two years old, with the majority acquiring infection as infants (Glezen et al., 1986). Despite the limited antigenic diversity of RSV, reinfections are common throughout life, which can largely be attributed to the limited development of durable and protective neutralizing antibodies against RSV (Openshaw & Chiu, 2013). Infants, the elderly, and individuals with compromised immune, pulmonary, or cardiac functions are among the most susceptible to RSV infection (Branche & Falsey, 2015; Ogra, 2004).

On a global scale, RSV is the leading cause of infant hospitalization for acute LTRIs (Hall, 2012). Globally in 2005, it was estimated that RSV was responsible for approximately 33.8 million cases of acute LRTIs in children under the age of five, and of those cases at least 3.4 million resulted in hospitalization (Nair et al., 2010). In addition, it was estimated that at least 66,000 children under the age of five died in 2005 as a result of RSV-induced severe LRTI, with 99% of deaths having occurred in developing countries (Nair et al., 2010). On an annual basis in the United States alone, RSV infections require medical attention in approximately 2.1 million cases in children less than five years of age (Borchers et al., 2013), and approximately 177,000 hospitalizations and at least 10,000 deaths in the elderly (Fearns & Deval, 2016).

RSV not only causes a significant health burden worldwide, but is also an economic burden. Estimates from 1997 suggested that the Canadian Health Care System spends approximately $18 million annually on RSV-associated infections in children up to four years of age (Langley et al., 1997). In 2000, the United States spent a staggering $652 million on RSV-associated medical costs (Paramore et al., 2004). From 1999 to 2003, high-risk adult and elderly RSV-associated hospitalization costs were estimated to exceed $1 billion dollars in the United States (Fearns & Deval, 2015; Falsey et al., 2005).

1.3 Clinical Presentation of Respiratory Syncytial Virus

Primary RSV infection is symptomatic and manifests as an upper respiratory tract infection, with symptoms including nasal discharge, congestion, cough, and a low-grade fever (Hall et al., 2013; Del Vecchio et al., 2013). Generally, the upper respiratory tract

symptoms persist for only a few days (Hall et al., 2013). However, 30% of RSV-associated upper respiratory tract infections in children up to two years of age spread to the lower respiratory tract, which can be fatal (Del Vecchio et al., 2013). Symptoms characteristic of an RSV-associated LRTI include a worsening cough, dyspnea, and wheezing (Ogra, 2004; Hall et al., 2013). Bronchiolitis is the most common diagnosis of RSV-associated LRTI and is characterized by increased swelling and death of small airway epithelial cells, which manifests as symptoms of wheezing, fever, coryza, cough, and respiratory distress (Leung et al., 2005; Del Vecchio et al., 2013). Generally, the symptoms of an acute RSV infection peak five days post-infection, resolving within ten days (Eiland, 2009; Hall et al. 2013). However, ciliated airway epithelial cells recover slowly and as a result coughing can persist for up to one month post-infection (Eiland, 2009).

Recurrent RSV infections in older children and adults are often accompanied by symptoms of an upper respiratory tract infection, including persistent flu-like symptoms that are generally more severe than the common cold (Borchers et al., 2013, Hall et al., 2013). The most common symptoms of a recurrent RSV infection include fever, sinusitis, and otitis media (Hall et al., 2013). In addition, up to one-fourth of secondary RSV infections progress to LRTI (Borchers et al., 2013; Hall et al., 2013). Recurrent RSV infections in the elderly are generally more severe as a result of other comorbid conditions, such as chronic obstructive pulmonary disease (Hall et al., 2013).

Viral LRTIs are a known risk factor for bacterial co-infections (Thorburn et al., 2006). Significantly higher levels of bacteria are commonly isolated from the nasopharynx and lower respiratory tract of children under the age of five with RSV infection (Chappell

et al., 2013; Thorburn et al., 2006). RSV is believed to promote bacterial co-infection by decreasing bacterial clearance and increasing bacterial adherence (Brealey et al., 2015). Interestingly, it has been suggested that the RSV attachment glycoprotein may function as a receptor on the surface of respiratory epithelial cells for bacterial binding (Brealey et al., 2015). Furthermore, bacterial co-infection may lead to increased severity of RSV infection and increased risk for pneumonia (Brealey et al., 2015; Chappell et al., 2013; Thornburn et al., 2006).

It is believed that up to 40% of children under the age of five admitted to the pediatric intensive care unit (PICU) as a result of severe RSV-associated LRTI experience bacterial co-infection (Thorburn et al., 2006). In addition, it was observed that children with bacterial co-infection require prolonged ventilator support (Thornburn et al., 2006). *Moraxella catarrhalis*, *Streptococcus pneumoniae*, *Haemophilus influenzae*, and *Staphylococcus aureus* are the most common bacterial species showing an increased load during RSV infection (Chappell et al., 2013).

Additionally, severe RSV bronchiolitis in children is considered an important risk factor in the development of wheezing and asthma (Bacharier et al., 2012; Sigurs et al., 2000). In one study, 48% of children that acquired severe RSV bronchiolitis during infancy were diagnosed with asthma prior to age seven (Bacharier et al., 2012). However, the mechanisms governing the association between RSV infection and asthma remain unclear (Bacharier et al., 2012; Sigurs et al., 2000).

1.4 Risk Factors for Severe Respiratory Syncytial Virus Infection

Premature infants, the elderly, as well as individuals with chronic lung disease, immune deficiencies, and congenital heart disease are at the greatest risk for severe RSV infections (Branche & Falsey, 2015; Hall et al., 2013; Ogra, 2004; Welliver, 2003). Premature infants are at a high risk for severe RSV infection since they have lower titers of maternally derived RSV-neutralizing antibodies and underdeveloped airways (Welliver, 2003). In addition, premature infants with chronic lung disease not only have underdeveloped lungs, but they also have deformed, inflamed, or hyperactive airways, rendering them more susceptible to RSV-induced inflammatory reactions (Welliver, 2003). Other factors that put young children at risk of RSV infection include day care attendance, a crowded home, and older siblings attending school or day care (Eiland, 2009; Hall et al., 2013). Children with risk factors for severe RSV infection experience prolonged hospitalizations, increased requirements for admission to PICUs, and ventilator support (Hall et al., 2013). Elderly patients are considered high risk since many have underlying conditions that may become exacerbated with RSV infection (Hall et al., 2013). Death as a result of RSV infection is most likely in the immunocompromised as they experience prolonged replication of RSV within the lungs and delayed recovery following infection (Welliver, 2003). Lastly, although no particular cardiac lesion is associated with a greater severity of RSV infection, individuals with congenital heart disease experience prolonged hospitalizations, administration to intensive care units, as well as a greater risk of respiratory failure and mortality (Welliver, 2003).

1.5 Transmission and Seasonality of RSV

RSV is a highly transmissible infection between individuals of all ages (Hall, 1983). The incubation period is approximately three to five days and the period of viral shedding is anywhere from three to eight days (Eiland, 2009). RSV is transmitted from direct contact with the respiratory secretions of an infected individual, which can be transmitted by sneezing, coughing, and breathing (Hall & Douglas, 1981; Hall et al., 2013). RSV transmission can also occur through contact with infected surfaces followed by self-inoculation through the nose, eyes, or upper respiratory tract (Hall et al., 2013). RSV can survive on stethoscopes for six hours, non-porous surfaces for 12 hours, and on skin for approximately 30 minutes (Eiland, 2009). In addition, nosocomial spread of RSV is problematic in pediatric wards and for high-risk patients (Hall et al., 2013).

Outbreaks of RSV in temperate regions occur seasonally and generally persist for 12 to 20 weeks (Hall et al., 2013). In temperate regions, RSV outbreaks generally occur from November to April in the Northern hemisphere and from March to October in the Southern hemisphere (Borchers et al., 2013; Hall et al., 2013). However, the seasonality of RSV outbreaks in tropical regions is less predictable, whereby multiple peaks of infection or constant infection have been documented (Borchers et al., 2013). Despite general time frames of peak infections based on geographical location, individual RSV outbreaks can vary greatly in both the timing and duration from year to year (Hall et al., 2013).

1.6 Taxonomy and Antigenic Diversity

RSV is a member of the order *Mononegavirales* and family *Paramyxoviridae* (Chang & Dutch, 2012). Viruses within this family consist of a lipid-encapsulated, negative-sense single-stranded RNA virus (Chang & Dutch, 2012). Other members of this family include measles, mumps, parainfluenza viruses, and human metapneumovirus (Chang & Dutch, 2012). Although viruses within the *Paramyxoviridae* family share many structural features, underlying mechanisms that govern their lifecycles may be unique to each virus (Chang & Dutch, 2012). The *Paramyxoviridae* family can further be classified into subfamilies, *Paramyxovirinae* and *Pneumovirinae,* which are composed of five and two genera, respectively (Chang & Dutch, 2012). RSV is a member of the *pneumovirinae* subfamily, as is human metapneumovirus (Chang & Dutch, 2012).

RSV has two major antigenic subtypes, denoted A and B, which differ in their attachment glycoproteins (G), fusion proteins (F), nucleoproteins (N), and phosphoproteins (P) (Ogra, 2004; Sullender, 2000). The greatest degree of genetic diversity between the subtypes is observed within the G protein, with only 53% sequence similarity (Sullender, 2000). Furthermore, there is genetic variation within the major antigenic subgroups, resulting in different strains, which are likely the result of selective pressures imposed on the virus by the host immune system (Ogra, 2004; Sullender, 2000). Nonetheless, the different strains within a major group exhibit a high degree of similarity. For example, the genetic sequence of the G protein was 94% similar between the A2 and Long strains of RSV A (Sullender, 2000). Genetic differences between RSV A and B also occur to a small

degree within the F, N, and P proteins (Fuentes et al., 2016; Johnson & Collins, 1990; Ogra, 2004).

Epidemiological studies have documented a predominance of RSV group A infections; however, both subtypes are known to circulate during the same epidemic or to alternate in dominance (Borchers et al., 2013; Sullender, 2000). Although the majority of studies suggest that RSV A is more virulent than RSV B, other studies have failed to observe an association between RSV group and virulence (Gilca et al., 2006; Hall et al., 2013; McConnochie et al., 1990; Sullender, 2000).

1.7 Respiratory Syncytial Virus Genome

RSV is an enveloped, non-segmented, and negative-sense single stranded RNA virus (Ogra, 2004). The small viral genome of 15.2 kilobases consists of 10 genes that code for 11 proteins; nine structural and two non-structural (Gomez et al., 2014). Each gene is transcribed into monocistronic messenger ribonucleic acid (mRNA). However, the mRNA encoding the M2 proteins, M2-1 and M2-2, has two overlapping open reading frames (Bawage et al., 2013).

RSV has three trans-membrane envelope glycoproteins, the attachment protein (G), the fusion protein (F), and the small hydrophobic protein (SH) (Borchers et al., 2013; Collins et al., 2013). The G and F proteins play important roles in viral attachment and host-cell penetration, respectively (Gomez et al., 2014). The F protein is also responsible for cell-to-cell spread of RSV by promoting the fusion of neighboring epithelial cell membranes, thereby forming syncytia (Ghildyal et al., 2012; Gomez et al., 2014). Together,

the F and G envelope proteins are the major determinants of RSV antigenicity, which induce the production of neutralizing antibodies (Ogra, 2004). The exact role of the SH protein in RSV pathogenesis remains unclear, but it does not appear to play a role in viral attachment or penetration (Borchers et al., 2013; Ghildyal et al., 2012). More recent studies have suggested that the SH protein inhibits cellular apoptosis of infected cells by forming a viporin ion channel in the lipid bilayer to increase membrane stability, ultimately prolonging the life of the infected cell and promoting viral replication (Araujo et al., 2016; Gomez et al., 2014).

The nucleoprotein (N), phosphoprotein (P), large polymerase (L), M2-1, and M2-2 are structural proteins that form the RNA-dependent RNA polymerase (RdRp) complex, which is crucial for RSV transcription and replication (Borchers et al., 2013). N proteins associate with the viral RNA to form the helical and highly stable nucleocapsid (NC) complex (Ghildyal et al., 2012; Ruigrok et al., 2011; Tawar et al., 2009). In a continuous manner, N proteins encapsulate the viral RNA to prevent RNase digestion of the viral genome (Ruigrok et al., 2011). Furthermore, the association of N proteins along the length of the viral genome helps to prevent an innate immune response through host cell toll-like receptor (TLR) signaling (Collins et al., 2013). The NC complex is the site of both RSV transcription and replication (Galloux et al., 2012). The RSV P protein is an important co-factor for the L polymerase, which possesses the catalytic activity of the RdRp complex (Galloux et al., 2012; Ruigrok et al., 2012; Sourimant et al., 2015). The tetrameric P protein is believed to connect the L polymerase and NC complex, thereby providing the L polymerase with access to the viral genome (Galloux et al., 2012; Ruigrok et al., 2011;

Sourimant et al., 2015). Furthermore, RSV P proteins are responsible for binding newly synthesized N proteins, denoted N°, to prevent them from precipitating or associating with host cell RNA (Galloux et al., 2015). The M2-1 protein is an anti-termination factor that strongly promotes transcription elongation, while the M2-2 protein acts as a regulatory 'switch' from transcription to viral replication (Bermingham & Collins, 1999; Collins et al., 2013; Galloux et al., 2012).

Another RSV structural protein, the matrix (M) protein, plays two important roles throughout infection (Ghildyal et al., 2012; Ogra, 2004). During the early infection process, the M protein plays an important role in regulating host cell transcription in the nucleus of infected airway epithelial cells (Ghildyal et al., 2012). However, later during the infection process, the M protein leaves the nucleus and is involved in virion assembly followed by budding (Ogra, 2004; Ghildyal et al., 2012). Lastly, the two non-structural proteins of RSV, NS1 and NS2, contribute to the survival and replication of RSV through their roles in immune evasion (Collins et al., 2013). NS1 and NS2 have both been shown to suppress apoptosis and host cell type I interferons (Bitko et al., 2007; Collins et al., 2013, Spann et al., 2004). NS1 and NS2 are present in infected cells at high levels; however, they are absent from virions (Bitko et al., 2007).

1.8 Respiratory Syncytial Virus Lifecycle

The lifecycle begins with attachment of RSV virions to airway epithelial cells through the G protein (Feldman et al., 1999). Through an electrostatic interaction, the G protein associates with heparin sulfate glycosaminoglycans (GAGs) located on the apical

surface of host cells (Feldman et al., 1999; Ghildyal et al., 2012). More specifically, both RSV A and B attachment (G) proteins contain a heparin-binding domain, which consists of positively charged amino acids residues that electrostatically interact with the negatively charged sulfate residues of host cell plasma membrane GAGs (Feldman et al., 1999).

Following attachment, the F protein initiates fusion of the virion with the lipid bilayer of the host cell (Ghildyal et al., 2012). F proteins are synthesized as inactive polypeptides, F_0, that trimerize and are activated through cleavage by a furin-like protease (Ghildyal et al., 2012; McLellan et al., 2011). Cleavage of F_0 generates three fragments, and the subsequent disulfide-bonding between the F1 and F2 fragments generates the active form of the protein that is inserted into the virion membrane (Ghildyal et al., 2012; McLellan et al., 2011). On the surface of the virion, the active F protein is in its pre-fusion conformation (Mastrangelo & Hegele, 2013; McLellan et al., 2011). However, binding of the F protein to its putative receptor nucleolin on the surface of target cells results in a conformational change to the post-fusion form and subsequent fusion (Mastrengelo & Hegele, 2013). In addition, considering that RSV infection is restricted to epithelial cells of the respiratory tract and the nucleolin receptor is present on the surface of many different cell types, other receptors or co-receptors may be involved in this process (Tayyari et al., 2011).

Following fusion, the NC complex and other viral proteins are released into the cytoplasm of infected cells (Ghildyal et al., 2012; Gomez et al., 2014). Within the cytoplasm of infected cells, the N and P proteins associate with unknown host cell proteins to form inclusion bodies (Cowton et al., 2006; García-Barreno et al., 1993; García-Barreno

et al., 1996; Ghildyal et al., 2012). Viral N, P, L, and M2-1 proteins, along with the viral genome, are sequestered within the inclusion bodies (García et al., 1993; García-Barreno et al., 1996; Ghildyal et al., 2012). RNA synthesis occurs within the cytoplasmic inclusion bodies, which are often referred to as RNA synthesis factories (Cowton et al., 2006).

Transcription of viral genes is one of the first events to occur within inclusion bodies (Collins et al., 2013). For transcription to occur, the RdRp is delivered to the NC complex by the P protein (Collins et al., 2013; Galloux et al., 2012; Sourimant et al., 2015). Upon binding to the promoter located within the 44 nucleotide 3' leader (Le) sequence, the RdRp initiates transcription of the viral genes (Cowton et al., 2006). Each gene is flanked by a conserved gene-start (GS) sequence at the 3' end and a conserved gene-end (GE) sequence at the 5' end (Cowton et al., 2006). The GS and GE sequences regulate viral transcription, whereby GS sequences initiate mRNA synthesis and GE sequences terminate synthesis (Collins et al., 2013). This organization results in transcription that occurs in start-stop fashion from the 3' Le sequence towards the 155 nucleotide 5' trailer (Tr) sequence (Collins et al., 2013; Cowton et al., 2006).

From the promoter, the RdRp scans the genome for the first GS sequence (Collins et al., 2013; Cowton et al., 2006). At the GS signal, the RdRp caps and methylates the 5' end of the to-be viral mRNA and begins transcribing the viral gene (Collins et al., 2013; Cowton et al., 2006). During mRNA transcription elongation, the RdRp complex is only responsive to GE sequences (Collins et al., 2013). Upon reaching a GE sequence, the RdRp complex polyadenylates the 3' end of the transcript thereby terminating transcription and releasing the transcript (Collins et al., 2013; Cowton et al., 2006). The RdRp complex

remains bound to the NC complex and continues to scan the genome for the next GS sequence to reinitiate mRNA synthesis (Collins et al., 2013; Cowton et al., 2006). The M2-1 protein is an important cofactor of the RdRp complex that plays a major role in promoting transcript elongation (Bermingham & Collins, 1999; Collins et al., 1996; Galloux et al., 2012). The M2-1 protein interacts with the L polymerase through its binding to the P protein to exert its anti-termination activity (Collins et al., 2013).

The RdRp complex tends to dissociate at gene junctions, resulting in a gradient in transcription and ultimately protein expression (Collins et al., 2013; Cowton et al., 2006). Since the promoter where transcription is initiated is located at the 3' end of the RSV genome, genes located at the 3' end are transcribed much more frequently than genes located at the 5' end (Collins et al., 2013; Cowton et al., 2006). The RSV genome is strategically organized, such that proteins required in large amounts (such as NS1 and NS2) are located at the 3' end of the genome, while proteins required in smaller amounts (such as the L polymerase) are located at the 5' end (Collins et al., 2013; Cowton et al., 2006). Following transcription, RSV transcripts are translated to protein by host cell machinery (Collins et al., 2013; Cowton et al., 2006; González et al., 2012).

The trigger responsible for the switch from RSV transcription to replication remains unknown (Bermingham & Collins, 1999; Cowton et al., 2006). One theory proposes that replication is initiated once a threshold level of the N° protein is synthesized to enable protective encapsidation of the newly replicated genome, while another suggests that the M2-2 protein is responsible for initiating the switch in a time-dependent manner (Berminghman & Collins, 1999; Collins et al., 2013).

Replication of the RSV genome begins when the RdRp complex binds to the promoter within the Le sequence and synthesizes a complete positive-sense antigenome (Cowton et al. 2006). During the process of replication, the RdRp synthesizes a complete copy of the RSV genome since it is unresponsive to both GS and GE sequences (Bermingham & Collins, 1999; Cowton et al., 2006; Gomez et al., 2014). A promoter within the 3' end of the antigenome, denoted TrC, directs replication of the antigenome to yield full-length negative-sense RSV genomes, which are packaged into virions (Cowton et al., 2006). As replication occurs, both the newly synthesized positive antigenomes and negative-sense genomes are encapsidated by N°, which is believed to contribute to the RdRp's ability to read through GE signals (Cowton et al., 2006).

Following replication, RSV NC complexes and proteins are assembled into virions that are released from the host cell membrane (Collins et al., 2013). The exact processes of virion assembly and subsequent budding have yet to be fully elucidated. However, all viral proteins must be localized together at lipid raft domains of the host cell membrane (Ghildyal et al., 2012; Henderson et al., 2002). Just prior to virion assembly, the M protein associates with the NC through the M2-1 protein to stop RNA synthesis (Ghildyal et al., 2012). The M protein also anchors NC complexes to the host cell microfilament network to be transported to the site of assembly (Ghildyal et al., 2012; Henderson et al., 2002; Marty et al., 2004).

On the other hand, F and G proteins are transported to the site of virion assembly through the secretory pathway (Ghildyal et al., 2012). Presently, few studies have explored the transport of SH proteins to the site of assembly (Ghildyal et al., 2012). Nonetheless,

once all RSV structural proteins have been transported to the lipid raft domains, the virion is ready to bud from the host cell membrane to infect adjacent cells (Brown et al., 2002; Ghildyal et al., 2012; Henderson et al., 2002; Marty et al., 2004).

The mechanism of RSV budding remains poorly understood, but current theories suggest that the process depends largely on M and F proteins in conjunction with host factors (Baviskar et al., 2013; Brown et al., 2002; Ghildyal et al., 2012). The M protein is known to mediate curvature of the host cell membrane, which is essential for budding (Ghildyal et al., 2012). On the other hand, the F protein is believed to stabilize the viral filaments, which are formed by oligomerization of the M protein and are crucial for budding (Förster et al., 2015; Ghildyal et al., 2012; Jeffree et al., 2007). Furthermore, it has been suggested that the F protein acts as a catalyst for the budding process, whereby its C-terminal tail facilitates the incorporation of assembled virions into viral filaments (Baviskar et al., 2013).

1.9 Respiratory Syncytial Virus Immune Evasion Tactics

Several RSV proteins play important roles in promoting survival and protecting the virus from detection by the host cell innate immune system. An N-terminally truncated version of the G protein, which lacks its membrane anchor, is secreted to interrupt host antibody neutralization of RSV (Borchers et al., 2013 ;Collins et al., 2013). The secreted form of the G protein is believed to act as a decoy antigen to prevent cell-mediated neutralization of RSV (Borchers et al., 2013; Collins et al., 2013). As mentioned previously, the SH protein promotes RSV survival by inhibiting apoptosis of infected cells (Araujo et

al., 2016; Gomez et al., 2014). However, the SH protein also inhibits signaling of the antiviral cytokine, tumor necrosis factor alpha (TNF-α) (Collins et al., 2014; Fuentes et al., 2007). Lastly, as mentioned previously in section **1.7**, NS1 and NS2 suppress both apoptosis and interferon I signaling in infected cells (Bitko et al., 2007; Collins et al., 2013, Spann et al., 2004). These protective strategies that occur throughout infection are important for promoting RSV survival.

1.10 Development of a Respiratory Syncytial Virus Vaccine

Presently, there is no vaccine available to prevent RSV infections. The current absence of a Food and Drug Administration (FDA)-approved vaccine stems largely from the strict regulations implemented following the unfortunate outcomes of a trial involving a formalin-inactivated vaccine in 1966 (Acosta et al., 2016; Guvenel et al., 2014; Neuzil, 2016). The preliminary findings of this trial were promising since 43% of vaccine recipients displayed a four-fold increase in neutralizing antibodies (Guvenel et al., 2014; Kim et al., 1969). Despite these promising initial findings, vaccinated children experienced exacerbated immune responses that lead to an enhanced disease state when naturally infected with RSV (Guvenel et al., 2014). In fact, 80% of recipients required hospitalization with two deaths (Guvenel et al., 2014; Kim et al., 1969). Postmortem examination of the lungs from the two fatalities revealed infiltration of neutrophils, lymphocytes, macrophages, and eosinophils (Acosta et al., 2016).

It was later revealed that formalin treatment of RSV actually altered the F protein epitopes, resulting in the production of antibodies that could bind but not neutralize F

proteins from the natural, circulating virus (Murphy & Walsh, 1988). These non-neutralizing antibodies likely contributed to the enhanced disease state since they were shown to form complexes in the lungs with RSV antigens (Murphy & Walsh, 1988). In addition, an increase in the type-2 helper T-cell (Th2) response contributed to exacerbating the infection by triggering an inflammatory cell response (Acosta et al., 2016; Collins & Graham, 2008; Gut et al., 2008). Th2 polarization leads to defective viral clearance and reduced cytotoxic T-cell activity (Gomez et al., 2014; Krishnamoorthy et al., 2012).

In addition to the strict regulations imposed following the formalin-inactivated vaccine, several other immunological factors may explain the lack of a safe and effective RSV vaccine. Generally, successful vaccines induce aspects of the protective immune response that are initiated by the host organism upon natural infection, while eliminating any associated pathology (Guvenel et al., 2014). However, since humans do not elicit a complete immune response following RSV infection, this approach may not lead to the development of an effective vaccine (Guvenel et al., 2014). Furthermore, populations at high risk for severe RSV infection generally exhibit impaired immune responses as a result of immaturity, immunodeficiency, or immunosenescence (Guvenel et al., 2014).

Nonetheless, different strategies are being investigated for the development of a safe and effective RSV vaccine. The main strategies being explored include protein-based, live-attenuated, and vector-based methods (Neuzil et al., 2016; Rezaee et al., 2017). Currently, the populations being considered for vaccination against RSV include pregnant women, the elderly, as well as infants and children (Rezaee et al., 2017).

Popular protein-based vaccines strategies include vaccination with particle-based or whole-inactivated RSV, and are promising for use in pregnant women and the elderly (Rezaee et al., 2017). Development of a maternal vaccine is actively being explored and several are in clinical trials since infants are at the greatest risk for severe RSV infection and are unlikely to acquire protection from active immunization (Broadbent et al., 2015; Mazur et al., 2015). The goal of this vaccination strategy is to increase the maternal levels of RSV neutralizing antibodies, which will be transferred across the placenta to the fetus, thereby providing protection throughout the first few months of life (Polack, 2015).

Live-attenuated vaccine strategies attenuate the virus through selective genome deletions, while maintaining a sufficient degree of replication to stimulate an antibody response. This is a promising vaccination strategy for infants and children since the likelihood of immune exacerbation following natural infection is low (Rezaee et al., 2017). An additional advantage of this strategy is that it can be administered intranasally, thereby stimulating both mucosal and humoral immunity (Rezaee et al., 2017). Despite several live-attenuated vaccines being evaluated in clinical trials, further studies are required (Branche & Falsey, 2015; Guvenel et al., 2014)

1.11 Respiratory Syncytial Virus Therapeutics

To date, there is only one prophylactic and one pharmaceutical option licensed for clinical use in the prevention and treatment of RSV (Rodriguez & Ramilo, 2014). Palivizumab is a humanized mouse monoclonal immunoglobulin G 1 (IgG1) antibody directed against the RSV F protein (Chu & Englund, 2013). Palivizumab neutralizes both

RSV A and B by blocking the fusion process (Chu & Englund, 2013; Turner et al., 2014). Palivizumab is administered prophylactically each month of the RSV season through intravenous or intramuscular injection (Rezaee et al., 2017; Turner et al., 2014). Previous clinical trials to evaluate the prophylactic use of palivizumab showed a 55% reduction in hospitalization of high-risk infants (Neuzil, 2016). However, palivizumab costs approximately $6,000 to treat a single patient during the RSV season (Eiland, 2009). As a result, its use is limited to infants at high-risk of severe RSV infection, such as pre-term infants (Krilov, 2011; Mejias & Ramilo, 2015; Rez et al., 2017; Rodriguez & Ramilo, 2014). An additional neutralizing antibody, motavizumab, was derived from palivizumab and despite its greater RSV neutralizing abilities, it was not licensed for clinical use as subcutaneous reactions were reported (Rodriguez & Ramilo, 2014).

Ribavirin, a broad-spectrum guanosine analogue, is the only licensed antiviral agent approved for the treatment of RSV (Chu & Englund, 2013; Krilov, 2011; Mejias & Ramilo, 2015; Rodriguez & Ramilo, 2014). Ribavirin can be administered orally, intravenously, or intranasally (Turner et al., 2004). However, intranasal administration through aerosolization is the most common method of delivery (Chu & Englund, 2013). Ribavirin inhibits RSV replication by interfering with RNA capping, inhibiting the viral polymerase, inducing lethal mutagenesis, or inhibiting inosine monophosphate, thereby depleting guanosine-5'-triphosphate (GTP) levels (Turner et al., 2014). However, ribavirin is not routinely used in the treatment of RSV infections since there is limited proven efficacy, a difficult administration procedure, a high cost of treatment, and potential toxicity (Collins & Melero, 2011). As a result, ribavirin use is limited to severe RSV infections in infants

and immunocompromised patients (Krilov, 2011). Current clinical management of most RSV-associated lower respiratory tract infections is supportive in nature, consisting of adequate oxygenation, intravenous hydration, and ventilator support, as required (Chu & England, 2013).

Currently, a number of antiviral therapies are being evaluated in clinical trials. The majority of RSV antivirals being evaluated are small molecules (Mejias & Ramilo, 2015). One promising small molecule, GS-5806 (Presatovir), is an inhibitor of RSV fusion that was recently evaluated in Phase II clinical trials (Rezaee et al., 2017). The small molecule was able to significantly reduce RSV viral load without serious adverse reactions (Rezaee et al., 2017). There are also a number of monoclonal antibodies being evaluated in clinical trials for prophylactic use (Mazur et al., 2015). One example is the inhalable nanobody ALX-017, which was shown to reduce RSV load and replication by inhibiting fusion, while maintaining a desirable safety profile (Rezaee et al., 2017). As a result, this nanobody is currently being evaluated in children up to 2 years old (Rezaee et al., 2017). An additional promising antibody being evaluated is the long-lasting MEDI-88 monoclonal antibody, which is directed against the RSV F protein (Mazur et al., 2015). Although the vast majority of antiviral therapies being evaluated are directed against the RSV F protein, several other therapies target the viral G, N, and P proteins, as well as the L polymerase (Broadbent et al., 2015; Mazur et al., 2015). Considering the global and economic burdens of RSV and the current lack of routine treatment, safe, practical, and cost-effective RSV antiviral therapies are required.

1.12.1 Novel Antiviral Therapeutic Development: Targeting the Respiratory Syncytial Virus P-NC Interaction

Previous studies have shown that the N protein, L polymerase, and P protein are crucial for RSV replication, and ultimately survival of the virus within infected host cells (Yu et al., 1995). As previously mentioned, the P protein plays an important role in both transcription and replication, since it is necessary for recognition of the NC complex by the L polymerase, and may function as the point of connection between the two proteins (Galloux et al., 2012). Early deletion studies showed that the C-terminus of the RSV P protein was crucial for interaction with the N protein (García-Barreno et al., 1996). In addition, it was shown that an antibody consisting of the terminal 21 amino acids of the P protein (220-241) was sufficient to displace the N protein from N-P complexes (García-Barreno et al., 1996). More recently, it was shown that the last nine amino acids of the RSV P protein are sufficient for binding the NC complex (Galloux et al., 2012; Tran et al., 2007).

Since the RSV P protein binding region required for interaction with the NC complex has been mapped, there are no cellular orthologs, and an antibody can be used to disrupt the wild-type interactions (García-Barreno et al., 1996; Sourimant et al., 2015), a novel therapeutic compound could be designed to disrupt the P-NC interactions. Through disruption of the interaction, this therapeutic compound could function by preventing the L polymerase from recognizing and associating with NC complexes. Under these conditions, RSV replication would be limited and/or abolished.

1.12.2 Novel Antiviral Therapeutic Development: Targeting the Respiratory Syncytial Virus L Polymerase, NC Complex, and P Protein Interactions

The RSV P protein forms homo-tetramers, which are believed to interact simultaneously with L polymerases and NC complexes to allow the polymerase to access the tightly wrapped viral RNA (Asenjo and Villanueva, 2000; Ruigrok et al., 2011; Sourimant et al., 2015). Recently, through a series of deletions and pull-downs, the domain on the RSV P protein responsible for binding the L polymerase was mapped to C-terminal amino acid residues 212 to 239 (Sourimant et al., 2015). Interestingly, the L polymerase and NC complex binding domains on the P protein overlap by 7 residues (Sourimant et al., 2015; Tran et al., 2007).

Designing an RSV therapeutic compound able to block the P protein's interactions with both the L polymerase and NC complexes is a promising and novel antiviral strategy. Targeting the interaction between the L polymerase and P protein is desirable for several reasons, including the fact that the L polymerase harbors the catalytic activity required for replication and transcription (Collins et al., 2013), and is transcribed less frequently than other viral genes, resulting in lower L polymerase protein levels (Collins et al., 2013; Cowton et al., 2006). However, targeting the P protein's interactions with both NC complexes and L polymerase may increase the efficacy of the therapeutic compound. In addition, since the binding domain on the P protein is larger for the L polymerase compared to the NC complex, it may show a higher affinity for the L protein (Sourimant et al., 2015). This may further improve the efficacy of the therapeutic compound, as its affinity may be greater for the L polymerase, which is more limited in availability than the N protein.

A therapeutic compound able to disrupt the wild-type interactions between the P protein, L polymerase, and NC complex may function by sequestering both L polymerase and NC complexes, thereby blocking important interactions required for RSV replication. Under these conditions, RSV replication would be significantly limited or completely abolished.

1.13 Peptide Mimetics

Protein interaction networks are essential to many biological pathways, as well as disease progression by bacterial and viral pathogens (Schaefer et al., 2013). These crucial protein interaction networks are established through protein-protein interactions, which in turn are mediated by small regions or "hot spots" within the interaction interface of the proteins (Ghildyal et al., 2012; Tsomaia, 2015). Due to their importance, these protein interactions are viable targets for novel therapeutic compounds to prevent or treat viral infections (Ghildyal et al., 2012; Tsomaia, 2015). Important protein-protein interactions can be disrupted using peptide mimetic compounds. Peptides are classified as proteins of 50 amino acids or less and play important roles in many biological pathways (McGregor, 2008; Tsomaia, 2015). As such, peptide mimetic compounds can be used as dominant-negative molecules that would outcompete wild-type protein interactions, thereby disrupting important biological interaction networks (Mason, 2010).

Peptides offer numerous advantages over small-molecule therapeutics, predominantly because they have a high specificity for their targets due to the larger binding pocket compared to a small molecule (McGregor, 2008; Tsomaia, 2015). A single mutation

in the target organism can hamper the binding of small molecules (Krishnamurty & Maly, 2011; Tsomaia, 2015). In contrast, therapeutic peptides target a much larger binding domain, and retain efficacy even in the presence of one or two mutations within their binding region (Tsomaia, 2015). This is a desirable feature of peptide mimetics since it limits the development of resistance to therapeutic molecules, which is a major issue with classical viral treatments (Pillay & Zomban, 1998). Furthermore, the high specificity of peptide therapeutics has resulted in desirable safety, efficacy, and tolerability profiles in humans (Fosgerau & Hoffmann, 2015). Another potential advantage of peptide mimetics is that they are often non-immunogenic when targeting a natural biological pathway (McGregor, 2008). However, immunogenicity could be an issue if the peptide is derived from a foreign species, such as viral pathogens (Fosgerau & Hoffmann, 2015).

Since many important protein-protein interactions occur in the intracellular environment, gaining cellular access is an important consideration for the use of peptide mimetics. One approach that can be used to allow peptides to cross cell membranes is fusion of the peptide to a cell penetrating peptide (CPP), which is typically a stretch of 8 to 30 basic amino acids that can interact with and facilitate passage of cargo through cellular membranes (Dinca et al., 2016; Jones & Sayers, 2012). Since peptide mimetics are much smaller than antibody derived therapeutics, they are able to effectively penetrate tissues and can more easily reach their intracellular targets when conjugated to a CPP (McGregor, 2008).

To date, the most successful example of a peptide mimetic therapeutic used to treat viral infection is enfuvirtide, a fusion inhibitor of HIV (Matthews et al., 2004). Enfurvirtide

is a 36 amino acid peptide that binds to and inhibits the gp41 HIV envelope protein, thereby preventing HIV-1 penetration into host cells (Matthews et al., 2004). In addition, the Mahony laboratory has had previous success in designing viable peptide mimetics capable of blocking important protein-protein interactions involved in influenza replication (unpublished data) and *Chlamydia pneumoniae* type III secretion (Stone et al., 2011). Furthermore, a previous student in the Mahony laboratory synthesized a peptide mimetic capable of inhibiting RSV replication by approximately 90% (unpublished data). With over 140 peptide therapeutic approaches currently in clinical trials (Fosgerau & Hoffmann, 2015), peptide mimetics offer promising new opportunities for the development of novel antiviral therapeutics.

1.14 Improving Peptide Stability Through the Albumin Binding Domain (ABD)

One challenge associated with the use of peptides is their limited efficacy, mainly resulting from their susceptibility to rapid renal clearance and degradation by proteases (McGregor, 2008). However, one approach that has improved their efficacy is by associating them with relatively large carrier molecules that will ultimately limit their degradation and clearance (McGregor, 2008).

Human serum albumin (HSA), a 66.5 kDa serum protein synthesized by hepatocytes in the liver, is found in large quantities in the blood (40 g/L) and is an ideal carrier molecule due to its long serum half-life of approximately 19 days (Jacobs et al., 2015; Sand et al., 2014). The long serum half-life of HSA is attributed to its ability to avoid endosomal degradation by binding to the neonatal Fc receptor (FcRn) (Sand et al., 2014).

This interaction is pH-dependent, whereby HSA has a high affinity for FcRn receptors in acidic environments but not at physiological pH (Sand et al., 2014). Through this mechanism, HSA can be recycled back to the cell membrane where it is released into circulation since the environment is at a physiological pH (Sand et al., 2014).

There are two common strategies for using HSA as a carrier molecule in recombinant protein therapeutics. The first is to synthesize a peptide mimetic that is fused directly to HSA. However, previous studies have shown that HSA can be challenging to express since a eukaryotic expression system is required for post-translational modifications (B. Li, Cao, Zhou, Liang, & Sun, 2013). Thus, an alternative approach is to attach a peptide mimetic to an albumin-binding domain (ABD). ABDs are short stretches of amino acids that have a high affinity for HSA (Nilvebrant & Hober, 2013). A number of ABDs have been characterized, and interaction between the ABD and HSA is known to be non-covalent, thereby allowing the peptide to exist in both a bound and unbound state (Nivelbrant & Hober, 2013). Through this mechanism, any associated peptide acquires the advantages of improved stability and decreased clearance while still existing in an unbound form to exert its therapeutic effects (Kontermann, 2011; Nivelbrant & Hober, 2013).

Streptococcal protein G, a protein localized on the surface of many streptococcal strains, contains specific amino acid sequences that interact with both HSA and IgG1 (Linhult et al., 2002; Nilvebrant & Hober, 2013). Upon further characterization of protein G, three individual ABD domains were identified; namely, ABD-1, ABD-2, and ABD-3. The 46 amino acid (~5 kDa) ABD-3 domain at the C-terminus of the protein was further characterized and was shown to be highly stable and soluble, contain a compact

hydrophobic core, and possess refolding-abilities following thermal and chemical denaturation, as well as being small and amenable to protein synthesis (Nilvebrant & Hober, 2013). The secondary structure of ABD-3 is composed of three alpha helices, with residues in helix II being critical for the interaction with HSA (Linhult et al., 2002). On the other hand, previous studies have shown that domain II of HSA is responsible for interacting with ABDs (Nilvebrant & Hober, 2013).

Previous studies have explored increasing the binding affinity of the ABD-3 domain for Streptococcal protein G for HSA (Jonsson et al., 2008; Sand et al., 2014). One novel variant, denoted ABD035, maintained a similar secondary structure to that of the wild-type ABD-3 domain, yet demonstrated both improved affinity for HSA and thermal stability (Jonsson et al., 2008). The ABD035 variant increased the half-life of several fusion proteins, and it was previously shown that a construct consisting of the ABD035 variant fused to an affibody molecule had a similar half-life and biodistribution to that of HSA (Andersen et al., 2011). In a different study, a single chain diabody (scDb) fused to ABD035 resulted in a two-fold increase in half-life of the therapeutic molecule (Frejd, 2012; Stork et al., 2009). More recently, a synthetic ABD, denoted ABDCon, was developed through consensus engineering (Jacobs et al., 2015). In a murine model, fusion of the ABDCon to a small protein, Tecon25, that lacks binding partners, prolonged its serum half-life from approximately 40 minutes to over 60 hours (Jacobs et al., 2015).

1.15 Thesis Objectives

The Mahony laboratory has previously demonstrated that an RSV P protein mimetic designed to block the wild-type interaction between the P protein and NC complex was able to inhibit RSV A and B replication *in vitro* by approximately 90 and 80%, respectively (unpublished data). This mimetic was designed to include the final 21 amino acids of the P protein from RSV A attached to the *E. coli* MBP carrier molecule to increase the mimetic's stability and solubility, as well as the HIV-1 Tat CPP for transport to the intracellular compartment of cells. Furthermore, a hexa-histidine tag was included in the recombinant fusion protein for purification and detection purposes, yielding the recombinant fusion protein His-MBP-Tat-RSVP$_{220\text{-}241}$. Dr. David Bulir cloned this construct and Jordan Nelson performed all experiments to evaluate its activity. A boxcar diagram of this construct is depicted in **Figure 6.1**.

Since the ultimate goal of the His-MBP-Tat-RSVP$_{220\text{-}241}$ fusion protein is RSV treatment in humans, a carrier molecule compatible for use in humans is required in place of the *E. coli* MBP carrier molecule. For this purpose, we chose the ABD035 carrier molecule since it is small, stable, highly soluble, and has a high affinity for HSA (Jonsson et al., 2008). The first goal of this thesis was to ultimately replace the MBP portion of the RSV P$_{220\text{-}241}$ fusion protein with an ABD035 carrier molecule and subsequently evaluate its activity. We hypothesized that RSV replication would still be attenuated when attached to the ABD035 carrier molecule.

The second goal of this thesis was to design a new peptide mimetic that could disrupt wild-type RSV P protein interactions with both the L polymerase and NC complex,

since it was recently shown that the two binding domains on the P protein overlap (Sourimant et al., 2015). This novel new peptide mimetic was designed to include the last 30 C-terminal amino acid residues of the RSV A P protein (denoted $RSVP_{212-241)}$. We hypothesized that this peptide mimetic would be more effective than its counterpart His-MBP-Tat-$RSVP_{220-241}$ in attenuating RSV replication since in theory it should be able to block two important interactions required for replication. For this part of my thesis, my objectives were to design, synthesize, and evaluate the peptide mimetic *in vitro*.

Chapter 2 – Materials and Method

2.1.1 Cloning of Expression Plasmids Using the Gateway® Cloning System

Protein mimetic constructs containing an ABD were cloned using the Gateway® Cloning System. The constructs were ordered as gBlock® Gene Fragments from Integrated DNA Technologies. The gBlocks® Gene Fragments were designed to include *attB* recombination sites for cloning into the Gateway® pDONR201 entry vector. The ABD-Tat-$RSVP_{220-241}$ gBlock contained codon optimized nucleotide sequences for the ABD035 peptide (LAEAKVLANRELDKYGVSDFYKRLINKAKTVGVEALKLHILAALP), a GGGS linker, the HIV-1 Tat CPP, an S linker, and the 21 C-terminal amino acids of the RSV phosphoprotein. The $RSVP_{212-241}$ construct was ordered as a gBlock that contained codon optimized nucleotide sequences for a GSAAS linker followed by the 30 C-terminal amino acid residues of the RSV phosphoprotein ((DEVSLNPTSEKLNNLLEGNDSDNDLSLEDF). Lastly, the Tat-$RSVP_{212-241}$ construct was ordered as an entry vector from Invitrogen (Thermo Fisher Scientific) and contained nucleotide sequences for the HIV-1 Tat CPP and the 30 C-terminal amino acids of the RSV A phosphoprotein.

According to the manufacturer's protocols, all gBlock® Gene Fragments were cloned into the pDONR201 vector via the Gateway® Cloning System BP reaction to generate entry vectors. Briefly, to perform a BP reaction, 25 ng of the gBlock® Gene Fragment was incubated with empty pDONR201 vector, Gateway® BP clonase mix, and TE buffer (10 mM Tris-HCl pH 8.0, 1 mM EDTA) for a minimum of one hour. Following the incubation, the BP reaction was terminated by adding 0.2 μg/μl of Proteinase K

(Invitrogen) and incubating the sample at 37˚C for 10 minutes. Subsequently, the BP reaction was transformed into chemically competent *E. coli* Turbo or DH5α cells (New England Biolabs, Ipswich MA), as described in section **2.2.2**. Entry vectors were purified from successful transformants, described in section **2.2.2**. Success of the BP reaction was confirmed through agarose gel electrophoresis and sequencing at the MOBIX sequencing facility (McMaster, Hamilton ON).

Expression plasmids were constructed using the Gateway® Cloning System LR reaction according to the manufacturer's protocols. Briefly, entry vectors were incubated with the desired destination vector (denoted pDEST), Gateway® LR clonase mix, and TE buffer for one hour. Constructs were cloned into pDEST17 to generate His fusion proteins, pDEST15 to generate GST fusion proteins, or pDEST-His-MBP to generate His-MBP fusion proteins. ABD constructs were cloned into pDEST17, pDEST15, and pDEST-His-MBP vectors, whereas the Tat-$RSVP_{212-241}$ and $RSVP_{212-241}$ constructs were cloned into pDEST-His-MBP. The LR reaction was terminated after one hour by adding 0.2 μg/μL of Proteinase K and incubating the sample at 37˚C for 10 minutes. The LR reaction was transformed into chemically competent *E. coli* Turbo cells, as described in section **2.2.2**. Entry vectors were purified from successful transformants and LR reaction products were screened for successful recombination using agarose gel electrophoresis and sequencing at the MOBIX Sequencing Facility (McMaster, Hamilton ON). Expression plasmids containing the desired inserts were transformed into chemically competent *E. coli* BL21 (DE3) or *E. coli* Rosetta (Life Technologies) cells to allow for expression of the desired protein.

2.1.2 Cloning of Expression Plasmids Using Inverse Polymerase Chain Reaction and the In-Fusion® Cloning System

The Tat-His-MBP-Tat-RSVP$_{212-241}$ and His-Arg9-MBP-RSVP$_{212-241}$ constructs were cloned using inverse PCR and In-Fusion® Cloning. The starting material for the Tat-His-MBP-Tat-RSVP$_{212-241}$ mimetic was a His-MBP-Tat-RSVP$_{212-241}$ expression vector, whereas the starting material for the His-Arg9-MBP-RSVP$_{212-241}$ mimetic was the pDEST-His-MBP vector. Primers used to insert the additional Tat CPP at the N-terminus of the original RSVP$_{212-241}$ construct and the Arg9 at the C-terminus of the His-tag of the pDEST-His-MBP vector were designed to be compatible with the In-Fusion® Cloning System. Specifically, In-Fusion® Cloning System primers require a 15 base-pair overlap, whereby the first 15 nucleotides of the 5' end of the forward primer are complementary to the first 15 nucleotides of the 5' end of the reverse primer. All primers used in this thesis were ordered as lyophilized stocks from Integrated DNA Technologies. The primers were re-suspended in UltraPure^{TM} DNase/RNase-Free Distilled Water (Invitrogen) to a master stock concentration of 100 μM. For use in inverse PCR, the primers were further diluted to 20 μM. All primers used in this thesis are outlined in **Table 6.2**.

Template vectors used to generate expression vectors for Tat-His-MBP-Tat-RSVP$_{212-241}$ and the His-Arg9-MBP destination vector (to generate His-Arg9-MBP-RSVP$_{212-241}$) were His-MBP-Tat-RSVP$_{212-241}$ expression vector and pDEST-His-MBP vector, respectively. The His-MBP-Tat-RSVP$_{212-241}$ expression vector was amplified, linearized, and an additional HIV-1 Tat CPP (YGRKKRRQRRR) was inserted at the N-terminus of the His-tag using inverse PCR with primer set A (see **Table 6.2),** as per the

manufacturer's protocols. The resulting linearized PCR products were mixed at a 4:1 ratio with 5x DNA loading dye (50% w/v sucrose, 0.05 M ethylenediaminetetraacetic acid (EDTA), 0.1% Bromophenol Blue, 4 M urea, pH 7.0) and electrophoresed on a 0.6% agarose-ethidium bromide gel at 120 volts (V) for 60 minutes using the PowerBac Basic Power Supply (BioRad). Subsequently, the gel was visualized via ultraviolet (UV) light using the GelDoc™ XR+ (Bio-Rad) system and Quantity One Software.

Desired PCR products were excised and purified from the gel using the Geneaid™ Gel/PCR DNA Fragments Extraction Kit. Subsequently, the linearized plasmid was re-circularized using the In-Fusion® Cloning System (Thermo Fisher Scientific), as per the manufacturer's protocols. Briefly, the In-Fusion® enzyme mix was incubated with linearized vector for 15 minutes at 50˚C followed by 5 minutes of incubation on ice. The re-circularized plasmids were then transformed into chemically competent *E. coli* DH5α cells (New England Biolabs, Ipswich MA), as described in section **2.2.2**. The expression plasmids of successful transformants were isolated as described in **2.2.2** and sequenced at the MOBIX sequencing facility (McMaster, Hamilton ON). Desired expression plasmids were then transformed into *E. coli* BL21 (DE3) cells.

The same protocol was followed to insert a nine-arginine (RRRRRRRRR) CPP following the His-tag of the pDEST-His-MBP vector using primer set B (see **Table 6.2**). In this case, the re-circularized plasmid was transformed into *E. coli* One Shot ccdB Survival cells (Thermo Fisher Scientific)**,** as described in section **2.2.2**. Subsequently, this destination was isolated and sequenced at the MOBIX Sequencing Facility (McMaster, Hamilton ON) prior to use in an LR reaction with the $RSVP_{212-241}$ entry vector.

2.2.1 Preparation of Chemically Competent *E. coli* Cells

E. coli strains used in this research include Turbo, DH5α, BL21 (DE3), and Rosetta. Each strain of *E. coli* was grown overnight in 5 mL of Luria-Bertani Broth (LB) (1% w/v tryptone, 0.5% w/v yeast extract, 1% w/v NaCl) at 37˚C while shaking at 250 rotations per minute (RPM). The overnight bacterial culture was inoculated into 100 mL of fresh LB at a ratio of 1:100 and then grown until an optical density at 600 nm (OD_{600}) of 0.5 was achieved. Subsequently, cells were incubated on ice for 15 minutes and pelleted by centrifugation at 3,000 RPM and 4˚C for 10 minutes. The media was removed and the cells were re-suspended in ice-cold 10 mM $MgSO_4$ prior to incubation on ice for 30 minutes. Cells were then pelleted by centrifugation at 3,000 RPM and 4˚C for 10 minutes. Subsequently, media was removed and cells were re-suspended in ice-cold 50 mM $CaCl_2$ and incubated on ice for 30 minutes. Cells were pelleted as described previously and then re-suspended in ice-cold 50 mM $CaCl_2$ + 15% v/v glycerol, divided into aliquots, and stored at -80˚C for future use.

2.2.2 Transformation of Chemically Competent *E. coli* Cells

To transform chemically competent *E. coli*, an aliquot of the desired cells were thawed on ice. Subsequently, approximately 100 ng of the desired plasmid was incubated with thawed *E. coli* on ice for 30 minutes. Cells were then heat shocked at 42˚C for 45 seconds and incubated on ice for 5 minutes. Following the incubation on ice, cells were grown for one hour at 37˚C in SOC medium (2% w/v tryptone, 0.5% w/v yeast extract, 10 mM NaCl, 2.5 mM KCl, 10 mM $MgCl_2$, and 20 mM glucose). Subsequently, 100 µL of the

transformed *E. coli* cells were plated using sterile glass beads on 1.5% agar plates supplemented with 30 µg/mL of kanamycin for entry plasmids or 100 µg/mL of ampicillin for expression plasmids. The plates were incubated overnight at 37˚C. Individual colonies from successful transformants were selected from the plate and grown overnight at 37˚C while shaking at 250 rpm in 5 mL of LB supplemented with either 30 µg/mL of kanamycin or 100 µg/mL ampicillin. Glycerol stocks of transformed *E. coli* were made by mixing 300 µL of overnight bacterial culture with 50% v/v glycerol at a 1:1 ratio. Glycerol stocks were stored at -80˚C for future use. Both entry and expression plasmids were purified from the remaining overnight culture using a High-Speed Plasmid Mini Kit (Geneaid), according to the manufacturer's protocol. All isolated plasmids were separated by electrophoresis using agarose gels, as described in **2.1.2**, after which plasmids believed to contain the desired product were sequenced at the MOBIX Sequencing Facility (McMaster University, Hamilton, ON). Following sequencing, expression plasmids were transformed into *E. coli* BL21 (DE3) cells.

2.3.1 Preliminary Assessment of Protein Expression and Solubility Using Mini-Expression Assays

Mini-expression solubility assays were performed to determine whether recombinant proteins could be expressed in a soluble form and to optimize protein expression for use in future large-scale experiments. *E. coli* cells transformed with the desired expression plasmid were grown overnight in 5 mL of LB supplemented with 100 µg/mL of ampicillin while shaking at 250 RPM and 37˚C. Overnight cultures were used to

inoculate anywhere from 3 to 30 mL of new LB supplemented with 100 µg/mL of ampicillin, and allowed to grow at 37˚C and 250 RPM until an OD_{600} of approximately 0.6 was achieved. The bacterial culture was aliquoted into tubes and protein expression was induced with 0.1, 0.2, or 0.5 mM IPTG at room temperature, 30˚C, or 37˚C while shaking at 250 RPM for at least 2 hours. Following induction, *E. coli* cells were harvested by centrifugation at 3,000 RPM for 10 minutes. The supernatant was decanted and pelleted cells were re-suspended in 200 µL of ice-cold 1X PBS. Subsequently, the cells were lysed on ice by sonication at 25 Watts for 10 seconds. Cellular debris was pelleted by centrifugation at 16,000 x *g* for 5 minutes, and the supernatant was transferred to a separate tube. Pellets, containing any insoluble protein, were re-suspended in 250 µL of 5X Laemmli buffer, while 50 µL of 5X Laemmli buffer was added to the supernatant samples. All samples were heated to 95˚C for approximately 15 minutes, separated by SDS-PAGE, and subsequently analyzed by Western blots, as described in section **2.4.1** and **2.4.2**.

2.3.2 Large-Scale Expression Recombinant Proteins

All His-tagged expression plasmids and GST-ABD-Tat-$RSVP_{220-241}$ expression plasmids used in this research were expressed in *E. coli* BL21 (DE3) cells. The GST-nucleoprotein (GST-N) and GST plasmids (kindly provided by Dr. David Bulir) were expressed in *E. coli* Rosetta cells. A small amount of *E. coli* glycerol stock containing the desired expression plasmid was inoculated into 100 mL of LB supplemented with 100 µg/mL of ampicillin and incubated overnight at 37˚C while shaking at 250 RPM. The following morning, approximately 15 mL overnight culture was inoculated into 1 L of LB

containing 100 μg/mL of ampicillin. For large-scale expression, we generally inoculated 6 L of LB. Bacterial cultures were grown in an incubator at 37˚C while shaking at 250 rpm. All His- and GST-tagged protein cultures were grown to an OD_{600} of approximately 0.6, except for the His-MBP-Tat-$RSVP_{212-241}$ cultures, which were grown to an OD_{600} of 2.0. Although protein expression was inducted by the addition of IPTG for all constructs, the expression conditions varied (see **Table 1**). Following induction of protein expression, *E. coli* cells were harvested by centrifugation at 12,000 x *g* and 4˚C for 5 minutes using a Sorvall® RC-5B refrigerated centrifuge. Harvested cells containing recombinant proteins to be used in GST pull-downs (see sections **2.6.5** and **2.6.7**) were re-suspended in 15 mL of tris-buffered saline (TBS) + 0.1% v/v Tween-20 (GST-ABD-Tat-$RSVP_{220-241}$) or PBS + 0.1% v/v Tween-20 (GST-N and GST). Harvested cells containing His-MBP and His-MBP-ABD-Tat-$RSVP_{220-241}$ recombinant proteins to be used in the Ni-NTA pull-downs (see section **2.6.6**) were re-suspended in 15 mL of TBS + 0.1% v/v Tween-20.

	Construct	Concentration of IPTG	Temperature	Length of Induction
GST-tagged Proteins	GST-ABD-Tat-$RSVP_{220-241}$	0.2 mM	37˚C	3 h
	GST	0.1 mM	37˚C	2 h
	GST-N	0.2 mM	16˚C + RT	3 h
His-tagged Proteins	His-MBP-Tat-$RSVP_{220-241}$	0.5 mM	RT	2 h
	His-MBP-ABD-Tat-$RSVP_{220-241}$	0.2 mM	16˚C + RT	2 h
	His-MBP	0.2 mM	RT	2 h
	His-MBP-Tat-$RSVP_{212-241}$	0.1 mM	30˚C	24 h
	Tat-His-MBP-Tat-$RSVP_{212-241}$	0.5 mM	37˚C	2 h
	His-Arg9-MBP-$RSVP_{212-241}$	0.2 mM	37˚C	2 h

Table 1. Expression conditions for the recombinant fusion proteins used in this thesis.

2.3.3 Affinity Purification of Glutathione S-transferase-tagged Proteins

E. coli cells harvested from large-scale expression, as described in section **2.3.2**, containing GST-ABD-Tat-RSVP$_{220\text{-}241}$ to be purified by glutathione affinity chromatography, were re-suspended in 20 mL of 1X PBS (pH 7.4). To inhibit proteases, two Pierce™ Protease Inhibitor Mini Tablets (EDTA-Free) (Thermo Fisher) were dissolved in the cell suspension. Cells were lysed by six pulse sonication cycles at 25 Watts with 20-second sonication intervals followed by 30-second rest intervals. The sonication process was performed on ice using the Fisher Scientific Sonic Dismembrator – Model 100. The cell lysate was centrifuged at 42,000 x *g* and 4˚C for 45 minutes. Subsequently, the supernatant was filtered through a 0.22 µM vacuum filter (Millipore) on ice.

To separate GST-tagged proteins from bacterial cell components, glutathione affinity chromatography was performed using the ÄKTA Fast Protein Liquid Chromatography (FPLC) Purification System (GE Healthcare). The filtered supernatant was loaded into a Superloop (GE Healthcare) and passed over a GSTrap^{TM} HP column pre-loaded with Glutathione Sepharose^{TM} High Performance medium (GE Healthcare). Subsequently, the column was washed with 1X PBS to remove any non-specifically bound proteins. Column-bound protein was eluted from the column in 500 mM Tris, + 0.015% reduced glutathione, pH 9.0. Eluted protein was collected and buffer exchanged into 1X PBS (pH 7.4, 8.51, 6.4, and 9) and 40 mM Tris-HCl + 400 mM NaCl (pH 8.57 and 6.5) using a HiPrep^{TM} 26/10 Desalting Column (GE Healthcare).

Following buffer exchange, the purified protein was filtered through an Acrodisc® Low-Protein Binding 0.22 μM Supor® Syringe filter (Pall) into an Amicon® Ultra-15 Centrifugal Filter Device (Millipore). The protein solution was concentrated at 2,000 x *g* and 4˚C for approximately 25 minutes. A small sample of the concentrated protein was collected for analysis by SDS-PAGE and Western blot, as described in sections **2.4.1** and **2.4.2**.

2.3.4 Affinity Purification of Histidine (His)-tagged Recombinant Proteins

E. coli cells harvested from large-scale expression, as described in section **2.3.2**, containing His-tagged recombinant proteins for purification using nickel affinity purification were re-suspended in 15 mL of ice-cold Nickel A buffer (20 mM Tris-HCl pH 7.0, 0.03% v/v LDAO, 0.02% v/v β-mercaptoethanol, 500 mM KCl, 10% v/v glycerol, 10 mM imidazole) with a pH of 7.4. To inhibit proteases, two Pierce™ Protease Inhibitor Mini Tablets (EDTA-Free) (Thermo Fisher) were dissolved in the cell suspension. His-MBP-ABD-Tat-RSVP$_{212\text{-}241}$ fusion protein was also purified under denaturing conditions. In that case, the harvested pelleted was re-suspended in 25 mL of Buffer C-10 (20 mM Tris-HCl pH 7.0, 0.02% β-mercaptoethanol, 375 mM KCl, 8 M urea, 10 mM imidazole). Cells were lysed by six pulse sonication cycles at 25 Watts with 20-second sonication intervals followed by 30-second rest intervals. The sonication process was performed on ice using the Fisher Scientific Sonic Dismembrator – Model 100. The cell lysate was centrifuged at 42,000 x *g* and 4˚C for 45 minutes. Subsequently, the supernatant was filtered through a 0.22 μM vacuum filter (Millipore) on ice.

To separate His-tagged proteins from bacterial cell components, nickel affinity chromatography was performed using the ÄKTA Fast Protein Liquid Chromatography (FPLC) Purification System (GE Healthcare). The filtered supernatant was loaded into a Superloop (GE Healthcare) and passed over a HisTrap™ HP column pre-loaded with Ni Sepharose™ (GE Healthcare). Subsequently, the column was washed three times with 5%, 10%, and 15% Nickel B Buffer (20 mM Tris-HCl pH 7.0, 0.03% LDAO, 0.02% β-mercaptoethanol, 500 mM KCl, 10% v/v glycerol, 300 mM imidazole, pHed to 7.4) to remove any non-specifically bound proteins. Column-bound protein was eluted from the column in 100% Nickel B Buffer. The same protocol was followed for the purification of His-MBP-ABD-Tat-RSVP$_{220-241}$ under denaturing conditions using Buffer D (20 mM Tris-HCl pH 7.0, 0.02% β-mercaptoethanol, 375 mM KCl, 8 M urea, 300 mM imidazole). Eluted protein was collected and buffer exchanged into 1X PBS (pH 7.4) using a HiPrep™ 26/10 Desalting Column (GE Healthcare).

The His-MBP-ABD-Tat-RSVP$_{220-241}$ protein was also buffer exchanged by dialysis overnight at 4˚C into 1X PBS (pH 7.4), 40 mM Tris-HCl + 500 mM NaCl (pH 7.4), 0.5X PBS (pH 7.4), 1X PBS + 10% glycerol (pH 7.4), and 1X PBS + 250 mM NaCl (pH 7.4). Briefly, following purification the protein sample was injected into a dialysis cassette and incubated in 2,000 mL of the exchange buffer and subsequently stirred for 2 hours at 4˚C. Following the incubation, the cassette was incubated in 2,000 mL of fresh buffer and incubated again for 2 hours while being stirred at 4˚C. Following the incubation, the cassette was incubated in 2,000 mL of fresh buffer overnight at 4˚C while being stirred.

Following buffer exchange using the desalting column or dialysis, the purified protein was filtered through an Acrodisc® Low-Protein Binding 0.22 µM Supor® Syringe filter (Pall) into an Amicon® Ultra-15 Centrifugal Filter Device (Millipore). The protein solution was concentrated at 2,000 x *g* and 4˚C for approximately 60 minutes. A small sample of the concentrated protein was collected for analysis by SDS-PAGE and Western blot and for quantification, as described in sections **2.4.1** and **2.4.2**. The remaining concentrated protein was divided into aliquots and stored at -80˚C for use in future experiments.

2.3.5 Quantification of Protein Concentration

To determine the concentration of purified recombinant proteins, the *DC* Protein Assay was performed, which is similar to the well-known Lowry Assay (Lowry, Rosebrough, Farr, & Randall, 1951). To generate protein standards of known concentration (0, 0.2, 0.6, 1, and 1.5 mg/mL), BSA was dissolved in the same buffer as the purified protein. The protein standards and aliquot of purified protein were mixed with 127.5 µL of DC™ Protein Reagent A (BioRad) followed by 1 mL of DC™ Protein Reagent B (BioRad) in a 1.5 mL cuvette. The absorbance of each sample was measured at a wavelength of 750 nm using an Ultrospec 4300 Pro UV/Visible Spectrophotometer. Absorbances of the BSA protein standards were plotted in Microsoft Excel to generate a standard curve. The unknown concentration of purified protein sample was determined using the line of best fit from the standard curve and the respective absorbance reading.

2.4.1 Sodium Dodecyl Sulfate Polyacrylamide Gel Electrophoresis

Protein samples were prepared for separation by electrophoresis by mixing the sample at a 1:4 ratio with 5X Laemmli buffer (4% w/v SDS, 100 mM Tris pH 7.0, 0.2 mM EDTA, 10% v/v glycerol, 0.002% bromophenol blue, 12.5% v/v β-mercaptoethanol). The samples were then heated at 95˚C for 15 minutes before being loaded onto a 12% polyacrylamide gel, which consisted of a resolving (375 mM Tris-HCl pH 6.8, 0.1% v/v SDS, 0.4% v/v tetramethylethylenediamine (TEMED), 12% v/v Acryl/Bis-Acryl, and 0.1% v/v ammonium persulfate (APS)) and a stacking (100 mM Tris-HCl pH 8.7, 0.1% v/v SDS, 0.4% v/v TEMED, 5% v/v Acryl/Bis-Acryl, and 0.1% APS) region. The solidified gel was placed into a mini-PROTEAN Tetra Cell (Bio-Rad), after which SDS-PAGE running buffer (25 mM Tris, 192 mM Glycine, and 0.1% w/v SDS) was added. Protein samples and a BLUelf Prestained Protein Ladder (FroggaBio), which was used to approximate the size of proteins, were loaded into wells. Protein samples were electrophoresed at 80 volts (V) for 20 minutes followed by 120 V for 80 minutes.

2.4.2 Western Blot Analysis

Western blot analysis was used to visualize His- or GST-tagged proteins separated by SDS-PAGE. The protein samples electrophoresed, as described in section **2.4.1**, were transferred to a nitrocellulose membrane using the iBlot Gel Transfer Device (Invitrogen), according to the manufacturers protocols. The nitrocellulose membrane was then blocked for one hour at room temperature while rocking in 20 mL of 5% w/v skim milk powder in phosphate-buffered saline (PBS) + 0.1% Tween-20. The membrane was then incubated

with primary antibody diluted in 20 mL of 5% w/v skim milk power in PBS + 0.1% v/v Tween-20 for one hour at room temperature while shaking. Primary antibodies used in this research include mouse anti-polyhistidine (Sigma-Aldrich) at a 1:10,000 dilution, mouse anti-GST (Sigma-Aldrich) at a concentration of 1:5,000, mouse anti-MBP (New England BioLabs) at a dilution of 1:10,000, and mouse anti-α-tubulin (GenScript) at a dilution of 1:5,000. Non-specifically bound antibodies were removed by washing the membrane three times for 5 minutes each time while shaking with PBS + 0.1% v/v Tween-20. Following the washes, the membrane was incubated for one hour at room temperature while shaking with goat anti-mouse conjugated to horseradish peroxidase secondary antibody diluted 1:5,000 in 20 mL of 5% w/v skim milk powder in PBS + 0.1% v/v Tween-20. The membrane was washed again three times and then incubated with enhanced chemiluminescence (ECL) solution (Pierce) for one minute at room temperature while shaking. Subsequently, the membrane was exposed to CL-XPosure™ (ThermoFisher) film paper in a dark room and developed using the Konica SRX-101A Tabletop Photo Processor, according to the manufacturers protocols.

2.4.3 Assessment of Protein Purity

To determine the purity of purified protein, samples of protein were separated by SDS-PAGE and transferred to a nitrocellulose membrane, as described in section **2.4.2**, and all proteins on the membrane were non-specifically detected using Ponceau S Stain (BioShop). Briefly, the membrane was incubated with Ponceau staining solution for 2 minutes while shaking. To clearly visualize bands, the membrane was washed three times

with double-distilled water (ddH_20). Images of the membrane were captured and the Ponceau staining solution was completely removed by washing with PBS + 0.1% v/v Tween-20. Following staining, the membrane was suitable for use in Western blot analysis.

2.5.1 Cell Culture: Passaging of Cell Lines

The cells used in this research, LLC-MK2 cells (rhesus monkey kidney epithelial cells) and HEp-2 (human HeLa contaminant carcinoma cells), were obtained from the ATCC. Both cells lines were propagated in Dulbecco's Modified Eagle Medium (DMEM) (Gibco) supplemented with 10% v/v fetal bovine serum (FBS). LLC-MK2 cells were propagated in 75 cm^2 tissue culture flasks (Greiner Bio-One), while HEp-2 cells were propagated in 25 cm^2 flasks. Cells were incubated at 37˚C and 5% CO_2 until reaching confluency. Once a confluent monolayer was obtained, cells were passaged into new flasks at a ratio of 1:3 to 1:10 in DMEM + 10% FBS depending on the timeline of future requirements. Briefly, the old media was aseptically aspirated and the cells were washed once with 1 mL of 0.05% Trypsin-EDTA (Invitrogen). Subsequently, the cells were incubated with 1 mL of 0.05% Trypsin-EDTA in a 25 cm^2 flask or 3 mL of 0.05% Trypsin-EDTA in a 75 cm^2 flask for approximately 5 minutes at 37˚C and 5% CO_2. Following trypsinization, 1 mL of DMEM + 10% FBS was added to detached cells in 25 cm^2 flasks, while 3 mL of DMEM + 10% FBS was added to detached cells in 75 cm^2 flasks to inhibit the action of trypsin. The cells were then re-suspended prior to being appropriately diluted in a new flask with DMEM + 10% FBS to a final volume of 5 mL for 25 cm^2 flasks or 10 mL for 75 cm^2 flasks.

2.5.2 Cell Culture: Seeding Plates

A confluent flask of LLC-MK2 cells was trypsinized, as described in **section 2.5.1**. Trypsin activity was inhibited by the addition of 7 mL of DMEM + 10% FBS and the detached cells were pelleted by centrifugation at 500 x *g* for 5 minutes. The media was aseptically aspirated and the cells were subsequently thoroughly re-suspended in 5 mL of DMEM + 10% FBS. A sample of the re-suspended cells was mixed at a 1:1 ratio with 0.4% Trypan Blue, and 10 µL was loaded onto a dual chamber cell counting slide (Bio-Rad). The cells were then counted using a TC20^{TM} Automated Cell Counter (Bio-Rad). Cells were seeded at various cell densities ranging from 22,500 cells/well to 375,000 cells/well depending on experimental requirements in 96-well, 24-well, or 6-well plates. The plates were then incubated at 37˚C and 5% CO_2 for 24 or 48 hours.

2.5.3 Cell Culture: RSV A Propagation

An RSV A long strain clinical sample of unknown titer was obtained from St. Joseph's Hospital Clinical Virology Laboratory (Hamilton ON). The frozen sample was thawed and added to a 25 cm^2 tissue culture flask containing a confluent monolayer of HEp-2 cells. The virus was allowed to absorb at 37˚C and 5% CO_2 for 4 hours, while being rocked every 15 minutes to enable distribution of the virus. Subsequently, 4 mL of REFEED medium was added to the flask, which was then incubated at 37˚C and 5% CO_2 for approximately 7 to 8 days. The cells and virus were harvested using a cell-scraper. The harvested virus and cells were subsequently transferred to 15 mL Falcon Tube containing sterile glass beads. The tube was vortexed twice for 30 seconds to lyse all of the cells. The

cellular debris was then pelleted by centrifugation at 500 x *g* for 5 minutes. Following centrifugation, the supernatant was filtered through an Acrodisc® Low-Protein Binding 0.22 µM Supor® Syringe filter (Pall) and subsequently divided into 250 µL aliquots. The aliquots were stored at -80˚C for future experiments.

2.5.4 Cell Culture: Determining the Titer of Propagated RSV A

The titer of RSV was determined by performing 1:10 serial dilutions of frozen RSV A aliquots in 100 µL of REFEED medium. The virus was added to confluent LLC-MK2 cells in a 96-well plate. The plate was centrifuged at 1,500 x *g* for 30 minutes and subsequently incubated at 37˚C and 5% CO_2 for 30 minutes. The viral media was aseptically aspirated, replaced with DMEM, and incubated at 37˚C and 5% CO_2 for 48 hours. Following the 48-hour incubation, the media was removed and the cells were washed twice with sterile 1X PBS. The cells were then fixed with ice-cold methanol for 20 minutes at room temperature. After fixation, cells were washed twice with PBS + 0.1% v/v Tween-20 before being blocked for one hour at 37˚C and 5% CO_2 with 5% BSA in PBS + 0.1% v/v Tween-20. Next, the cells were washed twice with PBS + 0.1% v/v Tween-20 and treated with a 1:1,000 dilution of mouse anti-RSV fusion protein (Abcam) primary antibody in 5% BSA in PBS + 0.1% v/v Tween-20 for one hour at 37˚C and 5% CO_2. Cells were washed seven times with PBS + 0.1% v/v Tween-20 before being treated for one hour at 37˚C and 5% CO_2 with a 1:200 dilution of goat anti-mouse-FITC (Cedarlane) secondary antibody in 5% BSA in PBS + 0.1% v/v Tween-20. Subsequently, cells were washed seven times with PBS + 0.1% v/v Tween-20 prior to a 20-minute room temperature incubation

with 0.05% Evan's Blue reagent. Cells were then washed twice with PBS + 0.1% v/v Tween-20 and visualized using an EVOS FL Cell Imaging System. To determine the titer, the number of infected cells was counted per well and multiplied by the appropriate dilution factor.

2.6.1 Assessing Protein Toxicity to LLC-MK2 Cells Using Light Microscopy Visualization

To assess the toxicity of the His-Arg9-MBP-$RSVP_{212-241}$ construct, the growth of LLC-MK2 cells was visualized in the presence of the recombinant protein. LLC-MK2 cells were seeded to under confluency in 96-well plates at a concentration of 22,500 cells/well in 100 µl of DMEM + 10% FBS, as described in section **2.5.2**. Media was removed and the cells were washed once with DMEM + 10% FBS prior to incubation in triplicate with PBS, 5 µM BSA, 80 µM human thioredoxin (hTrx) Δcys, and 50 µM or 150 µM His-Arg9-MBP-$RSVP_{212-241}$ diluted in DMEM + 10% FBS for 48 hours. The PBS and BSA were included in the experiment to demonstrate healthy cell growth whereas 80 µM hTrx Δcys was included to demonstrate cell toxicity. At time 0, 24, and 48 hours following incubation with the protein conditions, cells were visualized using a light microscope and images were captured.

2.6.2 Assessing Protein Toxicity Using a Spectrophotometer Cell Replication Assay

To assess the cellular toxicity of His-Arg9-MBP-$RSVP_{212-241}$ at the highest concentration to be used in inhibition of RSV studies, the growth of LLC-MK2 cells was

monitored in the presence of protein. LLC-MK2 cells were seeded to under confluency at a concentration of 35,000 cells/well on 24-well plates, as described in section **2.5.2**. The media was aspirated and cells were washed twice with 1X sterile PBS prior to incubation in triplicate with DMEM + 10% FBS alone, 2 mg/ml cycloheximide (Sigma-Aldrich), or 200 μM of His-Arg9-MBP-$RSVP_{212-241}$ diluted in DMEM + 10% FBS for 0, 24, and 48 hours. At the appropriate time point, media was removed from the wells and cells were washed twice with sterile 1X PBS. Subsequently, cells were trypsinized with 750 μl of 0.5% v/v Trypsin-EDTA for 10 minutes at 37˚C and 5% CO_2. Following trypsinization, detached cells were thoroughly re-suspended in trypsin and transferred to individual 1 cm spectrophotometer cuvettes. Absorbance at a wavelength of 800 nm using an Ultrospec 4300 Pro Spectrophotometer blanked against 750 μl of 0.5% v/v Trypsin-EDTA was measured. Absorbance at a wavelength of 800 nm is linearly dependent on cell density in any medium (Mohler, Charlton, & Blau, 1996). A peptide mimetic that is toxic to cells is expected to limit the proliferation of cells, such as cycloheximide, a known inhibitor of eukaryotic translation (Schneider-Poetsch et al., 2010).

2.6.3 Assessment of Cellular Uptake of His-MBP-Tat-$RSVP_{212-241}$ Using a Trypsinization Assay

To determine whether His-MBP-Tat-$RSVP_{212-241}$ was taken up by LLC-MK2 cells, a trypsinization uptake assay was performed. LLC-MK2 cells were seeded into a 24-well plate at a concentration of 150,000 cells/well, as described in **section 2.5.2**. The monolayer was washed three times with sterile 1X PBS. Cells were then incubated in duplicate with

10 μM His-MBP-Tat-$RSVP_{212-241}$ diluted in DMEM for 24 and 48 hours. At the appropriate time point, media was removed from the wells and the cells were washed twice with sterile 1X PBS. Subsequently, the cells were detached by incubation with 0.05% Trypsin-EDTA (Invitrogen) at 37˚C and 5% CO_2 for 10 minutes. The detached cells were collected and pelleted by centrifugation at 16,000 x *g* for 5 minutes. The supernatant was decanted and the pelleted cells were re-suspended in 100 μL of 5X Laemmli buffer, heated to 95˚C for 15 minutes, then separated by SDS-PAGE and analyzed by Western blot using mouse anti-His and mouse anti-α-tubulin primary antibodies, as described in sections **2.4.1** and **2.4.2**.

2.6.4 Assessment of Cellular Uptake of Recombinant Proteins Using a Cell Lysis Assay

To determine whether the His-Arg9-MBP-$RSVP_{212-241}$ fusion protein was taken up by cells, a cell lysis uptake assay was performed. LLC-MK2 cells were seeded in a 6-well plate at a concentration of 375,000 cells/well in 1 ml of DMEM + 10% FBS. The plate was incubated for 48 hours at 37˚C and 5% CO_2 to allow cells to adhere to the plate and reach confluency. Once the cells reached confluency, the growth media was removed and the cells were washed once with DMEM prior to being treated with 20 μM human thioredoxin Δcys (hTrx Δcys) (kindly provided by Christopher Chiang) or 50 μM His-Arg9-MBP-$RSVP_{212-241}$ in DMEM. Cells were incubated with recombinant fusion proteins at 37˚C and 5% CO_2 for 2 and 4 hours. At each time point, media was removed and cells were washed twice with 1X sterile PBS. Subsequently, cells were washed with ice-cold acid wash buffer (0.2 M glycine, 0.15 M NaCl, pH 3.0) for 5 minutes to remove any positively-charged Arg9 adsorbed to the negatively-charged proteoglycans of the cell membrane (Kameyama,

2007). Next, the cells were washed with 1X sterile PBS and incubated with 1 mL of radioimmunoprecipitation assay (RIPA) buffer (Thermofisher) containing 1 mM EDTA, 1 mM phenylmethylsulfonyl fluoride (PMSF), and 1 protease inhibitor tablet (Pierce) at room temperature for 10 minutes. Cells were then scraped from the wells using a cell scraper and lysates were collected and incubated on ice for 10 minutes. Following the incubation, the lysate was centrifuged at 16,000 x *g* and 4˚C for 15 minutes. A sample of the supernatant was re-suspended in 5x Laemmli buffer then boiled at 95˚C for 10 minutes. The boiled samples were run on a 12% SDS-PAGE gel, as described in section **2.4.1**, and analyzed via Western blot using mouse anti-His, mouse anti-MBP, and mouse anti-α-tubulin primary antibodies, as described in section **2.4.2**.

2.6.5 Glutathione S-transferase (GST) Pull-Down Assay to Assess the Interaction between GST-ABD-Tat-RSVP$_{220-241}$ and Human Serum Albumin (HSA)

GST pull-down assays were performed to explore whether two proteins could interact. A GST pull-down assay was performed between GST-ABD-Tat-RSVP$_{220-241}$ and HSA. The expression plasmid for GST-ABD-Tat-RSVP$_{220-241}$ was overexpressed in *E. coli* BL21 (DE3) cells, while the expression plasmid for GST was overexpressed in *E. coli* Rosetta (DE3) cells. For each of the GST-tagged recombinant proteins, 1 L of bacterial culture was grown at 37˚C while shaking at 250 RPM until reaching an OD_{600} of 0.6. At an OD_{600} of 0.6, expression of the GST-ABD-Tat-RSVP$_{220-241}$ and GST proteins were induced, as described in **section 2.3.2**. Following induction, cells were harvested for 5 minutes at 12,000 x *g* and 4˚C using a Sorvall® RC-5B refrigerated centrifuge. The harvested cells

were re-suspended in tris-buffered saline (TBS) + 0.1% v/v Tween-20 supplemented with an EDTA-free protease inhibitor tablet (Pierce) and subsequently lysed by sonication and cellular debris was pelleted, as described in section **2.3.3**.

GST-tagged recombinant protein cell lysates (bait) were incubated with 500 µL of Glutathione High Capacity Magnetic Agarose Beads (Sigma-Aldrich) for one hour while nutating at 4˚C. The beads were then pelleted by centrifugation at 500 x *g* and 4˚C for 5 minutes and the supernatants were removed. The beads were washed once with TBS + 0.1% v/v Tween-20 and re-suspended in 10 mL of ice-cold blocking buffer (5% w/v bovine serum albumin (BSA), 0.1% v/v Tween-20, 1X PBS) for one hour while nutating at 4˚C. The beads were pelleted by centrifugation at 500 x *g* and 4˚C for 5 minutes and subsequently re-suspended in 1 mL of TBS + 0.1% v/v Tween-20. A total of 15 µL of GST-ABD-Tat-RSVP$_{220\text{-}241}$ and GST beads were aliquoted in triplicate into separate 1.5 mL Eppendorf tubes containing 5, 2.5, or 1.25 µg of HSA. Tubes were nutated at 4˚C for 3 hours. Following the incubation, the beads were washed seven times with high salt wash buffer (500 mM NaCl, 20 mM Tris-HCl pH 7.4, 0.1% Triton X-100) using a magnetic stand. Following the final wash, the beads were re-suspended in 30 µl of Laemmli buffer, boiled at 95˚C for 10 minutes, run on a 12% SDS-PAGE gel (as described in section **2.4.1**), and analyzed by Western blot using mouse anti-HSA and mouse anti-GST primary antibodies, as described in section **2.4.2**.

2.6.6 Nickel-nitrilotriacetic acid (Ni-NTA) Agarose Bead Pull-Down

To explore whether the His-MBP-ABD-Tat-RSVP$_{220-241}$ construct maintained its interaction with HSA, a Ni-NTA agarose pull-down assay was performed. The expression plasmids for His-MBP-ABD-Tat-RSVP$_{220-241}$ and His-MBP were overexpressed in *E. coli* BL21 (DE3) cells. For each of the His-tagged recombinant proteins, 1 L of bacterial culture was grown at 37˚C while shaking at 250 RPM until an OD_{600} of 0.6 was achieved. At an OD_{600} of 0.6, expression of the His-MBP-ABD-Tat-RSVP$_{220-241}$ and His-MBP proteins were induced, as described in section **2.3.2**. Following induction, cells were harvested for 5 minutes at 12,000 x *g* and 4˚C using a Sorvall® RC-5B refrigerated centrifuge. The harvested cells were re-suspended in TBS + 0.1% v/v Tween-20 supplemented with an EDTA-free protease inhibitor tablet (Pierce) and subsequently lysed by sonication, after which cellular debris was pelleted, as described in section **2.3.3**.

His-tagged recombinant protein cell lysates (bait) were incubated with 500 µL of Ni-NTA Agarose Beads (Qiagen) for one hour while nutating at 4˚C. Beads were then pelleted by centrifugation at 500 x *g* and 4˚C for 5 minutes and the supernatants were removed. The beads were washed once with TBS + 0.1% v/v Tween-20 and re-suspended in 10 mL of ice-cold blocking buffer (5% w/v bovine serum albumin (BSA), 0.1% v/v Tween-20, 1X PBS) overnight while nutating at 4˚C. The beads were pelleted by centrifugation at 500 x *g* and 4˚C for 5 minutes and subsequently re-suspended in 1 mL of TBS + 0.1% v/v Tween-20. A total of 15 µL of His-MBP-ABD-Tat-RSVP$_{220-241}$- and His-MBP-bound beads were aliquoted in triplicate into separate 1.5 mL Eppendorf tubes containing 5, 2.5, or 1.25 µg of HSA. The tubes were nutated at 4˚C for 3 hours. Following

the incubation, the beads were washed 10 times with high salt wash buffer (500 mM NaCl, 20 mM Tris-HCl pH 7.4, 0.1% Triton X-100) using a magnetic stand. Following the final wash, the beads were re-suspended in 30 µl of Laemmli buffer, boiled at 95˚C for 10 minutes, run on a 12% SDS-PAGE gel (as described in section **2.4.1**), and analyzed by Western blot using mouse anti-HSA and mouse anti-His primary antibodies, as described in section **2.4.2**.

2.6.7 Glutathione S-transferase (GST) Pull-Down Assay to Assess the Interaction between GST-Nucleoprotein (GST-N) and His-Arg9-MBP-RSVP$_{212-241}$

A GST pull-down assay was performed to determine whether GST-N and His-Arg9-MBP-RSVP$_{212-241}$ interact. GST-N and GST were overexpressed in 1 L of *E. coli* Rosetta (DE3) cells. The bacterial cultures were grown at 37˚C while shaking at 250 RPM until reaching an OD_{600} of 0.6. At an OD_{600} of 0.6, expression of GST-N and GST proteins were induced, as described in section **2.3.2**. Following induction, cells were harvested for 5 minutes at 12,000 x *g* and 4˚C using a Sorvall® RC-5B refrigerated centrifuge. The harvested cells were re-suspended in PBS + 0.1% v/v Tween-20 supplemented with an EDTA-free protease inhibitor tablet (Pierce), subsequently lysed by sonication, and cellular debris was pelleted as described in section **2.3.3**.

GST-tagged protein cell lysates (bait) were incubated with 300 µL of Glutathione High Capacity Magnetic Agarose Beads (Sigma-Aldrich) for one hour while nutating at 4˚C. Beads were then pelleted by centrifugation at 500 x *g* and 4˚C for 5 minutes and the supernatants were removed. The beads were washed once with PBS + 0.1% v/v Tween-20

and re-suspended in 10 mL of ice-cold blocking buffer (5% w/v bovine serum albumin (BSA), 0.1% v/v Tween-20, 1X PBS) for one hour while nutating at 4˚C. Beads were pelleted by centrifugation at 500 x *g* and 4˚C for 5 minutes and subsequently re-suspended in 2 mL of blocking buffer, and 200 µL of GST-N- and GST-bound beads were aliquoted in triplicate into separate 1.5 mL Eppendorf tubes containing 1 mL of His-Arg9-MBP-$RSVP_{212-241}$. The tubes were incubated overnight at 4˚C while nutating. Following the incubation, the beads were washed seven times with high salt wash buffer (20 mM Tris-HCl, 500 mM KCl, 0.1% Triton X-100, pH 7.4) using a magnetic stand. Following the final wash, the beads were re-suspended in 60 µl of Laemmli buffer, heated at 95˚C for 15 minutes. The samples were then run on a 12% SDS-PAGE gel, as described in section **2.4.1**, and analyzed by Western blot using mouse anti-His and mouse anti-GST primary antibodies, as described in section **2.4.2**.

2.6.8 Assessment of RSV A Inhibition Using Indirect Immunofluorescence Microscopy

To determine whether the recombinant proteins could inhibit RSV A replication *in vitro*, inhibition assays using indirect immunofluorescence microscopy were performed. LLC-MK2 cells were seeded in a 96-well plate at a concentration of 50,000 cells/well in 100 µl of DMEM + 10% FBS, as described in section **2.5.2**. The plate was incubated for 24 hours at 37˚C and 5% CO_2 to allow the cells to adhere to the wells. Subsequently, the media was aspirated and the cells were washed once with DMEM. For the His-MBP-Tat-$RSVP_{212-241}$ experiment, cells were incubated with DMEM or 25 µM His-MBP-Tat-

$RSVP_{212-241}$ for 2 hours at 37˚C and 5% CO_2. For the His-MBP-Tat-$RSVP_{220-241}$ and His-Arg9-MBP-$RSVP_{212-241}$ experiment, cells were incubated with 0 µM of recombinant protein, 20 µM His-MBP-Tat-$RSVP_{220-241}$, or 25 µM, 50 µM, 100 µM, or 200 µM of His-Arg9-MBP-$RSVP_{212-241}$ in 100 µl of DMEM for 2 hours at 37˚C and 5% CO_2. Each of the recombinant protein conditions and controls were performed in triplicate. Following the incubation period, the cell media was aspirated and 100 µl of undiluted RSV A in REFEED medium was added to each of the wells, except for the negative control wells in which just REFEED medium was added. As a point of comparison, a total of three wells that were not exposed to recombinant protein were infected with RSV A. The plate was then centrifuged at 1,500 x *g* for 30 minutes and incubated at 37˚C and 5% CO_2 for an additional 30 minutes. Subsequently, the viral media was aseptically removed and replaced with the respective recombinant protein conditions or DMEM for the 0 µM peptide and virus-treated wells. The plate was incubated at 37˚C and 5% CO_2 for 48 hours then visualized by indirect immunofluorescence microscopy, as described in **section 2.5.4**. Images of representative and random fields of view were captured using the EVOS FL Cell Imaging System at 10x magnification for each of the experimental conditions. Percent inhibition (PI) was determined by dividing the average number of virus-infected cells in each peptide condition (P) by the average number of virus-infected cells in the virus only wells (V) and subtracting the resulting number from 1: PI = 1 – (P/V) x 100%.

2.6.9 Assessment of Whether Inhibition of RSV Replication Leads to Reduced Progeny Virus Using Indirect Immunofluorescence Microscopy

To determine whether inhibition of RSV A replication by the recombinant proteins His-MBP-Tat-RSVP$_{220-241}$ and His-Arg9-MBP-RSVP$_{212-241}$ results in a reduction in viral progeny, we performed a modified inhibition assay. LLC-MK2 cells were seeded in a 96-well plate at a concentration of 50,000 cells/well, as described in section **2.5.2**. The media was aspirated and the cells were washed once with DMEM. The cells were then treated in triplicate with 20 μM His-MBP-Tat-RSVP$_{220-241}$ or 200 μM His-Arg9-MBP-RSVP$_{212-241}$ in an RSV A inhibition assay, as described in section **2.6.8**. Following infection with RSV A and the second treatment with peptide for 48 hours, the supernatants, containing viral progeny, were used to infect new LLC-MK2 cells seeded in a 96-well plate. Supernatants from RSV A only treated wells were also used to infect new LLC-MK2 cells, as a point of comparison for the peptide condition. The infection process was followed as per section **2.6.8**. Following infection, the viral media was aseptically aspirated and the cells were incubated with DMEM for 48 hours at 37˚C and 5% CO_2. Following the 48-hour incubation, RSV A infection was visualized by indirect immunofluorescence microscopy, as per section **2.5.4**.

2.7 Statistical Analyses

All statistical analyses were performed using GraphPad Prism® Version 7.00 (GraphPad Software Inc., USA). The data are presented as the mean ± one standard deviation. One-way analysis of variance (ANOVA) with a *post hoc* Dunnett's test comparison was used to compare protein-treated groups with the RSV A-only treated

groups. A two-tailed student's t-test was used to compare percent inhibition for the 20 μM His-MBP-Tat-$RSVP_{220-241}$ and 25 μM His-Arg9-MBP-$RSVP_{212-241}$ protein conditions. For all tests, a p-value < 0.05 was considered statistically significant. A p-value < 0.001 was denoted *** and a p-value < 0.0001 was denoted ****.

Chapter 3 – Results

3.1 Development and Assessment of the Novel GST-ABD-Tat-RSVP$_{220-241}$ Fusion Protein

3.1.1 Development of GST-ABD-Tat-RSVP$_{220-241}$

Due to the potential immunogenicity of the bacterial MBP carrier, a carrier molecule compatible for use in humans is desirable for the peptide mimetics. The ABD035 carrier molecule was chosen since it is small in size, stable, highly soluble, and has high affinity for HSA (Jonsson et al., 2008). In addition, ABDs are believed to be less immunogenic since many bacteria that are part of the human body's natural flora express ABDs (Nivelbrant and Hober, 2013).

Initially, the ABD construct was fused to a hexa-histidine tag for purification and detection purposes, an HIV-1 Tat CPP for transport across cell membranes, and the RSVP$_{220-241}$ peptide mimetic. However, the construct could not be expressed and as a result the His-tag was replaced with a GST-tag to facilitate expression of the recombinant fusion protein. A boxcar diagram of the GST-ABD-Tat-RSVP$_{220-241}$ is depicted in **Figure 6.1**.

A gBlock gene fragment consisting of the nucleotide sequences for ABD-GGGS-Tat-S-RSVP$_{220-241}$ was cloned into the pDONR201 vector using the Gateway® Cloning System to generate an entry vector. Samples of the resulting entry vectors were analyzed by agarose-ethidium bromide gel electrophoresis (**Figure 3.1.1)**. The desired entry vectors were approximately 3,500 bp in length. Subsequently, desired entry vectors were used to clone the ABD-GGGS-Tat-S-RSVP$_{220-241}$ insert into the pDEST15 (GST) vector to generate an expression plasmid. Expression plasmids were sent to the MOBIX Sequencing Facility (McMaster, Hamilton ON) to confirm the DNA sequence.

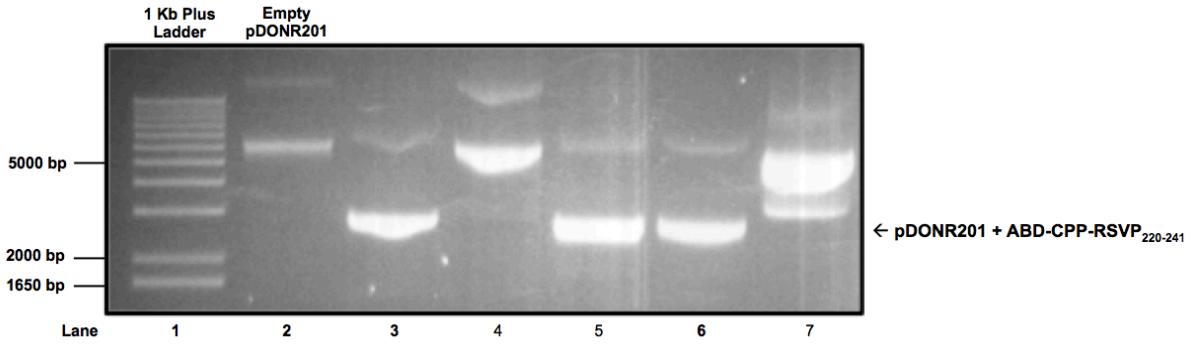

Figure 3.1.1. DNA agarose-ethidium bromide gel depicting insertion of ABD-Tat-RSVP$_{220-241}$ into pDONR201. *E. coli* Turbo cells were transformed with the Gateway BP reaction performed between pDONR201 and the ABD-Tat-RSVP$_{212-241}$ gBlock. Entry plasmids prepped from successful transformants were analyzed on a 1% agarose-ethidium bromide gel and visualized using the Quantity One Program for the GelDoc^{TM} XR+ System. A 1 Kb Plus Ladder was run to the left of the samples to indicate the approximate size of the plasmid samples. The plasmid of interest is approximately 3,400 bp. The presence of visible band shifts near the predicted size suggested ABD-Tat-RSVP$_{220-241}$ was inserted into the pDONR201 vector. These observations were confirmed by DNA sequencing of the resulting entry vectors at McMaster University's MOBIX Sequencing Facility.

3.1.2 Expression and affinity purification of GST-ABD-Tat-RSVP$_{220-241}$

The expression plasmid containing GST-ABD-Tat-RSVP$_{220-241}$ was transformed into *E. coli* BL21 (DE3) cells. A total of 6 L of transformed bacterial culture were prepared and the construct was purified by affinity chromatography using the ÄKTA FPLC protein purification system (GE Healthcare), as described in section **2.3.3**. The GST-ABD-Tat-RSVP$_{220-241}$ recombinant protein precipitated when buffer exchanged into several buffers, as described in section **2.3.3**. The buffer exchanged solution was centrifuged to pellet the precipitated protein and a sample of the soluble portion was analyzed on a 12% SDS-PAGE gel followed by Western blot using a mouse anti-GST primary antibody to evaluate breakdown and estimate the level of soluble protein (**Figure 3.1.2**). A visible band was

present near the predicted size of GST-ABD-Tat-RSVP$_{220-241}$ of 35.4 kDa. However, the band was faint, suggesting that little soluble protein was present. In addition, several breakdown products were visible.

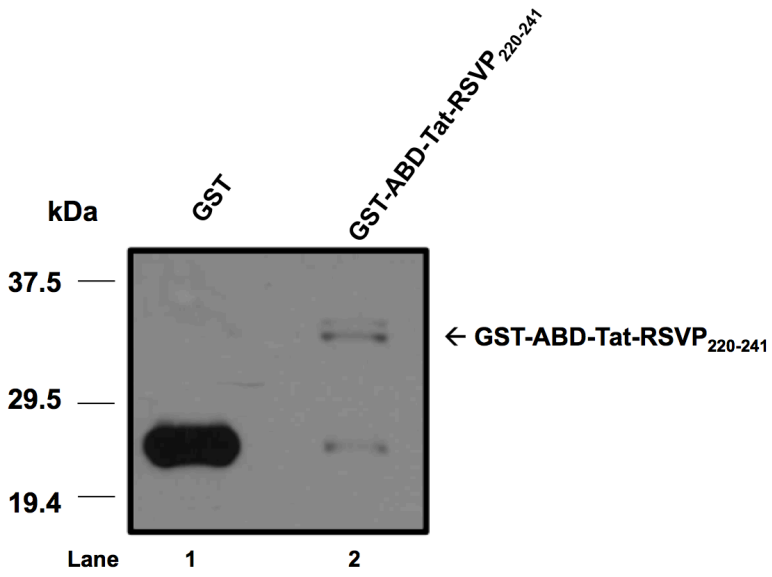

Figure 3.1.2. Purification of GST-ABD-Tat-RSVP$_{220-241}$. GST-ABD-Tat-RSVP$_{220-241}$ was overexpressed in 6 L of *E. coli* BL21 (DE3) cells and purified by affinity chromatography using the ÄKTA FPLC System with Unicorn 4.11 software. Cell lysate containing GST-ABD-Tat-RSVP$_{220-241}$ was passed through a GSTrap HP Column. Removal of any non-specifically bound proteins was accomplished by Nickel A, 5% Nickel B, 10% Nickel B, and 15% Nickel B washes, and the recombinant protein was eluted in 100% Nickel B. A sample of the eluted GST-ABD-Tat-RSVP$_{220-241}$ was run on a 12% SDS-PAGE gel and analyzed by Western blot using a mouse anti-His primary antibody (1:10,000). BLUelf Pre-Stained Protein Ladder was run to the left of the samples to indicate the approximate molecular weight of protein samples. The predicted molecular weight of the GST-ABD-Tat-RSVP$_{220-241}$ construct was 35.4 kDa. Visible bands near the estimated molecular weight suggested the protein was being expressed and purified. Furthermore, we observed breakdown of the recombinant protein as indicated by bands running at the same size as GST protein alone.

3.1.3 GST-ABD-Tat-RSVP$_{220-241}$ interacts with HSA

To explore whether the GST-ABD-Tat-RSVP$_{220-241}$ fusion protein interacts with HSA, a GST pull-down assay was performed. In this assay, GST protein alone was included as a negative control. GST and GST-ABD-Tat-RSVP$_{220-241}$ bound to magnetic glutathione-agarose beads (bait) were incubated separately with 5, 2.5, or 1.25 µg of HSA (prey) in triplicate. The beads were collected and washed several times under high salt conditions to remove any non-specifically bound proteins. Subsequently, the beads were re-suspended in Laemmli buffer, boiled, separated on a 12% SDS-PAGE gel, and analyzed by Western blot using mouse anti-HSA primary antibody or mouse anti-GST primary antibody as a loading control (**Figure 3.1.3 A**). HSA interacted with GST-ABD-Tat-RSVP$_{220-241}$, but not GST (**Figure 3.1.3 B**). The fact that the GST-ABD-Tat-RSVP$_{220-241}$ construct associated with HSA under high salt conditions suggested that it formed a stable interaction that may be maintained *in vivo*.

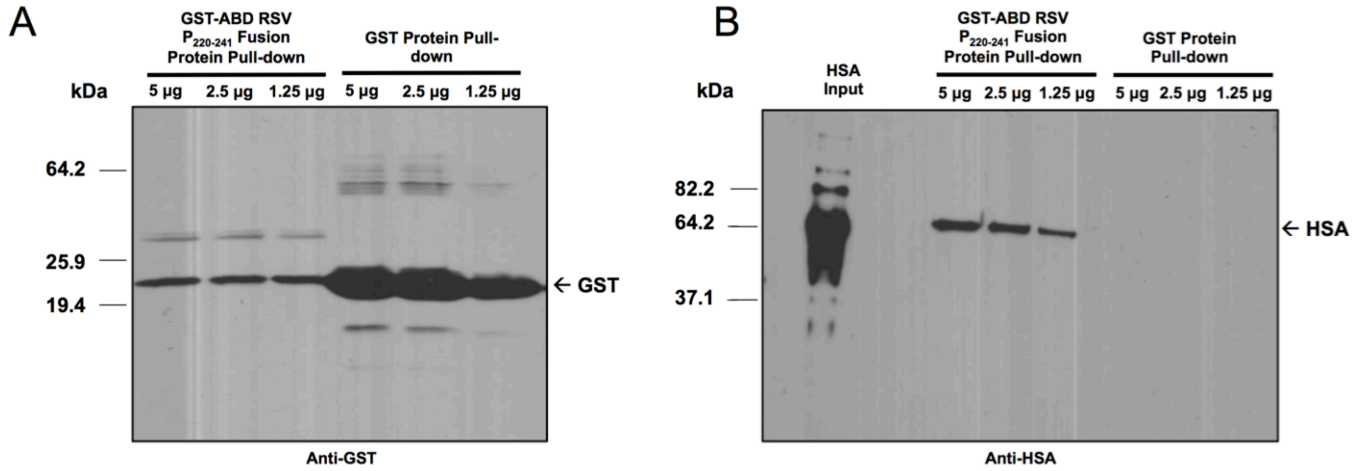

Figure 3.1.3. Interaction of HSA with GST-ABD-Tat-RSVP$_{220-241}$ in a GST pull-down. GST or GST-ABD-Tat-RSVP$_{220-241}$ (bait) were overexpressed in *E. coli* cells and cell lysates were incubated with glutathione high capacity magnetic agarose beads. GST- or GST-ABD-Tat-RSVP$_{220-241}$-bound beads were blocked for one hour at 4˚C while nutating with blocking buffer (5% w/v BSA, 0.1% v/v Tween-20, 1X PBS). Subsequently, the beads were incubated with 5, 2.5, or 1.25 µg of HSA (prey) for 3 hours at 4˚C while nutating. Beads were washed seven times with high salt wash buffer. Protein was eluted from the magnetic beads in Laemmli buffer, heated at 95˚C, run on 12% SDS-PAGE gels, and analyzed by Western blot using anti-GST (A) and anti-HSA (B) primary antibodies. BLUelf Pre-Stained Protein Ladder was run to the left of the samples to indicate the approximate molecular weight of protein samples. (A) An anti-GST Western blot was performed as a loading control. (B) The HSA input serves as an indication of the approximate protein size (66.5 kDa). From left to right, the wells following the HSA input were elution fractions from GST-ABD-Tat-RSVP$_{212-241}$ bound beads (in triplicate) and GST-bound beads (in triplicate).

3.2 Development and Assessment of the Novel His-MBP-ABD-Tat-RSVP$_{220-241}$ Fusion Protein

3.2.1 Development of His-MBP-ABD-Tat-RSVP$_{220-241}$

Since the GST-ABD-Tat-RSVP$_{220-241}$ recombinant protein was insoluble following buffer exchange into various solutions and the Mahony laboratory has previously purified and buffer exchanged His-MBP constructs, we changed the tag to His and added an additional carrier molecule of MBP. The entry vector known to contain the ABD-GGGS-

Tat-S-RSVP$_{220-241}$ insert described in section **3.1.1** was used to clone the insert into the pDEST-His-MBP vector to generate an expression plasmid. The expression plasmid was sent to the MOBIX Sequencing Facility (McMaster, Hamilton ON) to confirm the DNA sequence. A boxcar diagram of the construct is depicted in section **6.1**.

3.2.2 Expression and affinity purification of His-MBP-ABD-Tat-RSVP$_{220-241}$

The expression plasmid containing His-MBP-ABD-Tat-RSVP$_{220-241}$ was transformed into *E. coli* BL21 (DE3) cells. A total of 6 L of transformed bacterial culture was grown and purified by affinity chromatography using nickel affinity chromatography on the ÄKTA FPLC protein purification system (GE Healthcare), as described in section **2.3.4**. To determine whether the construct was being expressed and purified, a sample of purified protein was analyzed on a 12% SDS-PAGE gel followed by Ponceau staining prior to buffer exchange (**Figure 3.2.1**). A visible band was present near the predicted 51.6 kDa size of His-MBP-ABD-Tat-RSVP$_{220-241}$. We observed some breakdown and impurities in the purified solution. However, there was a large amount of purified His-MBP-ABD-Tat-RSVP$_{220-241}$. Unfortunately, the His-MBP-ABD-Tat-RSVP$_{220-241}$ recombinant protein also precipitated when buffer exchanged into several buffers, as described in section **2.3.4**.

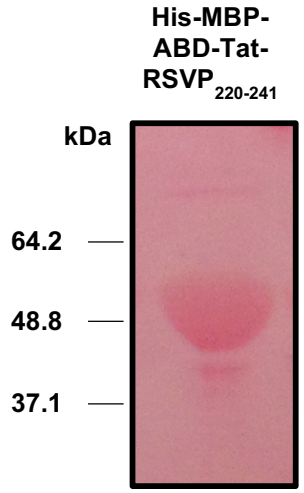

Figure 3.2.1. Purification of His-MBP-ABD-Tat-RSVP$_{220-241}$ visualized by Ponceau Stain. Prior to buffer exchange, an aliquot of purified His-MBP-ABD-Tat-RSVP$_{220-241}$ was run on a 12% SDS-PAGE gel alongside a BLUelf Prestained Protein Ladder (Froggabio). To visualize the protein, the gel was transferred to a nitrocellulose membrane using the iBlot Gel Transfer System (Invitrogen) and visualized using Ponceau S Stain. The presence of a band at the predicted molecular weight of 51.6 kDa suggested that the protein was expressed and purified. The presence of visible bands above and below the expected molecular weight was suggestive of contamination with bacterial proteins or breakdown products.

3.2.3 His-MBP-ABD-Tat-RSVP$_{220-241}$ interacts with HSA

To determine whether the His-MBP-ABD-Tat-RSVP$_{220-241}$ fusion protein interacted with HSA, a Ni-NTA agarose bead pull-down was performed. In this assay, His-MBP protein was included as a negative control. His-MBP and His-MBP-ABD-Tat-RSVP$_{220-241}$ were bound to Ni-NTA agarose beads (bait) and subsequently incubated separately with 5, 2.5, or 1.25 µg of HSA (prey) in triplicate. The beads were collected and washed several times under high salt conditions to remove any non-specifically bound proteins. Subsequently, the beads were re-suspended in Laemmli buffer, boiled, separated on a 12% SDS-PAGE gel, and analyzed by Western blot using mouse anti-HSA primary antibody or mouse anti-His primary antibody as a loading control (**Figure 3.2.2 A**). HSA

interacted with His-MBP-ABD-Tat-RSVP$_{220-241}$, but not His-MBP (**Figure 3.2.2 B**). The fact that the His-MBP-ABD-Tat-RSVP$_{220-241}$ construct associated with HSA under high salt conditions suggested this construct formed a stable interaction that may be maintained *in vivo*.

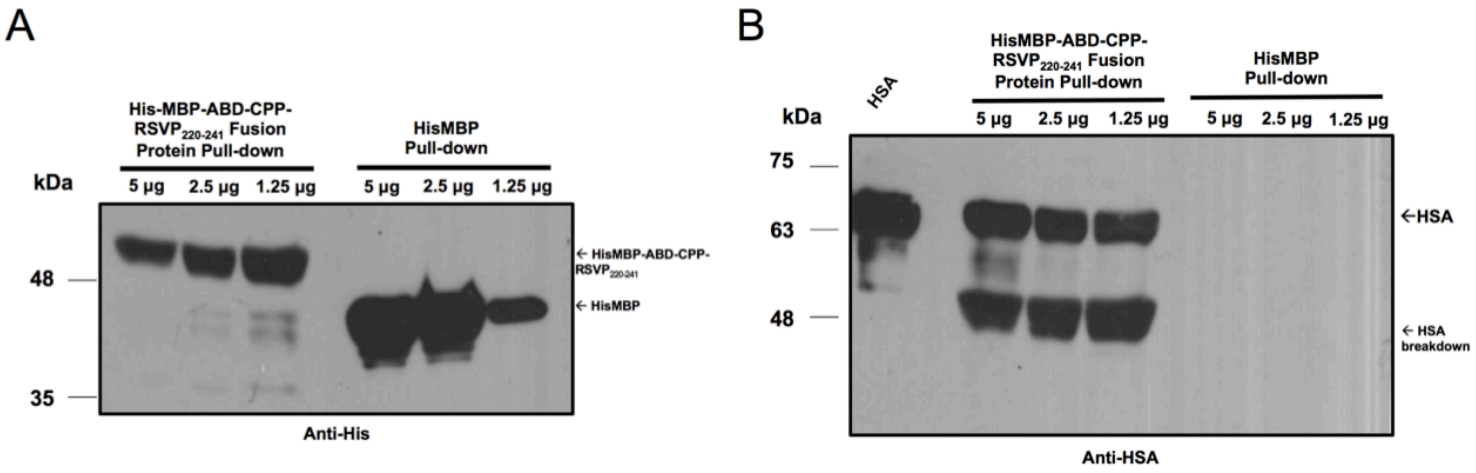

Figure 3.2.2. Interaction of HSA with His-MBP-ABD-Tat-RSVP$_{220-241}$ in a NI-NTA pull-down. His-MBP or His-MBP-ABD-Tat-RSVP$_{220-241}$ (bait) were overexpressed in *E. coli* cells and cell lysates were incubated with Ni-NTA agarose beads. His-MBP- or His-MBP-ABD-Tat-RSVP$_{220-241}$-bound beads were blocked for one hour at 4˚C while nutating with blocking buffer (5% w/v BSA, 0.1% v/v Tween-20, 1X PBS). Subsequently, the beads were incubated with 5, 2.5, or 1.25 µg of HSA (prey) for 3 hours at 4˚C while nutating. Beads were washed ten times with high salt wash buffer. Protein was eluted from the magnetic beads in Laemmli buffer, heated at 95˚C, and run on 12% SDS-PAGE gels and analyzed by Western blot using anti-His (A) and anti-HSA (B) primary antibodies. BLUelf Pre-Stained Protein Ladder was run to the left of the samples to indicate the approximate molecular weight of protein samples. (A) An anti-His Western blot was performed as a loading control (B) The HSA input serves as an indication of the approximate protein size (66.5 kDa). From left to right, the wells following the HSA input were elution fractions from GST-ABD-Tat-RSVP$_{212-241}$ bound beads (in triplicate) and GST-bound beads (in triplicate). Visible bands near the predicted molecular weight of HSA only in lanes corresponding to His-MBP-ABD-CPP-RSVP$_{220-241}$, suggested that HSA copurifies with His-MBP-ABD-RSVP$_{220-241}$ but not His-MBP under high salt conditions.

3.3 Development and assessment of the novel His-MBP-Tat-RSVP$_{212-241}$ fusion protein

3.3.1 Cloning of His-MBP-Tat-RSVP$_{212-241}$

Since the ABD fusion constructs could not be buffered exchanged, the next goal of my thesis was to design and evaluate the antiviral activity of an RSV P$_{212-241}$ peptide mimetic *in vitro*. In 2015, Sourimant and colleagues mapped the binding domain on RSV P responsible for interaction with the L polymerase to amino acid residues 212 to 239. Interestingly, they found that this binding domain overlapped with the domain on P responsible for binding NC complexes; namely, the terminal 9 amino acids (Sourimant et al., 2015). Based on these findings, I hypothesized that an RSVP$_{212-241}$ mimetic would be more effective in attenuating RSV replication than the previous His-MBP-Tat-RSVP$_{220-241}$ construct. Since the previous construct had inhibitory activity, I used its backbone in the design of the novel RSVP$_{212-241}$ mimetic, thereby creating a His-MBP-Tat-RSVP$_{212-241}$ construct. A boxcar diagram of this construct is shown in section **6.1**.

The Tat-RSVP$_{212-241}$ construct was ordered as an entry vector from Invitrogen (Thermo Fisher Scientific) and used in the Gateway® Cloning system with pDEST-His-MBP to generate an expression plasmid. Samples of the resulting expression plasmids were separated by agarose-ethidium bromide gel electrophoresis (**Figure 3.3.1)**. Several bands from different *E. coli* colonies appeared near the desired 6,800 bp size. These expression plasmids were sent to the MOBIX Sequencing Facility (McMaster, Hamilton ON) to confirm the DNA sequence.

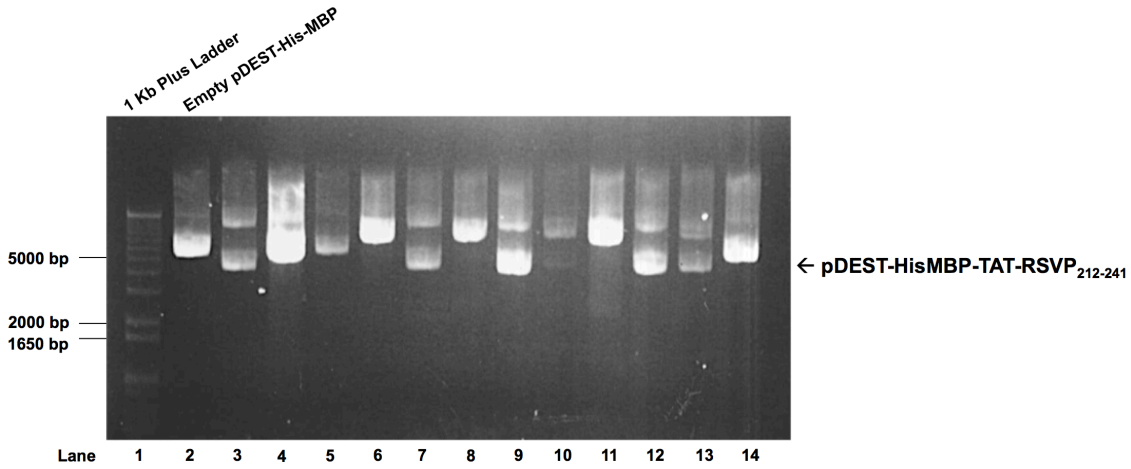

Figure 3.3.1. DNA agarose-ethidium bromide gel depicting insertion of Tat-RSVP$_{212-241}$ into pDEST-His-MBP. *E. coli* Turbo cells were transformed with the Gateway BP reaction performed between pDEST-His-MBP and the Tat-RSVP$_{212-241}$ gBlock. Entry plasmids prepped from successful transformants were analyzed on a 0.6% agarose-ethidium bromide gel and visualized using the Quantity One Program for the GelDoc^{TM} XR+ System. A 1 Kb Plus Ladder was run to the left of the samples to indicate the approximate size of the plasmid samples. The plasmid of interest was approximately 6,800 bps. The presence of visible band shifts near the predicted size suggested that Tat-RSVP$_{212-241}$ was inserted into the pDEST-His-MBP vector. These observations were confirmed by DNA sequencing.

3.3.2 Expression and affinity purification of His-MBP-Tat-RSVP$_{212-241}$

The expression plasmid containing His-MBP-Tat-RSVP$_{212-241}$ was transformed into *E. coli* BL21 (DE3) cells. A total of 6 L of transformed bacterial culture was grown and purified by nickel affinity chromatography on the ÄKTA FPLC protein purification system (GE Healthcare), as described in section **2.3.4**. Samples were collected throughout the purification process for expression, loss, and breakdown product analysis. Samples from the purification process, buffer exchange, and concentrated protein were analyzed on a 12% SDS-PAGE gel followed by Ponceau staining and Western blot using mouse anti-His primary antibody (**Figure 3.3.2 A** & **B**). The predicted size of His-MBP-Tat-RSVP$_{212-241}$ was estimated at 47.1 kDa using the online ExPasy Compute pI/MW tool. Bands visible

near the predicted size in the lanes corresponding to the 10% and 15% Nickel B washes suggested that some protein was eluted from the column. Breakdown products were visualized in samples corresponding to the 100% Nickel B elution and the final concentrated product. The absence of additional bands in lanes corresponding to the final protein product on the Ponceau stained membrane suggested that the sample was pure (**Figure 3.3.2 B**).

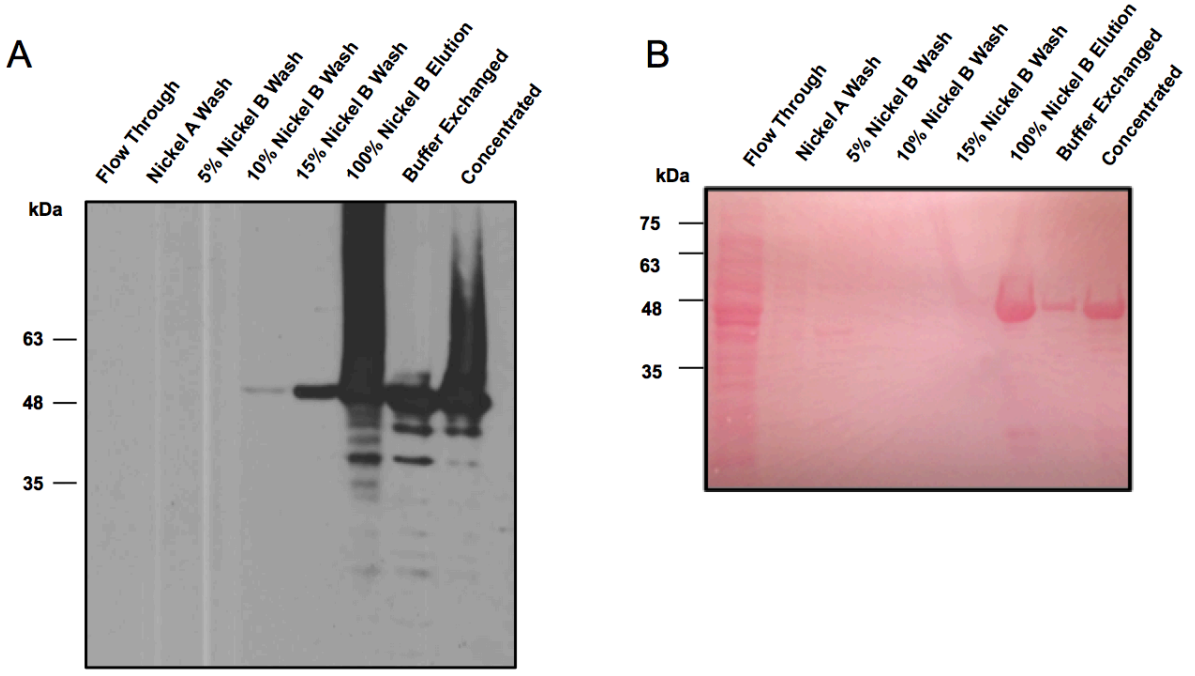

Figure 3.3.2. Purification of His-MBP-Tat-RSVP$_{212-241}$. Tat-His-MBP-Tat-RSVP$_{212-241}$ was overexpressed in 6 L of *E. coli* BL21 (DE3) cells and purified by affinity chromatography using the ÄKTA FPLC system with Unicorn 4.11 software. Cell lysate containing His-MBP-Tat-RSVP$_{212-241}$ was passed through a HisTrap Column. Removal of any non-specifically bound proteins was accomplished by Nickel A, 5% Nickel B, 10% Nickel B, and 15% Nickel B washes, and the peptide mimetic was eluted in 100% Nickel B. Samples were collected from the waste line during each step of the purification process and run on a 12% SDS-PAGE gel and analyzed by (A) Western blot using mouse anti-His primary antibody (1:10,000) and (B) Ponceau Stain. BLUelf Pre-Stained Protein Ladder was run to the left of the samples to indicate the approximate molecular weight of protein samples. The molecular weight of the peptide mimetic His-MBP-Tat-RSVP$_{212-241}$ was

predicted to be 47.1 kDa. Some fusion protein was lost from the column during the 10% and 15% Nickel B washes and multiple breakdown products are visible in fractions containing the elution, buffer exchanged, and concentrated protein.

3.3.3 His-MBP-Tat-RSVP$_{212-241}$ toxicity and activity

After purification of the His-MBP-Tat-RSVP$_{212-241}$ construct, we immediately explored whether it could attenuate RSV A replication *in vitro*. To test the ability of the construct to attenuate RSV replication, confluent monolayers of LLC-MK2 cells were incubated with 25 μM of His-MBP-Tat-RSVP$_{212-241}$ in triplicate for 2 hours, prior to infection with RSV A long strain. Following infection, cells were incubated again with the construct for 48 hours.

Following the 48-hour incubation, RSV infected cells were visualized using indirect immunofluorescence microscopy with a mouse anti-RSV F protein primary antibody and goat anti-mouse-FITC secondary antibody. Infection of cells in the wells treated with recombinant fusion protein was compared to virus only controls. We found that the His-MBP-Tat-RSVP$_{212-241}$ construct was toxic to LLC-MK2 cells, as cells sloughed off the monolayer (**Figure 3.3.3**). Furthermore, we observed no inhibition of RSV A replication between the peptide-treated monolayers and the virus-only monolayers (**Figure 3.3.3**).

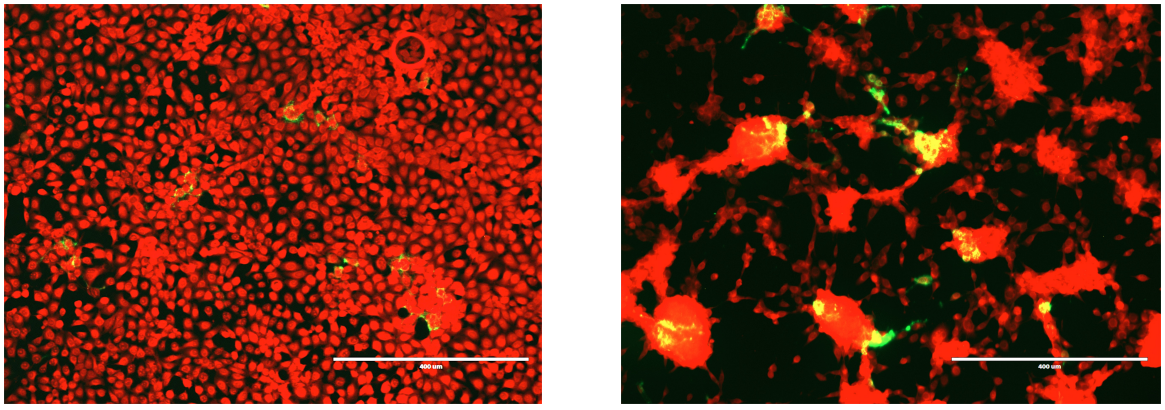

Figure 3.3.3. Inhibition of RSV A Replication by His-MBP-Tat-RSVP$_{212-241}$. LLC-MK2 cells were incubated with 25 µM His-MBP-Tat-RSVP$_{212-241}$ in DMEM for 2 hours, infected with RSV A, and subsequently incubated with a second round of peptide for 48 hours. Following the incubation period, cells were fixed in ice-cold methanol and visualized with indirect immunofluorescence microscopy using mouse anti-RSV fusion protein primary antibody and goat anti-mouse-FITC secondary antibody. Random and representative images of the stained LLC-MK2 cells were captured at 10X magnification using an Evos Light Microscope. RSV A-infected cells were stained green (FITC) and non-infected cells were stained red (0.05% Evan's Blue Reagent). These results suggested that the construct was toxic to cells, as visualized by the loss of and appearance of cells, and that the construct was non-inhibitory to RSV A.

3.3.4 His-MBP-Tat-RSVP$_{212-241}$ uptake by LLC-MK2 cells

Since RSV replication occurs within the cytoplasm of cells, the His-MBP-Tat-RSVP$_{212-241}$ fusion protein must be able to cross the cell membrane to block wild-type interactions and attenuate RSV replication. Despite the toxicity observed for the His-MBP-Tat-RSVP$_{212-241}$ construct, we performed an uptake assay to determine whether the construct was unable to inhibit RSV A replication since it was not able to enter LLC-MK2 cells. His-MBP-Tat-RSVP$_{212-241}$ was diluted to 20 µM in DMEM and incubated with confluent monolayers of LLC-MK2 cells in duplicate for 24 or 48 hours. Following incubation, the cells were washed, trypsinized, pelleted, re-suspended in Laemmli buffer,

and boiled. Protein within the samples was detected using a 12% SDS-PAGE gel followed by Western blot analysis using mouse anti-His primary antibody (**Figure 3.3.4 A**). A mouse anti-α-tubulin primary antibody was used as a loading control in this experiment (**Figure 3.3.4 B**). The absence of visible bands near the predicted size of 47.1 kDa suggested that the His-MBP-Tat-RSVP$_{212-241}$ construct was not taken up by LLC-MK2 cells.

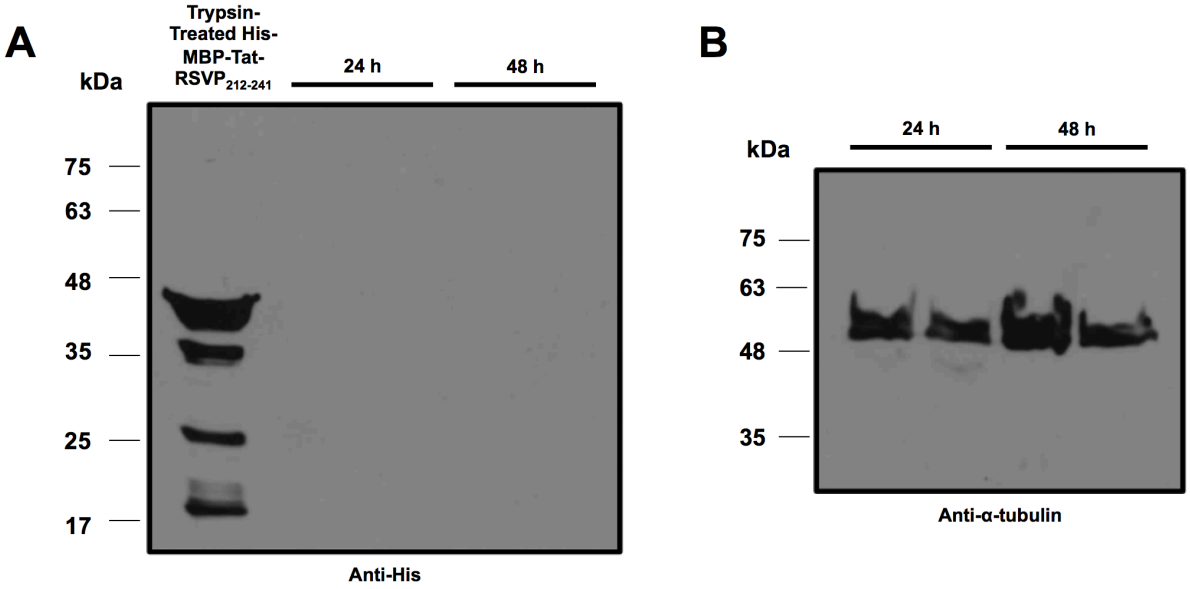

Figure 3.3.4. His-MBP-Tat-RSVP$_{212-241}$ was not detected in LLC-MK2 cells. LLC-MK2 cells were seeded to confluency in a 24-well plate. Purified His-MBP-Tat-RSVP$_{212-241}$ was diluted to 20 μM in DMEM and applied to LLC-MK2 cells for 24 and 48 hours. At the appropriate time intervals, the cells were harvested with 0.5 mg/ml Trypsin-EDTA. The cells were pelleted and re-suspended in Laemmli buffer. Protein samples were run on a 12% SDS-PAGE gel and analyzed by Western blot using mouse anti-His (1:10,000) and mouse anti-α-tubulin (1:10,000) primary antibodies. BLUelf Pre-Stained Protein Ladder was run to the left of the samples to indicate the approximate molecular weight of protein samples. (A) The protein samples were analyzed with mouse anti-His primary antibody and the lack of visible bands near the predicted size of 47.1 kDa suggested the His-MBP-Tat-RSVP$_{212-241}$ peptide mimetic was not taken up byLLC-MK2 cells. (B) Protein samples were analyzed using with mouse anti-α-tubulin as a loading control.

3.4 Development of the novel Tat-His-MBP-Tat-RSVP$_{212-241}$ fusion protein

3.4.1 Cloning of Tat-His-MBP-Tat-RSVP$_{212-241}$

Since the His-MBP-Tat-RSVP$_{212-241}$ construct was unable cross the plasma membrane of LLC-MK2 cells, we added an additional Tat CPP to the N-terminus of the construct. We chose the N-terminus since the Tat CPP is highly cationic, whereas the RSVP$_{212-241}$ portion is highly anionic. We hoped this separation in charge would allow the CPP to transport the construct across the cell membrane into the intracellular compartment.

Using inverse PCR and the In-Fusion® Cloning System, as described in section **2.1.2**, a Tat CPP was added to the N-terminus of the His-MBP expression plasmid containing Tat-RSVP$_{212-241}$. Products from the inverse PCR using an annealing temperature of 55˚C or 60˚C were analyzed on a 0.6% agarose-ethidium bromide gel. Both annealing temperatures resulted in a fragment at the desired length of approximately 6,800 bp (**Figure 3.4.1**). Other bands were visible under both conditions, and as a result the desired fragments were excised and purified from the gel. Subsequently, they were re-circularized using the In-Fusion® Cloning System to yield expression plasmids consisting of Tat-His-MBP-Tat-RSVP$_{212-241}$. A boxcar diagram of this construct is available in section **6.1**.

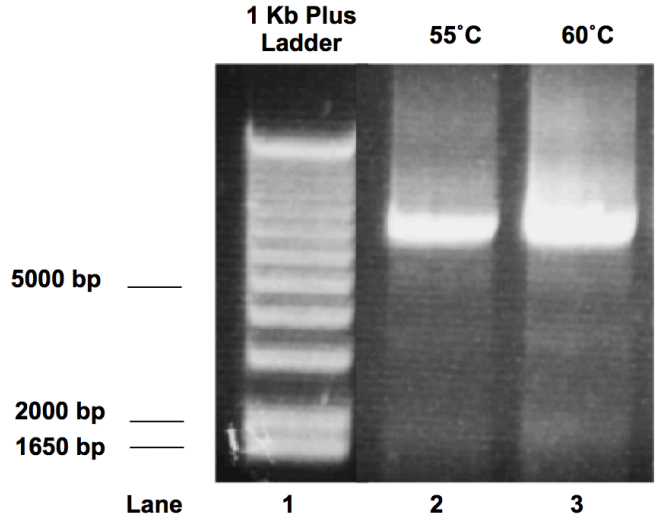

Figure 3.4.1. DNA agarose-ethidium bromide gel of the Tat-His-MBP-Tat-RSVP$_{212-241}$ inverse-PCR products. Inverse-PCR was performed to generate, linearize, and amplify a Tat-His-MBP-Tat-RSVP$_{212-241}$ expression vector. The inverse-PCR products were electrophoresed on a 0.6% agarose-ethidium bromide gel and visualized using the Quantity One Program for the GelDoc^{TM} XR+ System. A 1 Kb Plus Ladder was run to the left of the samples to indicate the approximate size of the PCR products. The PCR-product of interest is approximately 6,800 bps in size. The inverse-PCR products at annealing temperatures of 55˚C and 60˚C are depicted in lanes 2 and 3, respectively.

3.4.2 Expression and affinity purification of Tat-His-MBP-Tat-RSVP$_{212-241}$

The Tat-His-MBP-Tat-RSVP$_{212-241}$ expression plasmid was transformed into *E. coli* BL21 (DE3) cells. A total of 6 L of transformed bacterial culture was grown and purified by nickel affinity chromatography using the ÄKTA FPLC protein purification system (GE Healthcare), as described in section **2.3.4**. Samples were collected throughout the purification process for expression, loss, and breakdown product analysis. Samples from the purification process were analyzed on a 12% SDS-PAGE gel and Western blot using mouse anti-His primary antibody (**Figure 3.4.2**). The predicted size of Tat-His-MBP-Tat-RSVP$_{212-241}$ was estimated at 48.7 kDa using the online ExPasy Compute pI/MW tool.

Bands were visible at a lower molecular weight than expected, except for the eluted protein sample. These observations suggested that the construct's affinity for nickel column was reduced with large amounts of protein were lost in the flow through and during the wash steps. The presence of visible bands at lower molecular weight suggested significant breakdown of the construct. Although these observations suggested that the construct was purified, subsequent buffer exchange and concentration resulted in a total yield of 0.26 mg of Tat-His-MBP-Tat-RSVP$_{212-241}$.

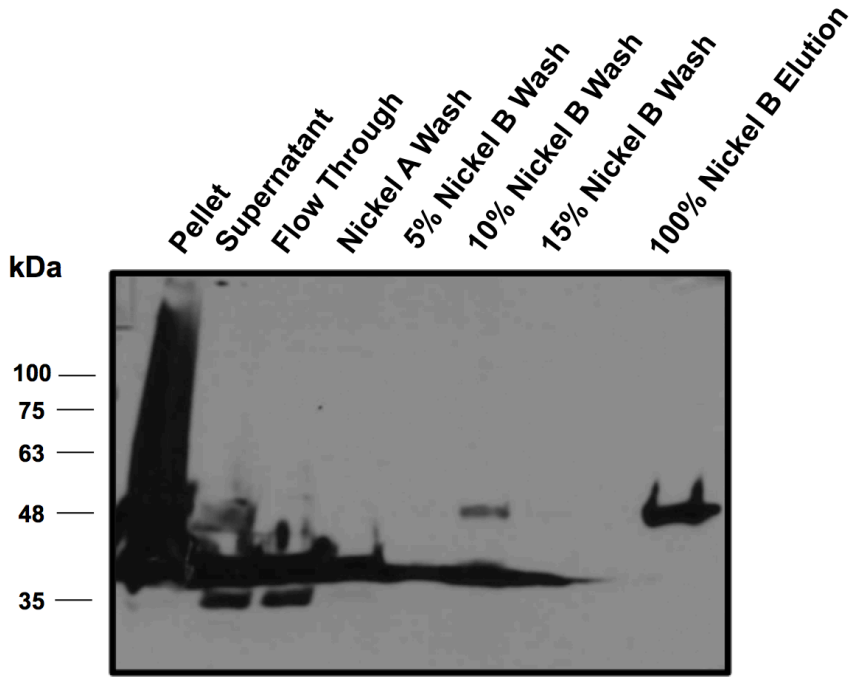

Figure 3.4.2. Analysis of Tat-His-MBP-Tat-RSVP$_{212-241}$ purification. Tat-His-MBP-Tat-RSVP$_{212-241}$ was overexpressed in 6 L of *E. coli* BL21 (DE3) cells and purified by affinity chromatography using the ÄKTA FPLC system with Unicorn 4.11 software. Cell lysate containing Tat-His-MBP-Tat-RSVP$_{212-241}$ was passed through a HisTrap Column. Removal of any non-specifically bound proteins was accomplished by Nickel A, 5% Nickel B, 10% Nickel B, and 15% Nickel B washes, and the peptide mimetic was eluted in 100% Nickel B. Samples were collected from the waste line during each step of the purification process and run on a 12% SDS-PAGE gel and analyzed by Western blot using mouse anti-His primary antibody (1:10,000). BLUelf Pre-Stained Protein Ladder was run to the left of the samples to indicate the approximate molecular weight of protein

samples. The molecular weight of the peptide mimetic Tat-His-MBP-Tat-RSVP$_{212-241}$ was predicted to be 48.7 kDa. Some protein was lost at each stage of the purification process (flow through, Nickel A wash, 5%, 10%, and 15% Nickel B washes) and multiple breakdown products are visible. However, there is no visible breakdown of the peptide in the 100% Nickel B elution fraction.

3.5 Development and assessment of the novel His-Arg9-MBP-RSVP$_{212-241}$ fusion peptide

3.5.1 Cloning of His-Arg9-MBP-RSVP$_{212-241}$

Since the Tat-His-MBP-Tat-RSVP$_{212-241}$ construct resulted in low yields of purified protein, we completely redesigned the RSVP$_{212-241}$ fusion protein. Another student in the Mahony laboratory demonstrated uptake of cargo proteins attached to a CPP consisting of nine arginine residues (Arg9). As a result, we used Arg9 as the CPP in my construct. In addition, since previous peptide mimetics designed in the Mahony laboratory that were successful in attenuating both influenza and RSV contained a His tag and the MBP carrier, we included a His tag and used the MBP molecule as the carrier. We used MBP as a carrier molecule for our peptide mimetic since MBP is known to increase expression yields and solubilization, as well as contribute to proper folding of conjugated proteins (Sun et al., 2011). Lastly, we positioned the CPP between the His-tag and the MBP carrier molecule to maintain the His-tag's affinity for the nickel column and separate the CPP from the RSVP$_{212-241}$ mimetic portion. A boxcar diagram for the His-Arg9-MBP-RSVP$_{212-241}$ construct is shown in section **6.1**.

A gBlock gene fragment consisting of GSAAS-RSVP$_{212-241}$ was cloned into the pDONR201 vector using the Gateway® Cloning System to generate an entry vector. Samples of the resulting entry vectors were analyzed by agarose-ethidium bromide gel

electrophoresis (**Figure 3.5.1)**. The desired entry vectors were approximately 2,600 bp in length. Each of the colonies of entry vectors ran close to the expected size, suggesting the cloning was successful.

The Arg9 CPP was inserted into the pDEST-His-MBP vector using inverse PCR followed by In-Fusion® Cloning, as described in section **2.1.2**. Products from the inverse PCR were analyzed on a 0.6% agarose-ethidium bromide gel, revealing a fragment near the desired length of approximately 8,200 bps (**Figure 3.5.2**). The desired fragment was excised and purified from the gel. Subsequently, the pDEST-His-Arg9-MBP vector was re-circularized using the In-Fusion® Cloning System.

The desired entry vector was used to clone the GSAAS-$RSVP_{212-241}$ insert into the pDEST-His-Arg9-MBP vector using the Gateway® Cloning System to generate an expression plasmid. Expression plasmids were sent to the MOBIX Sequencing Facility (McMaster, Hamilton ON) to confirm the DNA sequence.

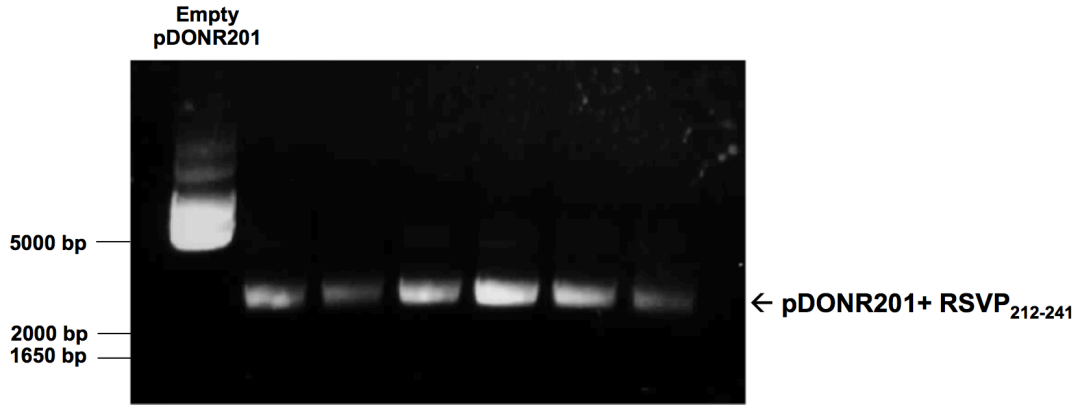

Figure 3.5.1. DNA agarose-ethidium bromide gel depicting insertion of $RSVP_{212-241}$ into pDONR201. *E. coli* Turbo cells were transformed with the Gateway BP reaction performed between pDONR201 and the $RSVP_{212-241}$ gBlock. Entry plasmids prepped from successful transformants were analyzed on a 1% agarose-ethidium bromide gel and visualized using the Quantity One Program for the GelDoc™ XR+ System. A 1 Kb Plus Ladder was run to the left of the samples to indicate the approximate size of the plasmid samples. The plasmid of interest is approximately 2,600 bps. The presence of visible band

shifts close to the predicted size suggest insertion of the $RSVP_{212-241}$ gBlock into the pDONR201 vector. These observations were confirmed by DNA sequencing.

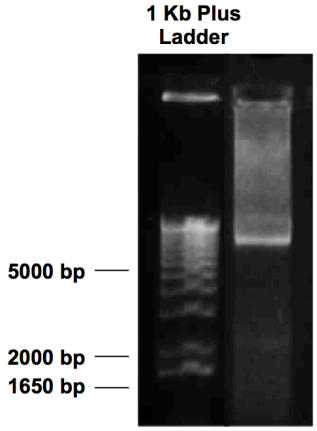

Figure 3.5.2. DNA agarose-ethidium bromide gel of the His-Arg9-MBP inverse-PCR products. Inverse-PCR was performed to generate, linearize, and amplify a His-Arg9-MBP destination vector. The inverse-PCR products were electrophoresed on a 0.6% agarose-ethidium bromide gel and visualized using the Quantity One Program for the GelDoc^{TM} XR+ System. A 1 Kb Plus Ladder was run to the left of the samples to indicate the approximate size of the PCR products. The PCR-product of interest is approximately 8,200 bps in size.

3.5.2 Expression and affinity purification of His-Arg9-MBP-$RSVP_{212-241}$

The His-Arg9-MBP-$RSVP_{212-241}$ expression plasmid was transformed into *E. coli* BL21 (DE3) cells. A total of 6 L of transformed bacterial culture was grown and purified by nickel affinity chromatography using the ÄKTA FPLC protein purification system (GE Healthcare), as described in section **2.3.4**. Samples were collected throughout the purification process for expression, loss, and breakdown product analysis. Samples from the purification process were separated on a 12% SDS-PAGE gel and subsequently analyzed by Western blot using a mouse anti-His primary antibody and Ponceau staining (**Figure 3.5.3 A** & **B**, respectively). The predicted size of the His-Arg9-MBP-$RSVP_{212-241}$

construct was estimated at 47.05 kDa using the online ExPasy Compute pI/MW tool. Bands near the expected size were visible in each lane, minus the lane corresponding to the 5% Nickel B wash. Visible bands in the pellet and flow through samples suggested that a fraction of His-Arg9-MBP-$RSVP_{212-241}$ was insoluble and not all protein was binding the column, respectively. Light bands present in the wash steps suggested that small amounts of protein were washed away from the column. In addition, some breakdown products were observed in the elution fraction. The size of the band at the expected molecular weight in the lane corresponding to the concentrated purified protein suggested that a significant amount of protein was purified. In fact, we generally obtain 15 mg of soluble His-Arg9-MBP-$RSVP_{212-241}$.

Furthermore, the presence of additional bands on the Ponceau stained membrane in the lane loaded with a sample from the purified protein solution suggested that the protein was approximately 90% pure (**Figure 3.5.3**. **B**). However, some of the bands corresponded to breakdown of the His-Arg9-MBP-$RSVP_{212-241}$ construct, as visualized by the Western blot (**Figure 3.5.3 A**).

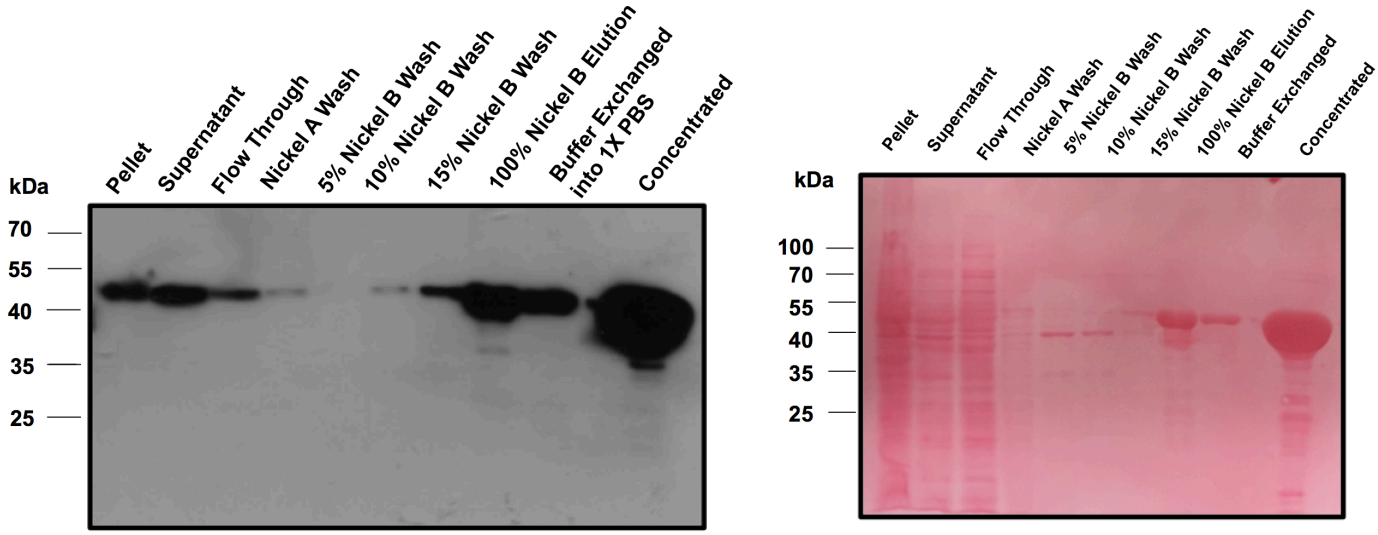

Figure 3.5.3. Analysis of His-Arg9-MBP-RSVP$_{212-241}$ purification and buffer exchange. His-Arg9-MBP-Tat-RSVP$_{212-241}$ was overexpressed in 6 L of *E. coli* BL21 (DE3) cells and purified by nickel affinity chromatography using the ÄKTA FPLC system with Unicorn 4.11 software. Cell lysate containing His-Arg9-MBP-RSVP$_{212-241}$ was passed through a HisTrap Column. Removal of any non-specifically bound proteins was accomplished by Nickel A, 5% Nickel B, 10% Nickel B, and 15% Nickel B washes. The peptide mimetic was eluted in 100% Nickel B, then was subsequently injected into a HiPrep Desalting Column to be buffer exchanged into 1X PBS. Samples were collected from the waste line or the collected fractions during each step of the purification and buffer exchange processes and run on a 12% SDS-PAGE gel and analyzed by (A) Western blot using mouse anti-His primary antibody (1:10,000) and (B) Ponceau Stain. BLUelf Pre-Stained Protein Ladder was run to the left of the samples to indicate the approximate molecular weight of protein samples. The molecular weight of the peptide mimetic His-Arg9-MBP-RSVP$_{212-241}$ was predicted to be 47.05 kDa. Some peptide was lost in the flow through, Nickel A wash, 5%, 10%, and 15% Nickel B washes. Additionally, minor breakdown products are visible in the 100% Nickel B and concentrated fractions.

3.5.3 His-Arg9-MBP-RSVP$_{212-241}$ is not toxic to LLC-MK2 cells

Considering that the ultimate goal of our peptide mimetics is therapeutic use in humans, we assessed the toxicity of the His-Arg9-MBP RSVP$_{212-241}$ construct toward LLC-MK2 cells. Toxicity of the construct was assessed by both visualization and a spectrophotometer cell replication assay. A fusion protein that is toxic to cells is expected

to limit cell proliferation, similar to the effect of cycloheximide, a known inhibitor of eukaryotic translation and cellular replication (Schneider-Poetsch et al., 2010).

Initially, toxicity was assessed by light microscopy visualization of cell growth. To perform this assay, under-confluent monolayers of LLC-MK2 cells in a 96-well plate were incubated in triplicate with 50 or 150 μM of His-Arg9-MBP-RSVP$_{212-241}$ for up to 48 hours. As a negative control, cells were incubated in triplicate with 5 μM BSA, a protein known to be non-toxic to cells. As a positive control, cells were incubated in triplicate with 80 μM hTrx Δcys, a concentration of protein known to be toxic to cells. At time 0, 24, and 48 hours, the plates were observed under the light microscope and random, representative images were captured (**Figure 3.5.4**). We observed healthy growth of cells incubated with 5 μM BSA and lysis of cells incubated with 80 μM hTrx Δcys. LLC-MK2 cells incubated with 50 and 150 μM His-Arg9-MBP-RSVP$_{212-241}$ grew over the 48-hour period and did not exhibit cell lysis, suggesting that the construct was not toxic to LLC-MK2 cells up to 150 μM.

However, we ultimately planned to test the activity of the His-Arg9-MBP-RSVP$_{212-241}$ construct up to a concentration of 200 μM. As a result, we performed a spectrophotometer cell replication assay to assess the toxicity of His-Arg9-MBP-RSVP$_{212-241}$ at 200 μM. LLC-MK2 cells were seeded to under-confluency in a 24 well-plate and incubated in triplicate with 200 μM His-Arg9-MBP-RSVP$_{212-241}$ diluted in DMEM + 10% FBS for 0, 24, and 48 hours. As a positive control, under-confluent LLC-MK2 cells were incubated in triplicate with 2 mg/ml cycloheximide diluted in DMEM + 10% FBS for 0, 24, and 48 hours. As a negative control, under-confluent LLC-MK2 cells were incubated

with DMEM + 10% FBS in triplicate for 0, 24 and 48 hours. At the appropriate time point, cells were harvested by trypsin and the cell density was assessed at 800 nm using a spectrophotometer. Absorbance readings at 800 nm are linearly dependent on the density of cells in any solution (Mohler et al., 1996).

The absorbance at each time point was averaged per triplicate condition and plotted as a bar graph to enable comparisons between the means (**Figure 3.5.5 A**). The averaged absorbances were also plotted as a line graph to depict growth of LLC-MK2 cells over time (**Figure 3.5.5 B**). At 24 and 48 hours, there was a decrease in absorbance of cells treated with cycloheximide indicative of some cell death. On the other hand, absorbance increased for cells incubated with both DMEM + 10% FBS and 200 μM His-Arg9-MBP-$RSVP_{212-241}$. Interestingly, higher absorbance readings were obtained from LLC-MK2 cells incubated with His-Arg9-MBP-$RSVP_{212-241}$.

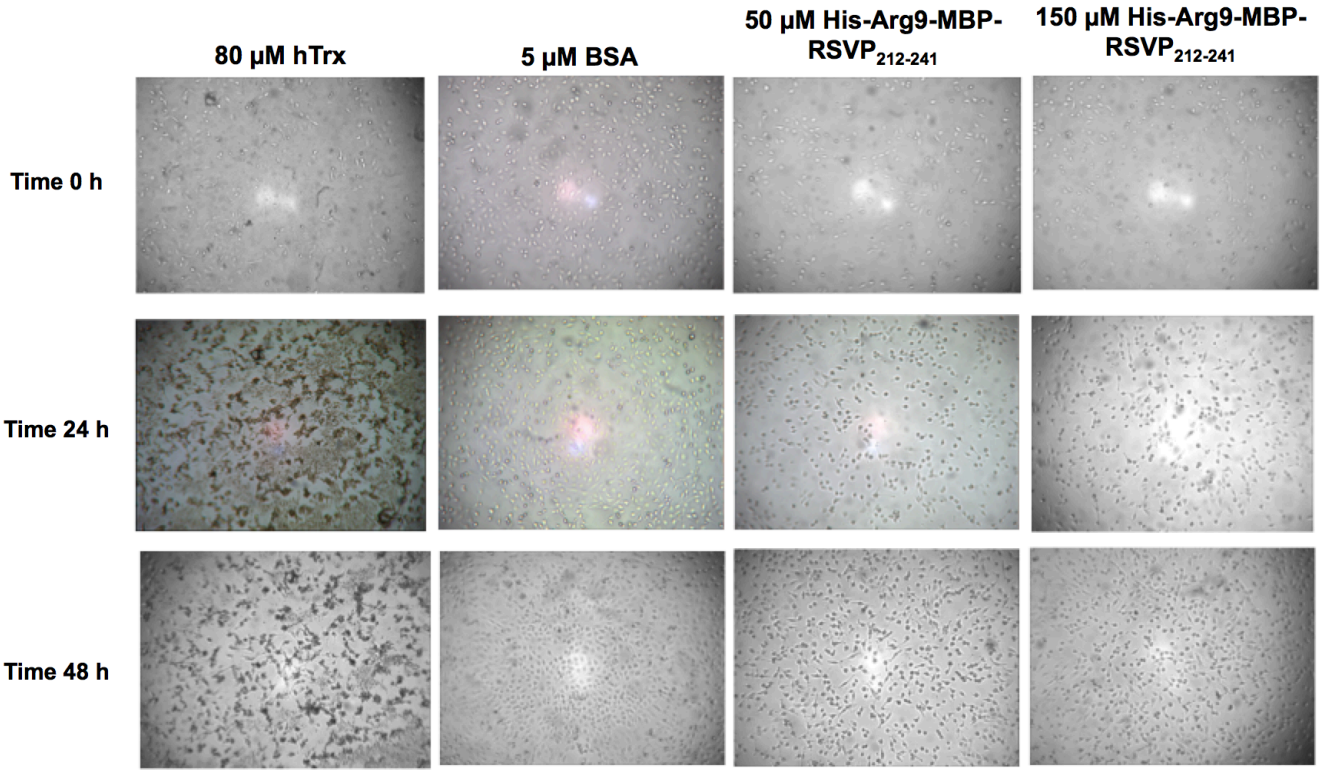

Figure 3.5.4. Growth of LLC-MK2 cells in the presence of BSA, hTrx, and His-Arg9-MBP-RSVP$_{212-241}$. In a 96 well plate, under-confluent LLC-MK2 cells were incubated with 5 µM BSA, 80 µM hTrx, 50 µM or 150 µM His-Arg9-MBP-RSVP$_{212-241}$ in triplicate for 0, 24, or 48 hours. At the appropriate time interval, the cells were visualized using a light microscope and images were captured. As seen at time 24 h, the cells had grown and appeared healthy when treated with 5 µM BSA, 50 µM or 150 µM His-Arg9-MBP-RSVP$_{212-241}$. However, cells treated with 80 µM hTrx Δcys lysed and did not demonstrate healthy growth. As at time 48h, cells treated with 5 µM BSA, 50 µM or 150 µM His-Arg9-MBP-RSVP$_{212-241}$ grew normally, whereas cells treated with 80 µM hTrx did not, appearing darker and unhealthy.

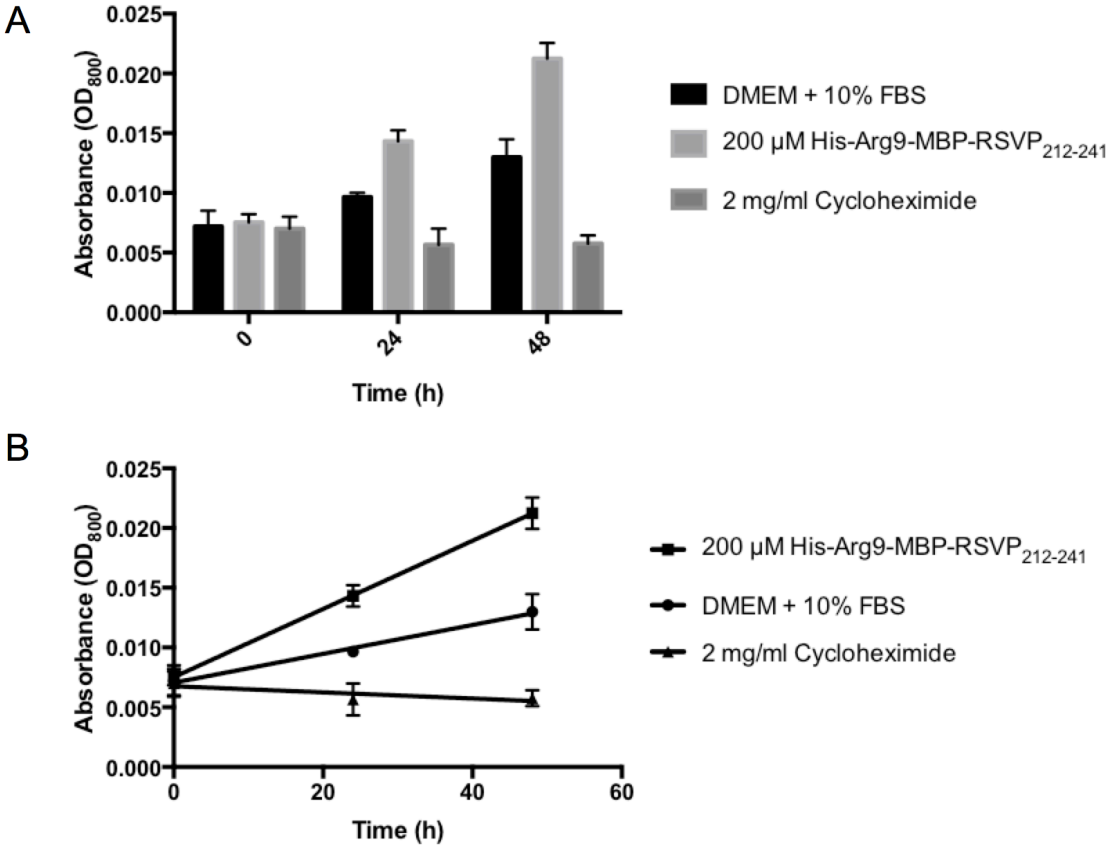

Figure 3.5.5. Growth of LLC-MK2 cells in the presence of His-Arg9-MBP-RSVP$_{212-241}$. In a 24 well plate, confluent LLC-MK2 cells were incubated with DMEM + 10% FBS, 2 mg/ml cycloheximide, or 200 µM His-Arg9-MBP-RSVP$_{212-241}$ in triplicate for 0, 24, or 48 hours. At the appropriate time interval, the cells were trypsinized and thoroughly re-suspended. The absorbance of the re-suspended cells was measured at 800 nm using an Ultrospec 4300 Pro UV/Visible spectrophotometer. (A) The absorbance readings were plotted as a bar graph to compare differences between the means or a (B) line graph to show growth over time. Error bars represent +/- one standard deviation from the mean. As seen at time 24 h, cells treated with DMEM + 10% FBS and 200 µ M His-Arg9-MBP-RSVP$_{212-241}$ replicated, whereas cells treated with 2 mg/ml cycloheximide did not. The same results can be seen after 48 h of treatment. Interestingly, cells treated with 200 µ M His-Arg9-MBP-RSVP$_{212-241}$ exhibited higher growth than the DMEM + 10% FBS control.

3.5.4 His-Arg9-MBP-RSVP$_{212-241}$ is taken up by LLC-MK2 cells

Since RSV replication occurs within the cytoplasm of cells, the His-Arg9-MBP-RSVP$_{212-241}$ fusion protein must be able to cross the cell membrane in order to block wild-

type interactions and attenuate RSV replication. To determine whether the construct could enter LLC-MK2 cells, an uptake assay was performed.

LLC-MK2 cells were seeded to confluency in a 6-well plate and incubated with 50 μM His-Arg9-MBP-$RSVP_{212-241}$ or as a positive control, 20 μM hTrx Δcys for 2 or 4 hours. At the appropriate time point, the cells were acid washed to remove exogenously bound protein and lysed using RIPA buffer. The cell lysates were collected and cellular debris was pelleted by centrifugation. A sample of the supernatant was re-suspended in Laemmli buffer, heated to 95˚C, separated on a 12% SDS-PAGE gel, and subsequently analyzed by Western blot using a mouse anti-His, mouse anti-MBP, or mouse anti- α-tubulin as a loading control.

As expected, hTrx was taken up by LLC-MK2 cells after 2 and 4 hours of incubation as indicated by bands near the predicted molecular weight of 18.7 kDa (**Figure 3.5.6 A**). No His-Arg9-MBP-$RSVP_{212-241}$ was detected in LLC-MK2 cells when mouse anti-His was the primary antibody used (**Figure 3.5.6 B**). The presence of bands near the predicted molecular weight of 47.05 kDa when mouse anti-MBP was the primary antibody used, suggested that His-Arg9-MBP-$RSVP_{212-241}$ was in fact taken up by LLC-MK2 cells (**Figure 3.5.6 C**). Furthermore, breakdown products can be visualized and suggested the construct was being broken down inside LLC-MK2 cells at the N-terminus preventing detection with an anti-His antibody. Lastly, the presence of bands near the 50 kDa α-tubulin size, confirm that cell lysates were properly loaded onto the gel (**Figure 3.5.6 D**).

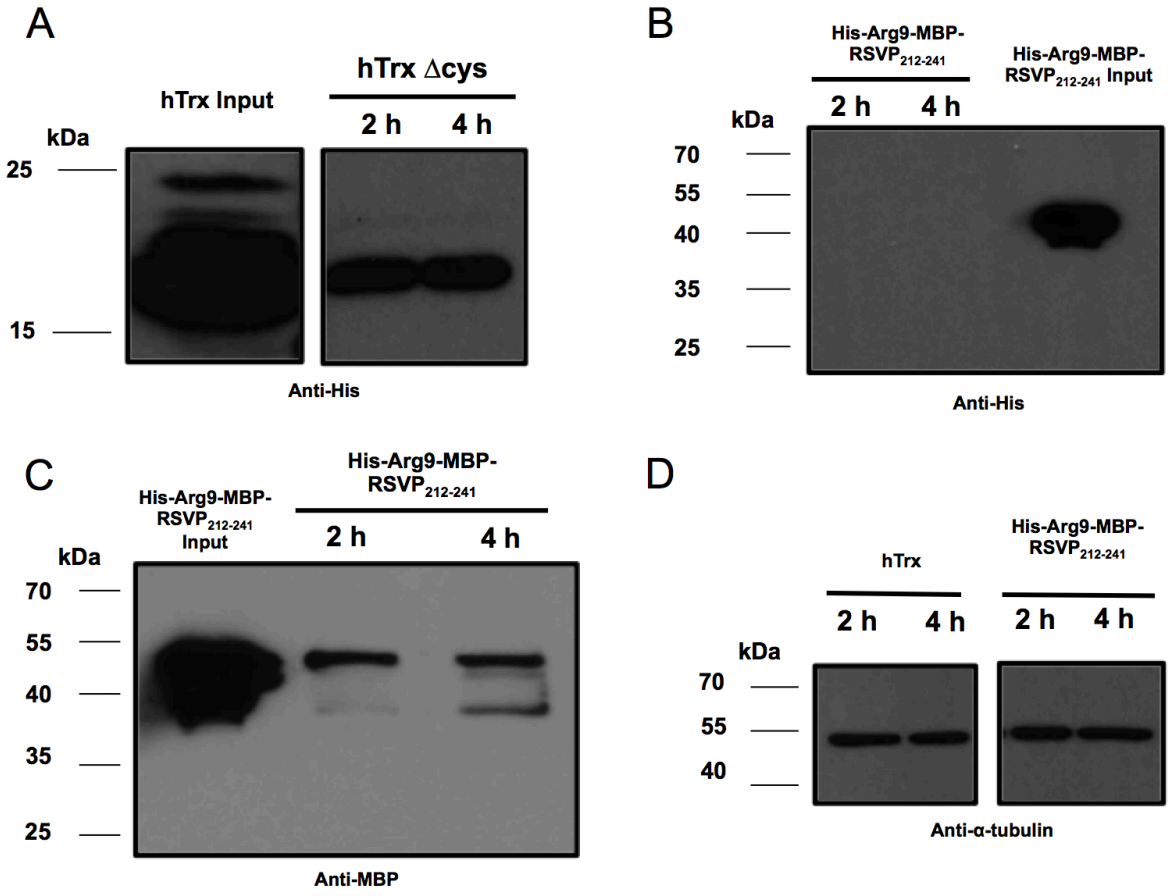

Figure 3.5.6. Uptake of His-Arg9-MBP-RSVP$_{212-241}$ by LLC-MK2 cells. Confluent monolayers of LLC-MK2 cells were incubated with 20 µ M of positive uptake control hTrx or 50 µ M His-Arg9-MBP-RSVP$_{212-241}$ in a 6-well plate for 2 or 4 hours. At the appropriate time point, the cells were washed twice with 1X sterile PBS and once with ice-cold acid wash buffer to remove any peptide exogenously bound to cells. Subsequently, the cells were lysed with RIPA buffer and cellular debris was removed through centrifugation. Samples of the supernatant were collected, mixed with Laemmli buffer, boiled at 95°C, run on a 12% SDS-PAGE gel, and analyzed by Western blot mouse anti-His (1:10,000), mouse anti-MBP (1:10,000), and mouse anti-α -tubulin (1:10,000) primary antibodies. BLUelf Pre-Stained Protein Ladder was run to the left of the samples to indicate the approximate molecular weight of the protein samples. (A) Western blot analysis of the positive uptake control hTrx cell lysates using anti-His primary antibody. The input lane consists of purified hTrx used in the assay and serves to indicate the approximate size of the peptide (18.7 kDa). Visible bands near the predicted molecular weight suggested that hTrx was taken up by LLC-MK2 cells following 2 and 4 h of incubation. (B) Western blot analysis of His-Arg9-MBP-RSVP$_{212-241}$ cell lysates using anti-His primary antibody. The input consisted of purified His-Arg9-MBP-RSVP$_{212-241}$ used in the assay and indicates the approximate size of the peptide (47.05 kDa). The absence of visible bands near the

predicted molecular size suggested that His-Arg9-MBP-$RSVP_{212-241}$ was not taken up by LLC-MK2 cells. (C) Western blot analysis of His-Arg9-MBP-$RSVP_{212-241}$ cell lysates using anti-MBP primary antibody. The input consisted of purified His-Arg9-MBP-$RSVP_{212-241}$ used in the assay and indicated the approximate size of the peptide (47.05 kDa). The presence of visible bands near the predicted molecular size suggested that His-Arg9-MBP-$RSVP_{212-241}$ was in fact being taken up by LLC-MK2 cells and was being degraded at the N-terminus once inside cells. (D) Western blot analysis of hTrx and His-Arg9-MBP-$RSVP_{212-241}$ cell lysates using anti-α -tubulin as the primary antibody as a loading control. Visible bands near the predicted size of α -tubulin (50 kDa) demonstrate that cell lysate was loaded into each of the lanes. Collectively, the figures showed that His-Arg9-MBP-$RSVP_{212-241}$ and hTrx were taken up by LLC-MK2 cells.

3.5.5 His-Arg9-MBP-$RSVP_{212-241}$ interacts with the RSV nucleoprotein

Having demonstrated that His-Arg9-MBP-$RSVP_{212-241}$ recombinant fusion protein was taken up by LLC-MK2 cells, the next step was to determine whether the construct could interact with the RSV nucleoprotein. Interaction with the L polymerase could not be evaluated since the L polymerase has yet to be successfully purified from bacteria (Noton et al., 2012) and no L polymerase antibody is currently available.

To determine whether the His-Arg9-MBP-$RSVP_{212-241}$ fusion protein interacts with RSV nucleoprotein, a GST pull-down assay was performed. In this assay, GST protein was included as a negative control. GST and GST-N bound to magnetic glutathione-agarose beads (bait) were incubated separately cell lysate containing His-Arg9-MBP-$RSVP_{212-241}$ (prey) in triplicate. The beads were collected and washed several times under high salt conditions to remove any non-specifically bound proteins. Subsequently, the beads were re-suspended in Laemmli buffer, heated to 95˚C, separated on a 12% SDS-PAGE gel, and subsequently analyzed by Western blot using mouse anti-His primary antibody or mouse anti-GST primary antibody as a loading control (**Figure 3.5.7 A**). His-Arg9-MBP-

$RSVP_{212-241}$ interacted with GST-N but not GST, as indicated by the presence of bands near the predicted size of 47.05 kDa in GST-N but not GST lanes (**Figure 3.5.7 B**). The fact that the construct associated with GST-N under high salt conditions suggested that it formed a stable interaction that may be maintained *in vivo*.

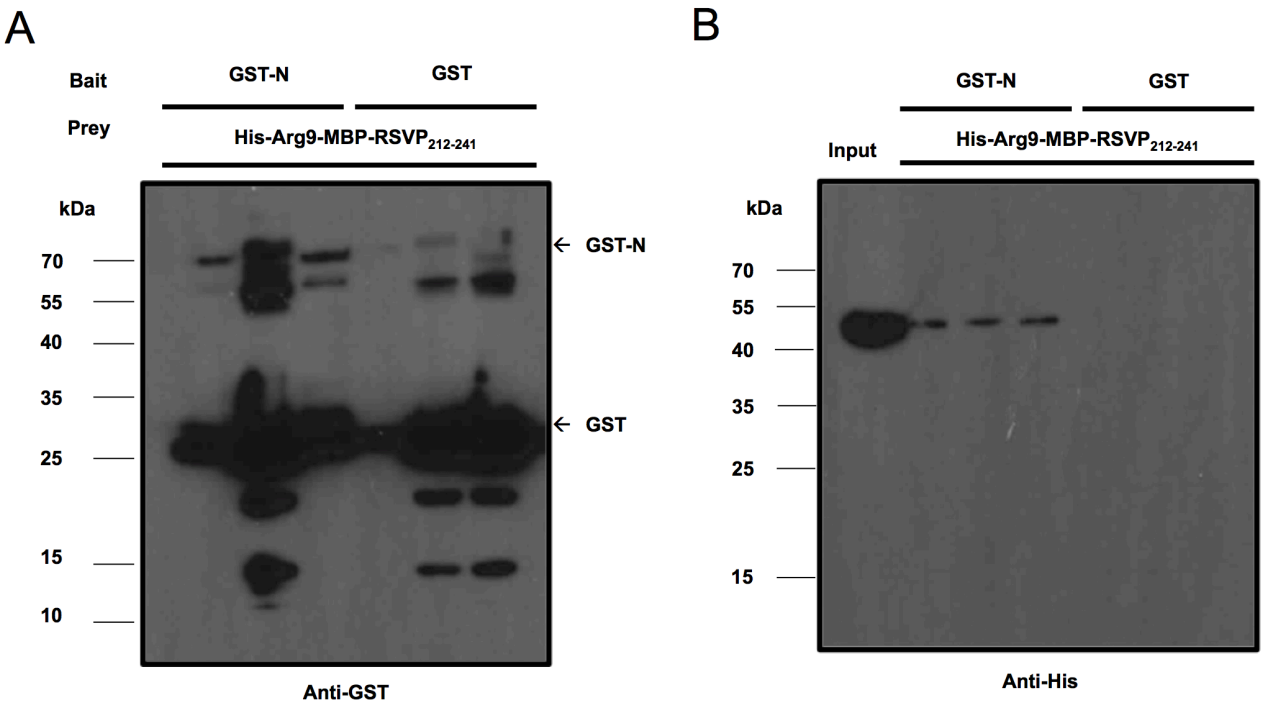

Figure 3.5.7. Interaction of His-Arg9-MBP-$RSVP_{212-241}$ with GST-N in a GST pull-down. GST or GST-N bait were overexpressed in *E. coli* and cell lysates were incubated with glutathione high capacity magnetic agarose beads. GST- or GST-N-bound beads were blocked for one hour at 4˚C while nutating with blocking buffer (5% w/v BSA, 0.1% v/v Tween-20, 1X PBS). Subsequently, the beads were incubated with cell lysate containing His-Arg9-MBP-$RSVP_{212-241}$ prey protein overnight at 4˚C while nutating. Beads were washed seven times with high salt wash buffer. Proteins were eluted from the magnetic beads in Laemmli buffer, boiled at 95˚C, and run on 12% SDS-PAGE gels and analyzed by Western blot using anti-GST (A) and anti-His (B) primary antibodies. BLUelf Pre-Stained Protein Ladder was run to the left of the samples to indicate the approximate molecular weight of protein samples. (A) As a loading control, protein samples were visualized using anti-GST primary antibody. (B) The input control is a sample of the cell lysate containing His-Arg9-MBP-$RSVP_{212-241}$ used in this assay and serves as an indication of approximate protein size (47.05 kDa). From left to right, the wells following the input control were elution fractions from GST-N bound beads (in triplicate) and GST-bound

beads (in triplicate). Visible bands near the predicted molecular weight of His-Arg9-MBP-$RSVP_{212-241}$ only in lanes corresponding to GST-N suggested that His-Arg9-MBP-$RSVP_{212-241}$ copurifies with GST-N, but not GST under high salt conditions.

3.5.6 His-Arg9-MBP-$RSVP_{212-241}$ attenuates RSV A replication in LLC-MK2 cells

Since His-Arg9-MBP-$RSVP_{212-241}$ was shown to be non-toxic, could cross the plasma membrane, and interacted with the N protein, its ability to attenuate RSV A replication *in vitro* was evaluated. The His-Arg9-MBP-$RSVP_{212-241}$ construct's activity was evaluated alongside the original RSV peptide mimetic that was able to attenuate RSV A replication by approximately 90%, 20 μM His-MBP-Tat-$RSVP_{220-241}$. LLC-MK2 cells were incubated in triplicate with DMEM, 20 μM His-MBP-Tat-$RSVP_{220-241}$, 25, 50, 100, or 200 μM His-Arg9-MBP-$RSVP_{212-241}$ for 2 hours prior to being infected with RSV A. Following infection, the cells were treated with a second round of DMEM or recombinant protein for 48 hours.

Following the 48-hour incubation, RSV infected cells were visualized using indirect immunofluorescence microscopy with a mouse anti-RSV F protein primary antibody and goat anti-mouse-FITC secondary antibody (**Figure 3.5.8 A**). RSV infection in wells treated with recombinant fusion proteins were compared to virus-only controls. All infected cells on each monolayer were counted and the triplicates were averaged. The average number of infected cells for the virus only and protein conditions were plotted as a bar graph (**Figure 3.5.8 B**). Percent inhibition was determined as described in section **2.6.8** and depicted as a bar graph (**Figure 3.5.8 C**). Compared to the RSV A only control, His-MBP-Tat-$RSVP_{220-241}$ inhibited RSV A replication by approximately 50.7% at 20 μM, while His-Arg9-MBP-$RSVP_{212-241}$ inhibited RSV A replication by 47.3% at 25 μM, 55.6% at 50 μM, 65.9% at

100 µM, and 94.8% at 200 µM. Furthermore, percent inhibition was not significantly different between the 20 µM His-MBP-Tat-RSVP$_{220-241}$ and 25 µM His-Arg9-MBP-RSVP$_{212-241}$ recombinant protein conditions.

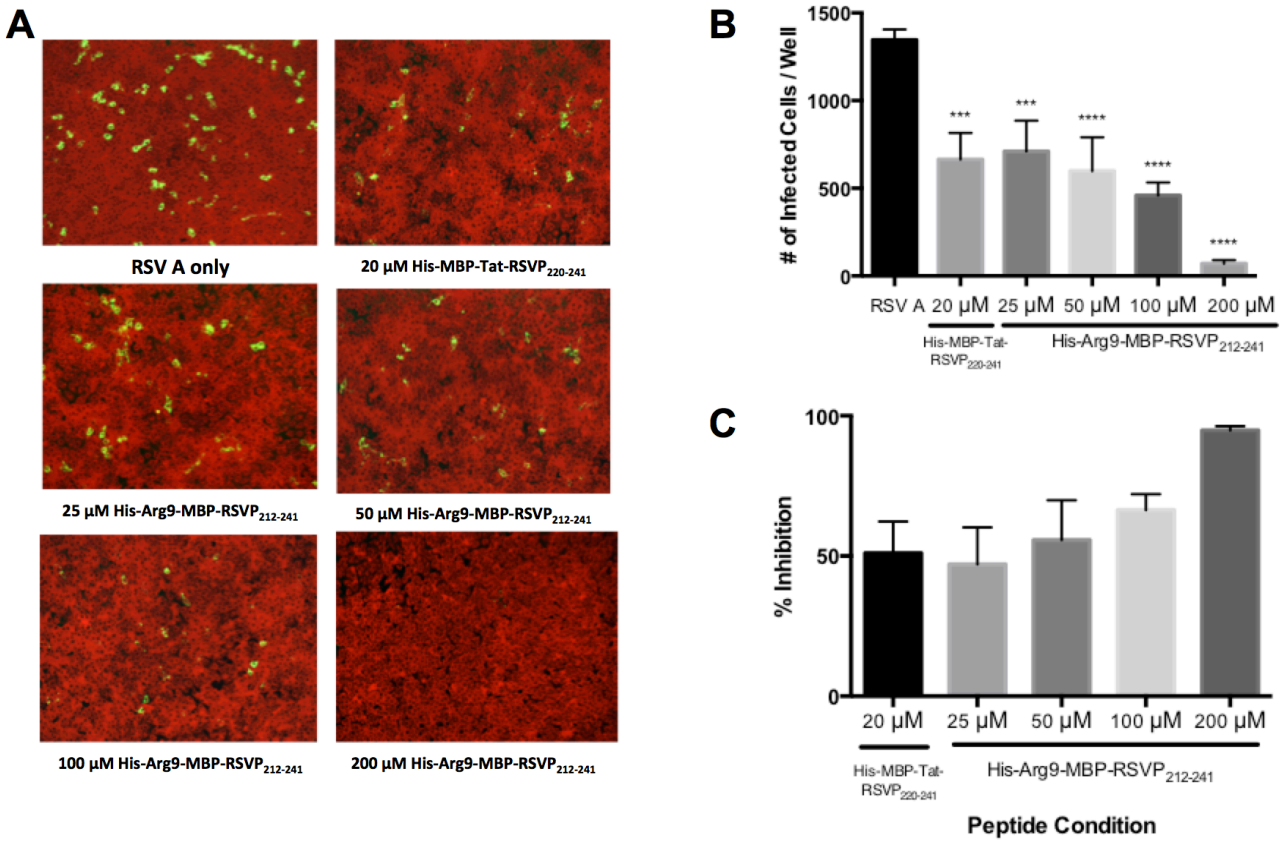

Figure 3.5.8. Inhibition of RSV A Replication by His-Arg9-MBP-RSVP$_{212-241}$. LLC-MK2 cells were incubated in triplicate with 20 µM His-MBP-Tat-RSVP$_{220-241}$, 25 µM, 50 µM, 100 µM, or 200 µM His-Arg9-MBP-RSVP$_{212-241}$ in DMEM for 2 hours, infected with RSV A, and subsequently incubated under the same peptide conditions for 48 hours. Following the incubation period, cells were fixed in ice-cold methanol and visualized with indirect immunofluorescence microscopy using mouse anti-RSV fusion protein primary antibody and goat anti-mouse-FITC secondary antibody. (A) Random and representative images of the stained LLC-MK2 cells were captured at 10X magnification using an Evos Light Microscope. RSV A-infected cells were stained green (FITC) and non-infected cells were stained red (0.05% Evan's Blue Reagent). (B) The total number of infected cells for each monolayer were counted and the mean of triplicates for each condition were plotted as a bar graph. The error bars represent one standard deviation from the mean. Statistical significance was calculated using a one-way ANOVA and *post hoc* Dunnett's multiple comparisons between the peptide groups and the virus-only treated groups using GraphPad

Prism 7.00 software. A p-value < 0.05 was considered statistically significant. The *** denotes a p-value < 0.001 and **** denotes a p-value < 0.0001. (C) Percent inhibition of RSV A replication by each peptide condition was calculated as described in the methods section and plotted as a bar graph with error bars representing one standard deviation from the mean.

3.5.7 Attenuation of RSV A replication by His-Arg9-MBP-RSVP$_{212-241}$ translates to reduced viral progeny production

After demonstrating that His-Arg9-MBP-RSVP$_{212-241}$ could attenuate RSV A replication, we explored whether this translated to decreased production of viral progeny. Confluent LLC-MK2 cells were incubated in triplicate with DMEM, 200 μM His-Arg9-MBP-RSVP$_{212-241}$ or 20 μM His-MBP-Tat-RSVP$_{220-241}$ prior to be infected with RSV A. Following infection, the cells were incubated with a second round of DMEM, 200 μM His-Arg9-MBP-RSVP$_{212-241}$ or 20 μM His-MBP-Tat-RSVP$_{220-241}$ for 48 hours. Subsequently, the supernatants, containing viral progeny, were used to infect new confluent monolayers of LLC-MK2 cells. After the infection, the cells were incubated with DMEM for 48 hours.

RSV infected cells were visualized using indirect immunofluorescence microscopy with a mouse anti-RSV F protein primary antibody and goat anti-mouse-FITC secondary antibody (**Figure 3.5.9 A**). RSV infection in wells treated with recombinant fusion proteins were compared to the virus only controls. All infected cells on each monolayer were counted and the triplicates were averaged. The average number of infected cells for the virus only and protein conditions were plotted as a bar graph (**Figure 3.5.9 B**). Percent inhibition was determined as described in section **2.6.8** and was depicted as a bar graph (**Figure 3.5.9 C**). Compared to the RSV A only control, His-MBP-Tat-RSVP$_{220-241}$ decreased RSV A replication by approximately 49% at 20 μM, while His-Arg9-MBP-

$RSVP_{212-241}$ decreased RSV A replication by 93.33% at 200 µM. These results suggested that attenuation of RSV A replication translated to reduced progeny production.

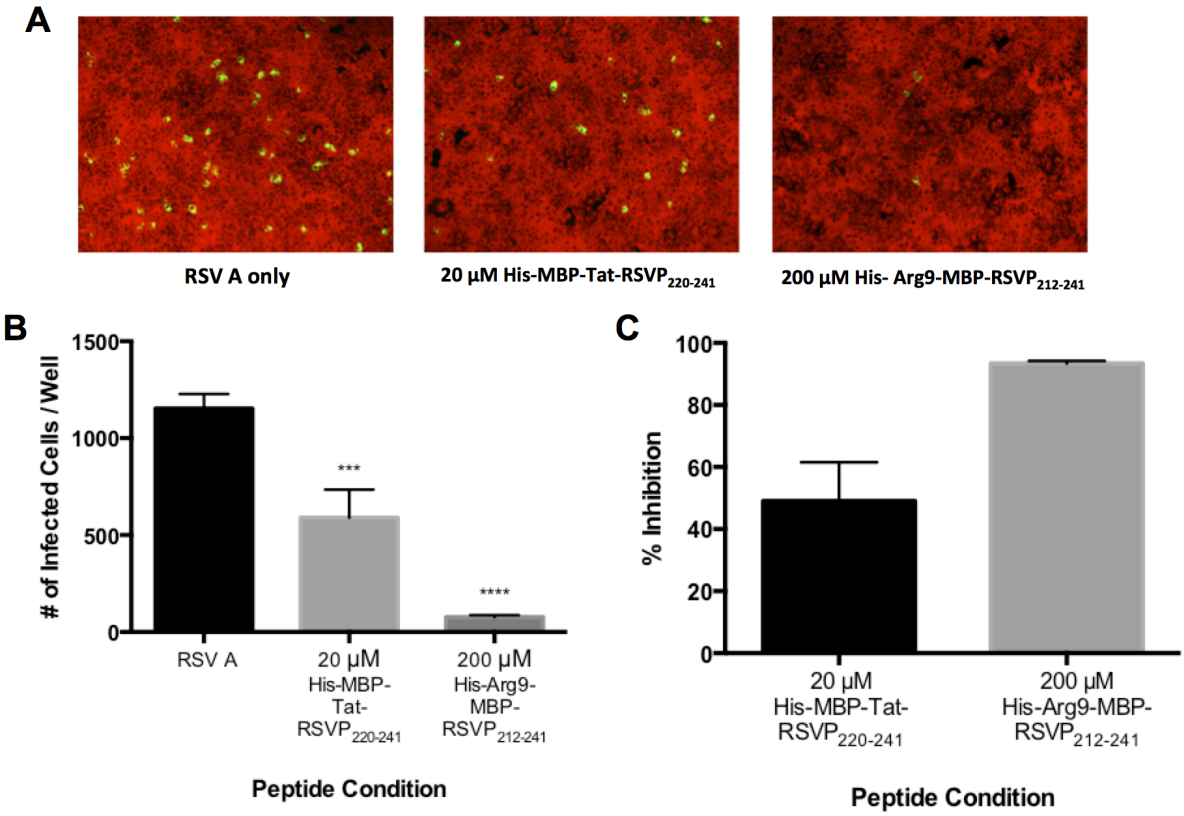

Figure 3.5.9. Inhibition of RSV A Progeny Virus Release by His-Arg9-MBP-$RSVP_{212-241}$. LLC-MK2 cells were incubated in triplicates with 20 µM His-MBP-Tat-$RSVP_{220-241}$ or 200 µM His-Arg9-MBP-$RSVP_{212-241}$ in DMEM for 2 hours, infected with RSV A, and subsequently incubated with a second round of peptide for 48 hours. Following the incubation period, the supernatants were used to infect new LLC-MK2 cells. Following the infection process, the cells were incubated with DMEM for 48 hours. After 48 hours, the cells were fixed in ice-cold methanol and visualized with indirect immunofluorescence microscopy using mouse anti-RSV fusion protein primary antibody and goat anti-mouse-FITC secondary antibody. (A) Random and representative images of the stained LLC-MK2 cells were captured at 10X magnification using an Evos Light Microscope. RSV A-infected cells were stained green (FITC) and non-infected cells were stained red (0.05% Evan's Blue Reagent). (B) The total number of infected cells for each monolayer were counted and the triplicate mean for each condition were plotted as a bar graph. The error bars represent one standard deviation from the mean. Statistical significance was calculated by a one-way ANOVA and *post hoc* Dunnett's multiple comparisons between the peptide groups and the virus-only treated groups using GraphPad Prism 7.00 software. A p-value < 0.05 was

considered statistically significant. The *** denotes a p-value < 0.001 and **** denotes a p-value < 0.0001. (C) Percent inhibition of RSV A viral progeny release by 20 μM His-MBP-Tat-$RSVP_{220-241}$ or His-Arg9-MBP-$RSVP_{212-241}$ was calculated and plotted as a bar graph with error bars representing one standard deviation from the mean.

Chapter 4 – Discussion and Future Directions

RSV is an important respiratory pathogen associated with significant global health and economic burdens (Fearns & Deval, 2016; Nair et al., 2010; Paramore et al., 2004; Rodriguez & Ramilo, 2014). With therapeutic options strictly limited to those at high-risk and no vaccine currently available (Acosta et al., 2016; Guvenel et al., 2014; Neuzil, 2016; Rodriguez & Ramilo, 2014), there is a current need for safe and cost-effective therapeutics. The application of peptide mimetics to target conserved and critical protein interaction networks is a novel approach that can be used to generate RSV antiviral therapeutics.

Previously, the Mahony laboratory created an RSV peptide mimetic based on previous studies showing that the nine terminal amino acids of the RSV P protein were required for binding to NC complexes and an antibody consisting of the 21 terminal amino acids of the P protein was able to displace the N protein from NC complexes (Galloux et al., 2012; García-Barreno et al., 1996; Tran et al., 2007). This original RSV peptide mimetic consisted of the 21 terminal amino acids of the RSV A P protein (amino acid residues 220-241) fused to a hexa-histidine tag for detection and purification purposes, the *E. coli* MBP carrier protein to increase stability and solubility, and the HIV-1 Tat CPP to enable uptake into cells as viral replication occurs within the cytoplasm of infected cells. This His-MBP-Tat-RSVP$_{220\text{-}241}$ construct was shown to attenuate RSV A and B replication in LLC-MK2 cells by approximately 90 and 80%, respectively.

4.1.1 ABD035 as a human carrier molecule

Although the *E. coli* MBP carrier molecule is useful for increasing the stability and solubility of conjugated peptide domains, it may be immunogenic in humans (Sun et

al., 2011; Zhao et al., 2013). As a result, our lab has investigated carrier molecules that can be used in humans. There are several suitable carrier molecules, and our lab has previously investigated elastin-like polypeptides (Meyer & Chilkoti, 1999) and human thioredoxin . As part of this thesis, we investigated ABD as a carrier molecule compatible for future use in humans.

We fused the ABD035 domain to the Tat-RSVP$_{220-241}$ construct. The ABD035 domain was engineered from the ABD3 domain of streptococcal protein G using affinity maturation to increase its affinity for HSA (Jonsson et al., 2008; Nilvebrant & Hober, 2013). Previous reports showed that the ABD035 variant maintained its secondary structure and showed affinity for HSA within the femtomolar range (Jonsson et al., 2008). Furthermore, this binding domain showed increased affinity to serum albumins from other species, including mouse (Jonsson et al., 2008), which would be advantageous considering *in vivo* studies are often performed using mouse models. Although it seems paradoxical to use a carrier molecule derived from bacteria for use in humans, ABDs are part of the natural flora within the human body and are therefore not expected to be immunogenic (Nilvebrant & Hober, 2013). Furthermore, the ABD035 variant would associate with HSA in human serum, which is a large protein that may protect the recombinant protein construct from detection by the immune system and degradation by proteases.

Initial efforts to express a His-ABD-Tat-RSVP$_{220-241}$ construct were unsuccessful. Although counterintuitive, we also included a GST or MBP carrier molecule to the ABD-Tat-RSVP$_{220-241}$ construct as both are known to increase the solubility, stability, and

proper folding of attached cargo (Sun et al., 2011; Zhao et al., 2013), which may improve expression of the construct. We could also incorporate a cleavable linker to remove the tag following purification. We initially fused the construct to a GST-tag and showed that GST-ABD-Tat-RSVP$_{220-241}$ interacted with HSA under high salt conditions. Our finding that GST protein alone did not pull-down HSA suggests that the interaction is specific to the ABD or ABD-Tat-RSVP$_{220-241}$ region. Furthermore, the interaction between GST-ABD-Tat-RSVP$_{220-241}$ may be maintained *in vivo* since it was stable under high salt conditions.

Unfortunately, the GST-ABD-Tat-RSVP$_{220-241}$ recombinant protein was unstable and precipitated out of solution upon buffer exchange into 1X PBS (pH 7.4, 8.51, 6.4, and 9) and 40 mM Tris-HCl + 400 mM NaCl (pH 8.57 and 6.5). The pH of the buffer exchange solution was at least one pH unit above or below the pI of the construct, as it is known that the solubility of a protein is minimal near its pI (Shaw et al., 2001). In addition, tris buffer was supplemented with high salt, which is known to decrease electrostatic interactions and aggregation (Lebendiker & Danieli, 2014). Despite these efforts, recombinant GST-ABD-Tat-RSVP$_{220-241}$ protein precipitated following buffer exchange. Previous studies that compared the properties of commonly used affinity tags showed that the GST affinity tag was the poorest at improving the solubility of fusion proteins (Rosano & Ceccarelli, 2014). As a result, we created a His-MBP-tagged ABD-Tat-RSVP$_{220-241}$ fusion protein since MBP is among the affinity tags with the greatest solubilizing activity (Rosano & Ceccarelli, 2014). However, the His-MBP version of the ABD-Tat-RSVP$_{220-241}$ fusion protein was again unstable and precipitated out of solution

upon buffer exchange into 1X PBS (pH 7.4), 40 mM Tris-HCl + 500 mM NaCl (pH 7.4), 0.5X PBS (pH 7.4), 1X PBS + 10% glycerol (pH 7.4), and 1X PBS + 250 mM NaCl (pH 7.4).

4.1.2 Precipitation of GST- or His-MBP-ABD-Tat-RSVP$_{220-241}$ – A problem of aggregation?

Although previous studies have supported the high solubility of ABD035, other protein-specific extrinsic and intrinsic factors can impact recombinant protein stability (Jonsson et al., 2008; Nivelbrant & Hober, 2013; Wang et al., 2010). Intrinsic factors include the structure of the fusion protein, whereas extrinsic factors include fusion protein environment (Wang et al., 2010). Common extrinsic factors that may have promoted aggregation leading to precipitation of both GST-ABD-Tat-RSVP$_{220-241}$ and His-MBP-Tat-RSVP$_{220-241}$ recombinant proteins include the pH of the buffers used, the buffering agent and concentration, and refolding properties (Wang et al., 2010). High protein concentration is an additional factor known to promote aggregation through enhanced protein-protein interactions (Wang et al, 2010). We observed high levels of purified His-MBP-ABD-Tat-RSVP$_{220-241}$ protein. Therefore, it is possible that the high concentration of recombinant protein in conjunction with the properties of the elution and dialysis buffers enhanced protein-protein interactions, causing aggregation and precipitation of the protein.

4.1.3 Precipitation of GST- or His-MBP-ABD-Tat-RSVP$_{220-241}$ – A problem with linker peptides?

Linker peptides are important for connecting individual protein domains and have several important functions such as promoting proper folding, solubility, and biological activity of recombinant proteins (Chen et al., 2013). There are three main categories of linker peptides, including rigid linkers that separate protein domains to prevent inter-domain interactions, flexible linkers to permit inter-domain interactions, and *in vivo* cleavable linkers (Chen et al., 2013; Fang et al., 2003). The length, amino acid composition, glycosylation, and flexibility or rigidity of linkers have substantial impacts on the stability and functional activity of fusion proteins (Arai et al., 2001; Gustavsson et al., 2001; Zhang et al., 2009). Flexible linkers are often composed of small polar or non-polar amino acid residues, such as serine or glycine, respectively (Chen et al., 2013). Small amino acid residues provide flexibility and allow for a greater degree of movement between the individual domains, and the incorporation of small polar amino acid residues in the linker can increase the stability of the construct in aqueous solution through hydrogen bonding to water molecules (Chen et al., 2013). A previous study showed that a flexible linker composed of glycine and serine residues increased the stability and folding of a single-chain variable fragment (Chen et al., 2013). Based on these findings, we included the commonly used GGGS flexible linker between the ABD035 and the Tat CPP domains, and a single serine residue between the Tat and RSVP$_{220-241}$ moieties of both the GST- and His-MBP-ABD-Tat-RSVP$_{220-241}$ construct. However, it is possible that a flexible linker in our ABD constructs allows for too much movement and interaction

between the fused domains, thereby promoting improper folding and aggregation. It has been shown that increasing the number of GGGS repeats in a flexible linker can increase its rigidity and reduce protein aggregation (Siegemund et al., 2012), which may have been a more suitable option for our ABD recombinant fusion proteins.

4.2.1 Targeting the RSV P-NC and P-L Interactions Using A Novel Peptide Mimetic

In 2015, Sourimant and colleagues determined that amino acid residues 212 to 239 on the RSV P protein were responsible for interacting with the L polymerase. The L polymerase-binding domain on P overlaps with the NC complex-binding domain by 7 amino acids (Galloux et al., 2012; Sourimant et al., 2015; Tran et al., 2007). Although, the Mahony lab previously demonstrated a high percent inhibition of RSV A and B using an RSV P protein mimetic consisting of the 21 terminal amino acids of the P protein at 20 μM (unpublished data), we hypothesized that a peptide mimetic able to block both L polymerase and NC complex interactions with wild-type RSV P protein would be more effective with a higher potency. Primarily, we hypothesized that this peptide mimetic would be more effective by targeting the L polymerase, since the L polymerase is expressed at a low level, whereas the N protein is highly expressed (Collins et al., 2013; Cowton et al., 2006; Sourimant et al., 2015). Initially, we cloned and expressed a His-MBP-Tat-RSVP$_{212-241}$ peptide mimetic. Considering our success with the previous His-MBP-Tat-RSVP$_{220-241}$, we used the same backbone structure and modified only the C-terminal sequence. However, His-MBP-Tat-RSVP$_{212-241}$ was toxic to cells and was not detected in LLC-MK2 cells. To improve transport across the cell membrane, we

generated a Tat-His-MBP-Tat-RSVP$_{212-241}$ construct, but, it was poorly purified. As a result, we created a final fusion protein, His-Arg9-MBP-RSVP$_{212-241}$.

4.2.2 His-MBP-Tat-RSVP$_{212-241}$ is toxic to LLC-MK2 cells

We cloned, expressed, and purified the recombinant protein His-MBP-Tat-RSVP$_{212-241}$. However, incubation of 20 μM of the construct with LLC-MK2 cells resulted in cells sloughing off the monolayer, suggesting that it was toxic at low concentrations. These observations may be explained by contamination with endotoxin, the overall arrangement of the recombinant fusion protein, or a combination of these two factors.

Endotoxins, commonly referred to as lipopolysaccharides (LPS), are a major component of Gram-negative bacterial cell membranes, such as *E. coli* (Magalhães et al., 2007). LPS organizes the bacterial cell membrane and maintains its stability (Magalhães et al., 2007). LPS is continuously released from *E. coli* cells throughout their lifecycle; however, a large amount of endotoxins are released following bacterial cell lysis (Magalhães et al., 2007). Furthermore, LPS has been shown to associate with basic, neutral, and acidic recombinant proteins (Magalhães et al., 2007). Therefore, virtually all recombinant proteins expressed in *E. coli* are contaminated to some degree with LPS (Magalhães et al., 2007; Mamat et al., 2015). Endotoxin is recognized by the toll-like receptor (TLR) 4 on the surface of epithelial cells and initiates an inflammatory response that ultimately leads to apoptosis (Cabrera-Benítez et al., 2016; Rietschel & Brade, 1992).

It is possible that preparations of His-MBP-Tat-$RSVP_{212-241}$ were contaminated with endotoxin, resulting in the observed cytotoxicity.

The cytotoxicity profile of a recombinant fusion protein with a CPP depends on the biochemical properties of the cargo, as well as the overall arrangement of the recombinant fusion protein (Dinca et al., 2016). Many cationic CPPs, such as Tat, are known to be tolerated at high concentrations by cells when fused to various cargo molecules (Dinca et al., 2016). However, the cytotoxicity prolife ultimately depends on the nature of the attached cargo, which can have toxic effects. For example, it was previously shown that Tat fused to a NEMO-binding domain peptide was cytotoxic, but fusion of Tat in the same manner to a STAT-1 peptide was non-toxic (Cardozo, et al., 2007). The arrangement of our His-MBP-Tat-$RSVP_{212-241}$ recombinant protein, whereby the Tat and $RSVP_{212-241}$ sequences are directly fused side-by-side may generate a cytotoxic combination.

4.2.3 His-MBP-Tat-$RSVP_{212-241}$ uptake and inhibition

We were unable to show uptake or inhibition of RSV A by His-MBP-Tat-$RSVP_{212-241}$ in LLC-MK2 cells. Upon further investigation of the fusion protein, we found that at a pH of 7.4, the charge of Tat was +7.8, while the charge of $RSVP_{212-241}$ was -8.2. Cationic CPPs are believed to deliver cargo molecules across the lipid bilayer through several different mechanisms, which will be discussed in section **4.2.6**. However, the first step in the uptake process involves an electrostatic interaction between the CPP, Tat (in this case), and the negatively charged components of the lipid bilayer (Heitz et al.,

2009). Thus, it is possible that the opposite charges of the Tat and $RSVP_{212-241}$ moieties may interact electrostatically, generating steric hindrance and preventing the CPP from associating with GAGs, ultimately blocking uptake (Heitz et al., 2009). However, it is challenging to definitively show that the cells did not take up the construct since incubation with the construct resulted in cells lifting off the monolayer. Thus, it is possible that His-MBP-Tat-$RSVP_{212-241}$ was taken up by LLC-MK2s leading to the observed toxicity. In addition, it is possible that the construct was taken up into cells, but was then cleaved or degraded by proteases, thereby preventing detection using a primary antibody directed against the His-tag.

Our observations that His-MBP-Tat-$RSVP_{212-241}$ did not attenuate RSV A replication in LLC-MK2 cells to any degree may be explained by our results suggesting that the construct was not taken across the cell membrane. However, if the construct was taken up by cells but not detected, it is possible that the biochemical characteristics of the fusion protein arrangement may explain our findings. For example, the bioactivity of the peptide mimetic may decrease as a result of steric hindrance. The MBP carrier molecule is rather bulky and has a molecular weight of approximately 42 kDa, while one of the binding targets, the RSV A L polymerase, has a molecular weight of approximately 250 kDa (Stec et al., 1991). As such, it is possible that steric hindrance between the MBP carrier molecule and L polymerase proteins prevents the peptide mimetic from blocking wild-type interactions.

4.2.4 Development of a Tat-His-MBP-Tat-RSVP$_{212-241}$ fusion protein

Since we hypothesized that the His-MBP-Tat-RSVP$_{212-241}$ fusion protein was not being transported across the lipid bilayer, we cloned an additional Tat CPP at the N-terminus of the previously used construct. We hypothesized that the additional Tat would not be involved in electrostatic interactions with the RSVP$_{212-241}$ domain as the two were located at different termini. However, an additional Tat CPP on the N-terminus of the His-tag appeared to disrupt the His-tag's affinity for the nickel column during purification, as significant amounts of protein were lost throughout the purification process. Ultimately, we only purified 0.26 mg of Tat-His-MBP-Tat-RSVP$_{212-241}$. The optimal placement of a His-tag is specific to each fusion protein; however, the most common placement is at either terminus of the recombinant protein (Bornhorst & Falke, 2000). One issue with an internally located affinity tag is that it may be inaccessible for binding to its immobilized matrix since it could be sterically affected or buried through protein folding (Bornhorst & Falke, 2000). It is possible that the addition of Tat to the N-terminus of the fusion protein prevented the His-tag from associating with the Ni-NTA column.

4.2.5 His-Arg9-MBP-RSVP$_{212-241}$ was not toxic to LLC-MK2 cells

We cloned, expressed, and purified a recombinant His-Arg9-MBP-RSVP$_{212-241}$ fusion protein. Considering that the ultimate purpose of designing this peptide mimetic is antiviral use in humans, it was important to ensure that the fusion protein was not toxic to cells. A recombinant protein toxic to cells is expected to inhibit cell growth or cause cell

death, as observed in the presence of cycloheximide, an inhibitor of eukaryotic translation (Schneider-Poetsch et al., 2010). We showed that this construct was not toxic to LLC-MK2 cells up to a concentration of 200 μM. Interestingly, for the spectrophotometric cell replication assay we observed higher absorbance readings for cells incubated with 200 μM His-Arg9-MBP-$RSVP_{212-241}$ compared to the control condition where cells were incubated with growth medium alone (DMEM + 10% FBS). Although 200 μM of this construct was not evaluated in the visualization assay, we observed minor differences in the morphology of cells incubated with 150 μM His-Arg9-MBP-$RSVP_{212-241}$. The higher absorbance readings for cells incubated with the peptide mimetic may be explained by the difference in cell morphology that resulted in less light reaching the detector (Stevenson et al., 2016).

4.2.6 Mechanism of Inhibition – Transport of His-Arg9-MBP-$RSVP_{212-241}$ across the lipid bilayer

Since RSV replication occurs within the cytoplasm of infected cells, the His-Arg9-MBP-$RSVP_{212-241}$ construct must be transported across the cell membrane to the cytoplasm to interact with its targets; namely, the RSV NC complex and L polymerase. We hypothesized that the Arg9 CPP domain allowed for internalization of the recombinant protein mimetic. In an uptake assay, we showed that His-Arg9-MBP-$RSVP_{212-241}$ was internalized by LLC-MK2 cells. Furthermore, we observed N-terminal breakdown of the protein preventing its detection with an anti-His antibody in Western blot analysis.

Currently, there are two possible routes of uptake for cationic CPPs, such as Tat and Arg9. The first, direct penetration, is an energy-independent process whereby the positively charged CPP interacts electrostatically with negatively charged components of the lipid bilayer, such as heparan sulfate (Dinca et al., 2016; Madani et al., 2011). This route of uptake is believed to occur at high CPP concentrations, when a large number of these electrostatic interactions result in membrane destabilization and subsequent internalization (Madani et al., 2011). The other proposed route of uptake is energy-dependent endocytosis (Dinca et al., 2016; Madani et al., 2011). Several different mechanisms of internalization by endocytosis have been described including caveolar, clathrin-mediated, and macropinocytosis (Dinca et al., 2016; Madani et al., 2011). With internalization by endocytosis, the fate of CPP-cargo depends on endosomal escape prior to degradation by lysosomes (Dinca et al., 2016). Endocytosis is believed to be the primary route of internalization of large cargo molecules conjugated to cationic CPPs (Dinca et al., 2016). Ultimately, the route of internalization depends on the CPP used, the concentration of CPP, the biochemical properties of the attached cargo, and the cell type (Dinca et al., 2016).

In our uptake assay, significantly less His-Arg9-MBP-RSVP$_{212\text{-}241}$ was detected inside LLC-MK2 cells than was added. This result suggested that only a small amount of the recombinant protein added was internalized. It is also possible that our construct was mainly internalized by endocytosis and that not all of the recombinant protein escaped the endosomes, resulting in its degradation by the time we analyzed the uptake samples.

4.2.7 Mechanism of Inhibition – Transport of His-Arg9-MBP-RSVP$_{212-241}$ across the lipid bilayer

To attenuate RSV replication through disruption of wild-type interactions between P-NC complexes and P-L polymerases, our construct His-Arg9-MBP-RSVP$_{212-241}$ must interact with NC complexes and L polymerases. To evaluate this, GST pull-downs were performed using full-length GST-tagged RSV N protein (GST-N) as bait and His-Arg9-MBP-RSVP$_{212-241}$ as prey. Unfortunately, we were unable to evaluate whether the fusion protein could interact with L polymerase since it has yet to be successfully purified from bacterial culture and there is currently no antibody available for its detection (Noton et al., 2012). Nonetheless, we showed that GST-N pulled-down His-Arg9-MBP-RSVP$_{212-241}$. Our observations that GST alone did not pull-down His-Arg9-MBP-RSVP$_{212-241}$ suggested that the interaction was specific to the N protein. In addition, the interaction between the fusion protein and N protein may be maintained *in vivo* since the interaction was stable *in vitro* under high salt conditions.

4.2.8 His-Arg9-MBP-RSVP$_{212-241}$ and His-MBP-Tat-RSVP$_{220-241}$ Inhibition

We showed that a His-Arg9-MBP-RSVP$_{212-241}$ fusion protein mimetic at 200 μM attenuated RSV A replication by 94.8%. Although my results did not corroborate with the 90% inhibition of RSV A replication by His-MBP-Tat-RSVP$_{220-241}$ at 20 μM in the past, I was able to demonstrate 50.7% inhibition at 20 μM. Furthermore, we were unable to conclude whether the His-Arg9-MBP-RSVP$_{212-241}$ recombinant protein was more effective than the original His-MBP-Tat-RSVP$_{220-241}$ construct since we observed no

significant difference in percent inhibition at 25 μM and 20 μM, respectively. We further confirmed attenuation of RSV A replication *in vitro* by showing that 200 μM of His-Arg9-MBP-$RSVP_{212-241}$ decreased RSV A progeny production by 93.33%. In addition, we showed that 20 μM His-MBP-Tat-$RSVP_{220-241}$ reduced RSV A progeny production by 49%.

There are several possible explanations for the low bioactivity of the His-Arg9-MBP-$RSVP_{212-241}$ construct. As mentioned previously, our uptake experiment showed that small amounts of the fusion protein were internalized into LLC-MK2 cells, which suggested that only a small amount of the recombinant fusion protein was contributing to the bioactivity of the construct. If we could improve uptake of the His-Arg9-MBP-$RSVP_{212-241}$ construct, we may be able to increase its bioactivity. It is also possible that the Arg9 CPP is delivering the construct to the nucleus, which would also decrease its bioactivity since RSV replication occurs in the cytoplasm. Previous studies have shown cationic CPPs generally transport cargo to the nucleus of cells (Dinca et al., 2016). Fusing the peptide mimetic to a CPP that specifically targets cargo to the cytoplasm of cells as opposed to the nucleus may increase antiviral bioactivity. Since we were unable to evaluate whether His-Arg9-MBP-$RSVP_{212-241}$ could interact with the RSV L polymerase, it is possible the construct does not interact with the L polymerase *in vitro*. In addition, steric hindrance between the fusion protein and its intended RSV targets may limit their binding capacity and decrease the bioactivity of His-Arg9-MBP-$RSVP_{212-241}$. These possible limitations offer several future avenues of research to better characterize the antiviral fusion protein. Lastly, the overall stability, folding, and bioactivity of a fusion

protein depends on the biochemical properties of individual domains, linkers, and the arrangement of the individual domains (Chen et al., 2013; Gräslund et al., 2008; Rosano & Ceccarelli, 2014; Zhang et al., 2009). Designing a successful fusion protein depends largely on trial and error (Chen et al., 2013; Gräslund et al., 2008; Rosano & Ceccarelli, 2014; Zhang et al., 2009). Thus, the current arrangement of His-Arg9-MBP-$RSVP_{212-241}$ may be suboptimal, thereby reducing its overall bioactivity.

4.3.1 Future Directions – Evaluate His-Arg9-MBP-$RSVP_{212-241}$ in BEAS-2B cells

In this thesis, the His-Arg9-MBP-$RSVP_{212-241}$ fusion protein was evaluated in LLC-MK2 cells, which are kidney epithelial cells from *Macaca mulatta* (rhesus monkey). RSV primarily infects ciliated columnar epithelial cells of the human respiratory tract (Zhang et al., 2002). The two cell lines possess unique biochemical properties, and as a result the peptide mimetic toxicity, uptake, and activity should be investigated in a cell culture line that more closely resembles the target tissue. The BEAS-2B cell line, which consists of human bronchial epithelial cells, is one possibility. However, immortalized cell lines derived from the human respiratory tract are often considered poorly representative of the *in vivo* complexity and true biochemical properties of the respiratory epithelium (Broadbent et al., 2016). As a result, it may be advantageous to evaluate the peptide mimetic in primary epithelial cells from donor patients.

4.3.2 Future Directions – Determine whether His-Arg9-MBP-RSVP$_{212-241}$ induces an antiviral response

Innate immunity is an intrinsic defense mechanism that enables cells to distinguish between self and invading pathogens (Lester & Li, 2014). Cells can make this distinction through pattern recognition receptors (PRRs), which detect conversed sequences or protein domains of invading pathogens known as pattern-associated molecular patterns (PAMPs) (Lester & Li, 2014). Engagement of PRRs, such as TLRs, activates signaling pathways that lead to the production of interferon, which is important for clearing viral infections (Kim & Lee, 2014; Lester & Li, 2014). Since the recombinant fusion protein is composed of protein domains that may be recognized as "non-self", the observed inhibition may be the result of a host cell antiviral response. Thus, future studies are required to evaluate whether the attenuation of RSV replication was the result of a host cell antiviral response. This can be achieved by exploring whether His-Arg9-MBP-RSVP$_{212-241}$ can inhibit a different virus from the *Paramyoxviridae* family, such as parainfluenza virus type 2 (PIV-2). In theory, the construct should not be able to attenuate PIV-2 replication. Thus, if inhibition is observed, it is likely the result of a host cell antiviral response. Additionally, this can be confirmed by investigating the activation of signaling molecules involved in the innate immune response and TLR signaling by Western blot using primary antibodies that detect phosphorylated forms of the signaling molecules.

4.3.3 Future Directions – Determine whether His-Arg9-MBP-$RSVP_{212-241}$ can attenuate RSV B replication *in vitro*

Antiviral activity of His-Arg9-MBP-$RSVP_{212-241}$ was only evaluated for RSV A Long Strain in this thesis. Although not tested, it is likely to inhibit other strains of RSV A since there is a very high degree of sequence similarity between the amino acid residues of the P proteins (Johnson & Collins, 1990). We believe that His-Arg9-MBP-$RSVP_{212-241}$ would be able to attenuate RSV B replication *in vitro* since there is a high degree of sequence similarity in amino acid residues 212 to 241 for both RSV groups. Previous studies have observed sequence similarities of 90% between the P protein amino acid residues of RSV A and B, with the majority of divergence occurring between amino acid residues 59 to 85 (Johnson & Collins; 1990). In fact, it was shown that sequence similarities outside of the divergent domain were 96% (Johnson & Collins; 1990). Collectively, these findings suggest that the mimetic may inhibit RSV B, which would be advantageous since RSV B is known to co-circulate with RSV or act as the dominant infecting group during an epidemic (Sullender, 2000).

4.3.4 Future Directions – Attaching $RSVP_{212-241}$ to a human carrier molecule

Although the *E. coli* MBP is a suitable carrier molecule to increase the expression, stability, and solubility of recombinant fusion proteins, it is likely to be immunogenic in humans (Sun et al., 2011; Zhao et al., 2013). A carrier molecule suitable for use in human is required to reduce clearance and degradation of the protein antiviral His-Arg9-MBP-$RSVP_{212-241}$. We were unable to use the ABD as a carrier molecule in this thesis;

however, several other members of the Mahony lab are investigating other human carrier molecules such human thioredoxin and elastin-like polypeptides. In addition, the peptide mimetic could be fused to HSA as a carrier molecule. There are several advantages to using HSA as a carrier molecule including reduction of renal clearance, prolonged half-life through FcRn recycling, and lack of immunogenicity (Jacobs et al., 2015; Sand et al., 2014).

4.4 Closing Remarks

RSV is the leading cause of acute lower respiratory tract infections in children and causes severe morbidity and mortality in the elderly and immunocompromised. RSV can cause repeated infections throughout life and represents a significant health and economic burden worldwide. Despite continuous research efforts, there is no vaccine for the prevention of RSV and no pharmaceutical options for its routine treatment. Palivizumab and ribavirin, the only FDA-approved pharmaceutical options for the prevention and treatment of RSV, respectively, are strictly provided to infants and children at risk of severe infection. Thus, the current need for RSV antivirals is clear. One novel approach is the use of a recombinant protein with a short peptide mimetic domain capable of blocking wild-type interactions between the P, NC, and L proteins of the RdRp complex. In theory, since those interactions are crucial for replication and ultimately survival, the novel peptide mimetic should attenuate RSV infection. We showed that a novel $RSVP_{212-241}$ fused to a bacterial carrier molecule, a detection tag, and an Arg9 CPP could attenuate RSV A replication and progeny production *in vitro*. However, further studies are required

to fully characterize the His-Arg9-MBP-RSVP$_{212-241}$ fusion protein, increase its bioactivity, and fuse the peptide mimetic portion to a more suitable carrier molecule for future evaluation *in vivo*.

CHAPTER 5 – REFERENCES

Andersen, J. T., Pehrson, R., Tolmachev, V., Daba, M. B., Abrahmsén, L., & Ekblad, C. (2011). Extending half-life by indirect targeting of the neonatal Fc receptor (FcRn) using a minimal albumin binding domain. *Journal of Biological Chemistry*, *286*(7), 5234–5241. http://doi.org/10.1074/jbc.M110.164848

Araujo, G. C., Silva, R. H. T., Scoot, L. P. B., Araujo, A. S., Souza, F. P., Junio de Oliveira, R. (2016). Structure and functional dynamics characterization of the ion channel of the human respiratory syncytial virus (hRSV) small hydrophobic protein (SH) transmembrane domain by combining molecular dynamics with excited normal modes. *J Mol Model 22*, 286. DOI 10.1007/s00894-016-3150-6

Asenjo, A. and Villanueva, N. (2000). Regulated but not constitutive human respiratory syncytial virus (HRSV) P protein phosphorylation is essential for oligomerization. *FEBS Letters 476*, 279-284.

Bacharier, L. B., Cohen, R., Schweiger, T., Yin-Declue, H., Christie, C., Zheng, J., … Castro, M. (2012). Determinants of asthma after severe respiratory syncytial virus bronchiolitis. *The Journal of Allergy and Clinical Immunology*, *130*(1), 91–100.e3. http://doi.org/10.1016/j.jaci.2012.02.010

Baviskar, P. S., Hotard, A. L., Moore, M. L., & Oomens, A. G. P. (2013). The respiratory syncytial virus fusion protein targets to the perimeter of inclusion bodies and facilitates filament formation by a cytoplasmic tail-dependent mechanism. *Journal of Virology*, *87*(19), 10730–41. http://doi.org/10.1128/JVI.03086-12

Bawage, S. S., Tiwari, P. M., Pillai, S., Dennis, V., & Singh, S. R. (2013). Recent advances in diagnosis, prevention, and treatment of human respiratory syncytial virus. *Advances in Virology*. Retrieved from http://www.hindawi.com/journals/av/2013/595768/

Bermingham, A., & Collins, P. L. (1999). The M2-2 protein of human respiratory syncytial virus is a regulatory factor involved in the balance between RNA replication and transcription. *Proceedings of the National Academy of Sciences of the United States of America*, *96*(20), 11259–64. Retrieved from http://www.ncbi.nlm.nih.gov/pubmed/10500164

Bitko, V., Shulyayeva, O., Mazumder, B., Musiyenko, A., Ramaswamy, M., Look, D. C., & Barik, S. (2007). Nonstructural Proteins of Respiratory Syncytial Virus Suppress Premature Apoptosis by an NF- B-Dependent, Interferon-Independent Mechanism and Facilitate Virus Growth. *Journal of Virology*, *81*(4), 1786–1795. http://doi.org/10.1128/JVI.01420-06

Blount, R. E., Morris, J. A., & Savage, R. E. (1956). Recovery of cytopathogenic agent from chimpanzees with coryza. *Proceedings of the Society for Experimental Biology*

and Medicine. Society for Experimental Biology and Medicine (New York, N.Y.), *92*(3), 544–549. http://doi.org/10.3181/00379727-92-22538

Borchers, A. T., Chang, C., Gershwin, M. E., & Gershwin, L. J. (2013). Respiratory syncytial virus, a comprehensive review. *Clinical Reviews in Allergy & Immunology*, *45*, 331–79. http://doi.org/10.1007/s12016-013-8368-9

Bornhorst, J. A. & Falke, J. J. (2000). Purification of proteins using polyhistidine affinity tags. *Methods Enzymol 326*, 245-254.

Branche, A. R., & Falsey, A. R. (2015). Respiratory Syncytial Virus Infection in Older Adults: An Under-Recognized Problem. *Drugs & Aging*, *32*(4), 261–269. http://doi.org/10.1007/s40266-015-0258-9

Brealey, J. C., Sly, P. D., Young, P. R., & Chappell, K. J. (2015). Viral bacterial co-infection of the respiratory tract during early childhood. *FEMS Microbiology Letters*, *362*(10). https://doi.org/10.1093/femsle/fnv062

Broadbent, L., Groves, H., Shields, M. D., & Power, U. F. (2015). Respiratory syncytial virus, an ongoing medical dilemma: An expert commentary on respiratory syncytial virus prophylactic and therapeutic pharmaceuticals currently in clinical trials. *Influenza and Other Respiratory Viruses*, *9*(4), 169–178. http://doi.org/10.1111/irv.12313

Broadbent, L., Villenave, R., Guo-Parke, H., Douglas, I., Shields, M. D., & Power, U. F. (2016). *In vitro* modeling of RSV infection and cytopathogenesis in well-differentiated human primary airway epithelial cells (WD-PAECs). *Methods Mol Biol 1442*, 119-139.

Brown, G., Rixon, H. W. M., & Sugrue, R. J. (2002). Respiratory syncytial virus assembly occurs in GM1-rich regions of the host-cell membrane and alters the cellular distribution of tyrosine phosphorylated caveolin-1. *The Journal of General Virology*, *83*(Pt 8), 1841–50. http://doi.org/10.1099/0022-1317-83-8-1841

Cabrera-Benítez, N. E., Pérez-Roth, E., Ramos-Nuez, A., Sologuren, I., Padrón, J. M., Slutsky, A. S., & Villar, J. (2016). Inhibition of endotoxin-induced airway epithelial cell injury by a novel family of pyrrol derivatives. *Laboratory Investigation 96*, 632-640. doi:10.1038/labinvest.2016.46

Cardozo, A. K., Buchillier, V., Mathieu, M., Chen, J., Ortis, F., Ladriere, L., Allaman-Pillet, N., Poirot, O., Kellenberger, S., Beckmann, J. S., Eizirik, D. L., Bonny, C., & Maurer, F. (2007). Cell-permeable peptides induce dose- and length-dependent cytotoxic effects. *Biochim Biophys Acta 1768*(9), 2222-2234.

Chang, A., & Dutch, R. E. (2012). Paramyxovirus fusion and entry: multiple paths to a common end. *Viruses*, *4*(4), 613–36. http://doi.org/10.3390/v4040613

Chanock, R. M., Parrott, R.H., Vargosko, A.J., Kapikian, A.Z., Knight, V., and Johnson, K.M. (1962). IV. Respiratory syncytial virus. *Am J Public Health Nations Health 52*(6), 918-925.

Chappell, K. J., Brealey, J. C., Mackay, I. M., Bletchly, C., Hugenholtz, P., Sloots, T. P., Sly, P. D., & Young, P.R. (2013). *Medical Microbiology & Diagnosis (S1)*. doi:10.4172/2161-0703.S1-005

Chen, X., Zaro, J., & Shen W.C. (2013). Fusion protein linkers: property, design, and functionality. *Adv Drug Deliv Rev 65*(10), 1357-1369.

Chu, H. Y., & Englund, J. A. (2013). Respiratory syncytial virus disease: prevention and treatment. *Current Topics in Microbiology and Immunology*, *372*, 235–58. http://doi.org/10.1007/978-3-642-38919-1_12

Collins, P. L., Fearns, R., & Graham, B. S. (2013). Respiratory syncytial virus: virology, reverse genetics, and pathogenesis of disease. *Current Top Microbiol Immunol 372*, 3–38. doi:10.1007/978-3-642-38919-1_1

Collins, P. L., & Graham, B. S. (2008). Viral and Host Factors in Human Respiratory Syncytial Virus Pathogenesis. *The Journal of Virology*, *82*, 2040–2055. http://doi.org/10.1128/jvi.01625-07

Collins, P. L., Hill, M. G., Cristina, J., & Grosfeld, H. (1996). Transcription elongation factor of respiratory syncytial virus, a nonsegmented negative-strand RNA virus. *Proceedings of the National Academy of Sciences of the United States of America*, *93*(1), 81–5. Retrieved from http://www.ncbi.nlm.nih.gov/pubmed/8552680

Collins, P. L., & Melero, J. A. (2011). Progress in understanding and controlling respiratory syncytial virus: Still crazy after all these years. *Virus Research*. http://doi.org/10.1016/j.virusres.2011.09.020

Cowton, V. M., McGivern, D. R., & Fearns, R. (2006). Unravelling the complexities of respiratory syncytial virus RNA synthesis. *Journal of General Virology*, *87*(7), 1805–1821. http://doi.org/10.1099/vir.0.81786-0

Del Vecchio, A., Ferrara, T., Maglione, M., Capasso, L., & Raimondi, F. (2013). New perspectives in Respiratory Syncitial Virus infection. *The Journal of Maternal-Fetal & Neonatal Medicine*, *26*(sup2), 55–59. http://doi.org/10.3109/14767058.2013.831282

Dinca, A., Chien, W.-M., & Chin, M. T. (2016). Intracellular Delivery of Proteins with Cell-Penetrating Peptides for Therapeutic Uses in Human Disease. *International Journal of Molecular Sciences*, *17*(2), 263. http://doi.org/10.3390/ijms17020263

Eiland, L. S. (2009). Respiratory syncytial virus: diagnosis, treatment, and prevention. *J Pediatr Pharmacol Ther 14*, 75-85.

Falsey, A. R., Hennessey, P. A., Formica, M. A., Cox, C., & Walsh, E. E. (2005) Respiratory syncytial virus infection in elderly and high risk-adults. *N Engl J Med 352*, 1749-1759. DOI: 10.1056/NEJMoa043951

Fang, M., Jiang, Z., Yang, Z., Yin, C., Li, H., Zhao, R., Zhang, Z., Lin, Q., & Huang, H. (2003). Effects of interlinker sequences on the biological properties of bispecific single-chain antibodies. *Chinese Science Bulletin 48*(21), 2277-2283.

Fearns, R. & Deval, J. (2016). New antiviral approaches for respiratory syncytial virus and other mononegaviruses: inhibiting the RNA polymerase. *Antiviral Research 134*, 63-76.

Feldman, S. A., Hendry, R. M., & Beeler, J. A. (1999). Identification of a linear heparin binding domain for human respiratory syncytial virus attachment glycoprotein G. *Journal of Virology*, *73*(8), 6610–7. Retrieved from http://www.ncbi.nlm.nih.gov/pubmed/10400758

Fosgerau, K., & Hoffmann, T. (2015). Peptide therapeutics: current status and future directions. *Drug Discovery Today*, *20*(1), 122–128. http://doi.org/10.1016/j.drudis.2014.10.003

Frejd, F. Y. (2012). Half-Life Extension by Binding to Albumin through an Albumin Binding Domain. In *Therapeutic Proteins* (pp. 269–283). Weinheim, Germany: Wiley-VCH Verlag GmbH & Co. KGaA. http://doi.org/10.1002/9783527644827.ch14

Fuentes, S., Coyle, E. M., Beeler, J., Golding, H., Khurana, S., Nair, H., … Beigel, J. (2016). Antigenic Fingerprinting following Primary RSV Infection in Young Children Identifies Novel Antigenic Sites and Reveals Unlinked Evolution of Human Antibody Repertoires to Fusion and Attachment Glycoproteins. *PLOS Pathogens*, *12*(4), e1005554. http://doi.org/10.1371/journal.ppat.1005554

Fuentes, S., Tran, K. C., Luthra, P., Teng, M. N., & He, B. (2007). Function of the respiratory syncytial virus small hydrophobic protein. *Journal of Virology*, *81*(15), 8361–6. http://doi.org/10.1128/JVI.02717-06

Galloux, M., Gabiane, G., Sourimant, J., Richard, C.-A., England, P., Moudjou, M., …

Eleouet, J.-F. (2015). Identification and characterization of the binding site of the respiratory syncytial virus phosphoprotein to RNA-free nucleoprotein. *Journal of Virology*, *89*(7), 3484–3496. http://doi.org/10.1128/JVI.03666-14

Galloux, M., Tarus, B., Blazevic, I., Fix, J., Duquerroy, S., & Eléouët, J.-F. (2012). Characterization of a viral phosphoprotein binding site on the surface of the respiratory syncytial nucleoprotein. *Journal of Virology*, *86*(16), 8375–87. http://doi.org/10.1128/JVI.00058-12

García-Barreno, B., Delgado, T., & Melero, J. A. (1996). Identification of protein regions involved in the interaction of human respiratory syncytial virus phosphoprotein and nucleoprotein: significance for nucleocapsid assembly and formation of cytoplasmic inclusions. *Journal of Virology*, *70*(2), 801–8. Retrieved from http://www.ncbi.nlm.nih.gov/pubmed/8551618

García, J., García-Barreno, B., Vivo, A., & Melero, J. A. (1993). Cytoplasmic Inclusions of Respiratory Syncytial Virus-Infected Cells: Formation of Inclusion Bodies in Transfected Cells That Coexpress the Nucleoprotein, the Phosphoprotein, and the 22K Protein. *Virology*, *195*(1), 243–247. http://doi.org/10.1006/viro.1993.1366

Ghildyal, R., Jans, D. A., Bardin, P. G., & Mills, J. (2012). Protein-protein interactions in RSV assembly: potential targets for attenuating RSV strains. *Infectious Disorders Drug Targets*, *12*(2), 103–9. Retrieved from http://www.ncbi.nlm.nih.gov/pubmed/22335497

Gilca, R., De Serres, G., Tremblay, M., Vachon, M.-L., Leblanc, E., Bergeron, M. G., … Boivin, G. (2006). Distribution and clinical impact of human respiratory syncytial virus genotypes in hospitalized children over 2 winter seasons. *The Journal of Infectious Diseases*, *193*(1), 54–8. http://doi.org/10.1086/498526

Glezen, W. P., Taber, L. H., Frank, A. L., and Kasel, J. A. (1986) Risk of primary infection and reinfection with respiratory syncytial virus. *Am J Dis Child 140*(6), 543-546.

Gomez, R. S., Guisle-Marsollier, I., Bohmwald, K., Bueno, S. M., & Kalergis, A. M. (2014). Respiratory Syncytial Virus: Pathology, therapeutic drugs and prophylaxis. *Immunology Letters*, *162*(1), 237–247. http://doi.org/10.1016/j.imlet.2014.09.006

González, P. A., Bueno, S. M., Carreño, L. J., Riedel, C. A., & Kalergis, A. M. (2012). Respiratory syncytial virus infection and immunity. *Reviews in Medical Virology*, *22*(4), 230–44. http://doi.org/10.1002/rmv.1704

Gräslund, S., Nordlund, P., Weigelt. J., Hallberg, B. M., Bray, J., Gileadi, O., Knapp, S., Oppermann, U., Arrowsmith, S., Hui, R., Ming, J., … & Gunsalus, K. C. (2008).

Protein production and purification. *Nat Methods 5*(2), 135-146.

Gustavsson, M., Lehtio, J., Denman, S., Teeri, T. T., Hult, K., & Martinelle, M. (2001). Stable linker peptides for a cellulose-binding domain-lipase fusion protein expressed in *Pichia pastoris*. *Pritein Eng 14*, 711-715.

Gut, W., Pancer, K., Abramczuk, E., Czescik, A., Dunal-Szczepaniak, M., Lipka, B., & Litwinska, B. (2013). RSV respiratory infection in children under 5 y.o.--dynamics of the immune response Th1/Th2 and IgE. *Przegl Epidemiol*, *67*(1), 17–22,105–109.

Guvenel, A. K., Chiu, C., & Openshaw, P. J. (2014). Current concepts and progress in RSV vaccine development. *Expert Review of Vaccines*, *13*(3), 333–44. http://doi.org/10.1586/14760584.2014.878653

Hall, C. B. (1983). The nosocomial spread of respiratory syncytial viral infections. *Ann. Rev. Med. 34*, 311-319.

Hall, C. B. (2012). The burgeoning burden of respiratory syncytial virus among children. *Infectious Disorders Drug Targets*, *12*(2), 92–7. http://doi.org/10.2174/187152612800100099

Hall, C. B., & Douglas, R. G. (1981). Modes of transmission of respiratory syncytial virus. *The Journal of Pediatrics*, *99*(1), 100–3. Retrieved from http://www.ncbi.nlm.nih.gov/pubmed/7252646

Hall, C. B., Simões, E. A. F., & Anderson, L. J. (2013). Clinical and Epidemiologic Features of Respiratory Syncytial Virus. *Current Topics in Microbiology and Immunology*, *372*, 39–57. http://doi.org/10.1007/978-3-642-38919-1_2

Heitz, F., Morris, M. C., & Divita, G. (2009). Twenty years of cell-penetrating peptides: from molecular mechanisms to therapeutics. *British Journal of Pharmacology 157*(2), 195-206.

Henderson, G., Murray, J., & Yeo, R. P. (2002). Sorting of the Respiratory Syncytial Virus Matrix Protein into Detergent-Resistant Structures Is Dependent on Cell-Surface Expression of the Glycoproteins. *Virology*, *300*(2), 244–254. http://doi.org/10.1006/viro.2002.1540

Jacobs, S. A., Gibbs, A. C., Conk, M., Yi, F., Maguire, D., Kane, C., & O'neil, K. T. (2015). Fusion to a highly stable consensus albumin binding domain allows for tunable pharmacokinetics. *Protein Engineering, Design and Selection*. http://doi.org/10.1093/protein/gzv040

Jeffree, C. E., Brown, G., Aitken, J., Su-Yin, D. Y., Tan, B.-H., & Sugrue, R. J. (2007).

Ultrastructural analysis of the interaction between F-actin and respiratory syncytial virus during virus assembly. *Virology*, *369*(2), 309–23. http://doi.org/10.1016/j.virol.2007.08.007

Johnson, P. R., & Collins, P. L. (1990). Sequence comparison of the phosphoprotein mRNAs of antigenic subgroups A and B of human respiratory syncytial virus identifies a highly divergent domain in the predicted protein. *Journal of General Virology 71*, 481-485.

Jones, A. T., & Sayers, E. J. (2012). Cell entry of cell penetrating peptides: tales of tails wagging dogs. *Journal of Controlled Release*, *161*(2), 582–591. http://doi.org/10.1016/j.jconrel.2012.04.003

Jonsson, A., Dogan, J., Herne, N., Abrahmsén, L., & Nygren, P.-A. (2008). Engineering of a femtomolar affinity binding protein to human serum albumin. *Protein Engineering, Design & Selection : PEDS*, *21*(8), 515–27. http://doi.org/10.1093/protein/gzn028

Kameyama, S., Horie, M., Kikuchi, T., Omura, T., Tadokoro, A., Takeuchi, T., Nakase, I., Sugiura, Y., & Futaki, S. (2007). Acid wash in determining cellular uptake of Fab/cell-permeating peptide conjugates. *Peptide Science 88*, 98-107.

Kim, H. W., Canchola, J. G., Brandt, C. D., Pyles, G., Chanock, R. M., Jensen, K., & Parrott, R. H. (1969). Respiratory syncytial virus disease in infants despite prior administration of antigenic inactivated vaccine. *American Journal of Epidemiology*, *89*(4), 422–434.

Kim, T. H. & Lee, H. K. (2014). Innate immune recognition of respiratory syncytial virus infection. *BMB Reports 47*(4), 184-191.

Kontermann, R. E. (2011). Strategies for extended serum half-life of protein therapeutics. *Current Opinion in Biotechnology*. http://doi.org/10.1016/j.copbio.2011.06.012

Krilov, L. R. (2011). Respiratory syncytial virus disease: update on treatment and prevention. *Expert Review of Anti-Infective Therapy*, *9*(1), 27–32. http://doi.org/10.1586/eri.10.140

Krishnamoorthy, N., Khare, A., Oriss, T. B., Raundhal, M., Morse, C., Yarlagadda, M., … Ray, P. (2012). Early infection with respiratory syncytial virus impairs regulatory T cell function and increases susceptibility to allergic asthma. *Nature Medicine*, *18*(10), 1525–1530. http://doi.org/10.1038/nm.2896

Krishnamurty, R. and Maly, D. J. (2011). Biochemical mechanisms of resistance to small-molecule protein kinase inhibitors. *ACS Chem Biol 5*(1), 121-138.

Langley, J. M., Wang, E. E. L., Law, B. J., Stephens, D., Boucher, F. D., Dobson, S., McDonald, J., MacDonald N. E., Mitchell, I., & Robinson, J. L. (1997). Economic evaluation of respiratory syncytial virus infection in Canadian children: A Pediatric Investigators Collaborative Network on Infections in Canada (PICNIC) study. *Journal of Pediatrics*, *131*(1), 113–7. http://doi.org/10.1542/peds.100.6.943

Lebendiker, M. & Danieli, T. (2014). Production of prone-to-aggregate proteins. *FEBS Letters 588*(2), 236-246.

Lester, S. N., and Li, K. (2014). Toll-like receptors in antiviral innate immunity. *J Mol Biol 426*(6), 1246-1264. doi: 10.1016/j.jmb.2013.11.024

Leung, A. K. C., Kellner, J. D., and Davies, H. D. (2005). Respiratory syncytial virus bronchiolitis. *Journal of the National Medical Association 97*(12), 1708-1713.

Li, B., Cao, Y., Zhou, L., Liang, C., & Sun, F. (2013). A novel protein expression system-PichiaPink^{TM}- and a protocol for fast and efficient recombinant protein expression. *African Journal of Biotechnology*, *10*(83), 19464–19472. http://doi.org/10.4314/AJB.V10I83.

Linhult, M., Binz, H. K., Uhlén, M., & Hober, S. (2002). Mutational analysis of the interaction between albumin-binding domain from streptococcal protein G and human serum albumin. *Protein Science : A Publication of the Protein Society*, *11*(2), 206–213. http://doi.org/10.1110/ps.02802

Lowry, O.H., Rosebrough, N. J., Farr, A. L., and Randall, R.J. (1951). Protein measurement with the folin phenol reagent. *Journal of Biological Chemistry 193*, 265-275.

Madani, F., Lindberg, S., Langel, U., Futaki, S., & Graslund, A. (2011). Mechanisms of cellular uptake of cell-penetrating peptides. *Journal of Biophysics 2011*, Article ID: 414729. doi: 10.1155/2011/414729

Mamat, U., Wilke, K., Bramhill, D., Schromm, A. B., Lindner, B., Kohl, T. A., Corchero, J. L., Villaverde, A., Schaffer, L., Head, S. R., Souvignier, C., Meredith, T. C., & Woodward, R. W., (2015). Detoxifying *Escherichia coli* for endotoxin-free production of recombinant proteins. *Microbial Cell Factories 14*, 57.

Magalhães, P. O., Lopes, A. M., Mazzola, P. G., Rangel-Yagui, C., Penna, T. C. V., & Pessoa, A. Jr. (2007). Methods of endotoxin remove from biological preparations: a review. *J Pharm Pharmaceut Sci 10*(3), 388-404.

Marty, A., Meanger, J., Mills, J., Shields, B., & Ghildyal, R. (2004). Association of

matrix protein of respiratory syncytial virus with the host cell membrane of infected cells Brief Report. *Arch Virol*, *149*, 199–210. http://doi.org/10.1007/s00705-003-0183-9

Mason, J. M. (2010). Design and development of peptides and peptide mimetics as antagonists for therapeutic intervention. *Future Medicinal Chemistry*, *2*(12), 1813–22. https://doi.org/10.4155/fmc.10.259

Mastrangelo, P., & Hegele, R. G. (2013). RSV Fusion: Time for a New Model. *Viruses*, *5*, 873–885. http://doi.org/10.3390/v5030873

Matthews, T., Salgo, M., Greenberg, M., Chung, J., DeMasi, R., & Bolognesi, D. (2004). Enfuvirtide: the first therapy to inhibit the entry of HIV-1 into host CD4 lymphocytes. *Nature Reviews. Drug Discovery*, *3*(3), 215–25. http://doi.org/10.1038/nrd1331

Mazur, N. I., Martin??n-Torres, F., Baraldi, E., Fauroux, B., Greenough, A., Heikkinen, T., … Bont, L. (2015). Lower respiratory tract infection caused by respiratory syncytial virus: Current management and new therapeutics. *The Lancet Respiratory Medicine*. http://doi.org/10.1016/S2213-2600(15)00255-6

McConnochie, K. M., Hall, C. B., Walsh, E. E., & Roghmann, K. J. (1990). Variation in severity of respiratory syncytial virus infections with subtype. *The Journal of Pediatrics*, *117*(1 Pt 1), 52–62. Retrieved from http://www.ncbi.nlm.nih.gov/pubmed/2115082

McGregor, D. P. (2008). Discovering and improving novel peptide therapeutics. *Current Opinion in Pharmacology*, *8*(5), 616–619. http://doi.org/10.1016/j.coph.2008.06.002

McLellan, J. S., Yang, Y., Graham, B. S., & Kwong, P. D. (2011). Structure of respiratory syncytial virus fusion glycoprotein in the postfusion conformation reveals preservation of neutralizing epitopes. *Journal of Virology*, *85*(15), 7788–96. http://doi.org/10.1128/JVI.00555-11

Mejias, A., & Ramilo, O. (2015). New options in the treatment of respiratory syncytial virus disease. *Journal of Infection*. http://doi.org/10.1016/j.jinf.2015.04.025

Mohler, W.A., Charlton, C. A., & Blau, H. M. (1996). Spectrophotometric quantitation of tissue culture cell number in any medium. *Biotechniques 21*(2), 260-266.

Munywoki, P. K., Koech, D. C., Agoti, C. N., Kibirige, N., Kipkoech, J., Cane, P. A., … Nokes, D. J. (2015). Influence of age, severity of infection, and co-infection on the duration of respiratory syncytial virus (RSV) shedding. *Epidemiology and Infection*, *143*(4), 804–12. http://doi.org/10.1017/S0950268814001393

Murphy, B. R., & Walsh, E. E. (1988). Formalin-inactivated respiratory syncytial virus vaccine induces antibodies to the fusion glycoprotein that are deficient in fusion-inhibiting activity. *Journal of Clinical Microbiology*, *26*(8), 1595–7. Retrieved from http://www.ncbi.nlm.nih.gov/pubmed/2459154

Nair, H., Nokes, D. J., Gessner, B. D., Dherani, M., Madhi, S. a, Singleton, R. J., … Campbell, H. (2010). Global burden of acute lower respiratory infections due to respiratory syncytial virus in young children: a systematic review and meta-analysis. *Lancet*, *375*(9725), 1545–55. http://doi.org/10.1016/S0140-6736(10)60206-1

Nair, H., Verma, V. R., Theodoratou, E., Zgaga, L., Huda, T., Simões, E. A. F., … Campbell, H. (2011). An evaluation of the emerging interventions against Respiratory Syncytial Virus (RSV)-associated acute lower respiratory infections in children. *BMC Public Health*, *11 Suppl 3*, S30. http://doi.org/10.1186/1471-2458-11-S3-S30

Neuzil, K. M. (2016). Progress toward a Respiratory Syncytial Virus Vaccine. *Clinical and Vaccine Immunology : CVI*, *23*(3), 186–8. http://doi.org/10.1128/CVI.00037-16

Nilvebrant, J., & Hober, S. (2013). The albumin-binding domain as a scaffold for protein engineering. *Computational and Structural Biotechnology Journal*, *6*(March), e201303009. http://doi.org/10.5936/csbj.201303009

Noton, S. L., Deflube, L. R., Tremaglio, C. Z., & Fearns, R. (2012). The respiratory syncytial virus polymerase has multiple RNA synthesis activites at the promoter. *PLOS Pathogens 8*, e1002980.

Ogra, P. L. (2004). Respiratory syncytial virus: The virus, the disease and the immune response. *Paediatric Respiratory Reviews*, *5*(SUPPL. A). http://doi.org/10.1016/S1526-0542(04)90023-1

Openshaw, P. J. & Chiu, C. (2013). Protective and dysregulated T cell immunity in RSV infection. *Current Opinion in Virology 3*, 468-474.

Paramore, L. C., Ciuryla, V., Ciesla, G., & Liu, L. (2004). Economic impact of respiratory syncytial virus-related illness in the US: an analysis of national databases. *PharmacoEconomics*, *22*(5), 275–84. Retrieved from http://www.ncbi.nlm.nih.gov/pubmed/15061677

Pillay, D. and Zambon, M. (1998). Antiviral drug resistance. *BMJ 317*, 660-662.

Polack, F. P. (2015). The changing landscape of respiratory syncytial virus. *Vaccine*, *33*(47), 6473–8. http://doi.org/10.1016/j.vaccine.2015.06.119

Rezaee, F., Linfield, D. T., Harford, T. J., & Piedimonte, G. (2017). Ongoing developments in RSV prophylaxis: a clinician's analysis. *Current Opinion in Virology 24*, 70-78.

Rietschel, E. T. & Brade, H. (1992). Bacterial endotoxins. *Sci Amer 276*, 54-61.

Rodriguez, R., & Ramilo, O. (2014). Respiratory syncytial virus: How, why and what to do. *Journal of Infection*, *68*(SUPPL1). http://doi.org/10.1016/j.jinf.2013.09.021

Rosano, G. L., & Ceccarelli, E. A. (2014). Recombinant protein expression in *Escherichia coli*: advances and challenges. *Frontiers in Microbiology 5*. doi: 10.3389/fmicb.2014.00172

Ruigrok, R. W., Crépin, T., & Kolakofsky, D. (2011). Nucleoproteins and nucleocapsids of negative-strand RNA viruses. *Current Opinion in Microbiology*, *14*(4), 504–510. http://doi.org/10.1016/j.mib.2011.07.011

Sand, K. M. K., Bern, M., Nilsen, J., Dalhus, B., Gunnarsen, K. S., Cameron, J., … Andersen, J. T. (2014). Interaction with both domain I and III of albumin is required for optimal pH dependent binding to the neonatal Fc Receptor (FcRn). *The Journal of Biological Chemistry*, 0–23. http://doi.org/10.1074/jbc.M114.587675

Schaefer, M. H., Lopes, T. J. S., Mah, N., Shoemaker, J. E., Matsuoka, Y., Fontaine, J.-F., … Andrade-Navarro, M. A. (2013). Adding protein context to the human protein-protein interaction network to reveal meaningful interactions. *PLoS Computational Biology*, *9*(1), e1002860. http://doi.org/10.1371/journal.pcbi.1002860

Schneider-Poetsch, T., Ju, J., Eyler, D.E., Dang, Y., Bhat, S., Merrick, W.C., Green, R., Shen, B., & Liu, J.O. (2010). Inhibition of eukaryotic translation elongation by cycloheximide and lactimidomycin. *Nat Chem Biol 6*, 209-217.

Shaw, K. L., Grimsley, G. R., Yakovlev, G. I., Makarov, A. A., & Pace, N. A. (2001). The effect of net charge on the solubility, activity, and stability of ribonuclease Sa. *Protein Sci 10*(6), 1206-1215.

Siegemun, M., Pollak, N., Seifert, O., Wahl, K., Hanak, K., Vogel, A., Nussler, A. K., Gottsch, D., Munkel, S., Bantel, H., Kontermann, R. E., & Pfizenmaier, K. (2012). Superior antitumoral activity of dimerized targeted single-chain TRAIL fusion proteins under rention of tumor selectivity. *Cell Death and Disease 3*, e295.

Sigurs, N., Bjarnason, R., Sigurbergsson, F., & Kjellman, B. (2000). Respiratory syncytial virus bronchiolitis in infancy is an important risk factor for asthma and allergy at age 7. *American Journal of Respiratory and Critical Care Medicine*, *161*(5), 1501–7. http://doi.org/10.1164/ajrccm.161.5.9906076

Sourimant, J., Rameix-Welti, M.-A., Gaillard, A.-L., Chevret, D., Galloux, M., Gault, E., & Eléouët, J.-F. (2015). Fine mapping and characterization of the L-polymerase-binding domain of the respiratory syncytial virus phosphoprotein. *Journal of Virology*, *89*(8), 4421–4433. http://doi.org/10.1128/JVI.03619-14

Spann, K. M., Tran, K.-C., Chi, B., Rabin, R. L., & Collins, P. L. (2004). Suppression of the Induction of Alpha, Beta, and Gamma Interferons by the NS1 and NS2 Proteins of Human Respiratory Syncytial Virus in Human Epithelial Cells and Macrophages. *Journal of Virology*, *78*(8), 4363–4369. http://doi.org/10.1128/JVI.78.8.4363-4369.2004

Stec, D.S., Hill, M. G., & Collins, P. L. (1991). Sequence analysis of the polymerase L gene of human respiratory syncytial virus and predicted phylogeny of nonsegmented negative-strand viruses. *Virology 183*(1), 273-287.

Stevenson, K., McVey, A. F., Clark, I. B. N., Swain, P. S., & Pilizota, T. (2016). General calibration of microbial growth in microplate readers. *Scientific Reports 6*. doi:10.1038/srep38828

Stone, C. B., Bulir, D. C., Emdin, C. A., Pirie, R. M., Porfilio, E. A., Slootstra, J. W., & Mahony, J. B. (2011). Chlamydia Pneumoniae CdsL Regulates CdsN ATPase Activity, and Disruption with a Peptide Mimetic Prevents Bacterial Invasion. *Frontiers in Microbiology*, *2*, 21. http://doi.org/10.3389/fmicb.2011.00021

Stork, R., Campigna, E., Robert, B., Müller, D., & Kontermann, R. E. (2009). Biodistribution of a bispecific single-chain diabody and its half-life extended derivatives. *Journal of Biological Chemistry*, *284*(38), 25612–25619. http://doi.org/10.1074/jbc.M109.027078

Sullender, W. M. (2000). Respiratory syncytial virus genetic and antigenic diversity. *Clinical Microbiology Reviews*, *13*(1), 1–15, table of contents. Retrieved from http://www.ncbi.nlm.nih.gov/pubmed/10627488

Sun, P., Tropea, J. E., & Waugh, D. S. (2011). Enhancing the solubility of recombinant proteins in *Esherichia coli* by using hexahistidine-tagged maltose-binding protein as a fusion partner. *Methods in Molecular Biology 705,*259-274

Tawar, R. G., Duquerroy, S., Vonrhein, C., Varela, P. F., Damier-Piolle, L., Castagné, N., … Rey, F. A. (2009). Crystal structure of a nucleocapsid-like nucleoprotein-RNA complex of respiratory syncytial virus. *Science (New York, N.Y.)*, *326*(5957), 1279–83. http://doi.org/10.1126/science.1177634

Tayyari, F., Marchant, D., Moraes, T. J., Duan, W., Mastrangelo, P., & Hegele, R. G.

(2011). Identification of nucleolin as a cellular receptor for human respiratory syncytial virus. *Nature Medicine*, *17*(9), 1132–1136.

Thorburn, K., Harigopal, S., Reddy, V., Taylor, N., & van Saene, H. K. F. (2006). High incidence of pulmonary bacterial co-infection in children with severe respiratory syncytial virus (RSV) bronchiolitis. *Thorax*, *61*(7), 611–5. http://doi.org/10.1136/thx.2005.048397

Tran, T.-L., Castagné, N., Bhella, D., Varela, P. F., Bernard, J., Chilmonczyk, S., … Eléouët, J.-F. (2007). The nine C-terminal amino acids of the respiratory syncytial virus protein P are necessary and sufficient for binding to ribonucleoprotein complexes in which six ribonucleotides are contacted per N protein protomer. *The Journal of General Virology*, *88*(Pt 1), 196–206. http://doi.org/10.1099/vir.0.82282-0

Tsomaia, N. (2015). Peptide therapeutics: Targeting the undruggable space. *European Journal of Medicinal Chemistry*, *94*, 459–470. http://doi.org/10.1016/j.ejmech.2015.01.014

Turner, T. L., Kopp, B. T., Landgrave, L. C., Hayes, D. Jr., & Thompson, R. (2014). Respiratory syncytial virus: current and emerging treatment options. *ClinicoEconomics and Outcomes Research 6*, 217-225.

Wang, W., Nema, S., & Teagarden, D. (2010). Protein aggregation - Pathways and influencing factors. *International Journal of Pharmaceutics 390*, 89-99.

Welliver, R. C. (2003). Review of epidemiology and clinical risk factors for severe respiratory syncytial virus (RSV) infection. *The Journal of Pediatrics*, *143*(5 Suppl), S112–7. Retrieved from http://www.ncbi.nlm.nih.gov/pubmed/14615709

Wyde, P. R. (1998). Respiratory syncytial virus (RSV) disease and prospects for its control. *Antiviral Research*. http://doi.org/10.1016/S0166-3542(98)00029-1

Yu, Q., Hardy, R. W., & Wertz, G. W. (1995). Functional cDNA clones of the human respiratory syncytial (RS) virus N, P, and L proteins support replication of RS virus genomic RNA analogs and define minimal *trans*-acting requirements for RNA replication. *Journal of Virology 69*(4), 2412-2419.

Zhang, L., Peeples, M. E., Boucher, R. C., Collins, P. L., & Pickles, R. J. (2002). Respiratory syncytial virus infection of human airway epithelial cells is polarized, specific to ciliated cells, and without obvious cytopathology. *J Virol 76*(11), 5654-5666. doi: 10.1128/JVI.76.11.5654-5666.2002

Zhang, J., Yun, J., Shang, Z., Zhang, X., & Pan, B. (2009). Design and optimization of a

linker for fusion protein construction. P*rogress in Natural Science 19*, 1197-1200.

Zhao, X., Li, G., & Liang, S. (2013). Several affinity tags commonly used in chromatographic purification. *Journal of Analytical Methods in Chemistry 2013*, 1-8. http://dx.doi.org/10.1155/2013/581093

Zhou, H., Thompson, W. W., Viboud, C. G., Ringholz, C. M., Cheng, P.-Y., Steiner, C., … Shay, D. K. (2012). Hospitalizations associated with influenza and respiratory syncytial virus in the United States, 1993-2008. *Clinical Infectious Diseases : An Official Publication of the Infectious Diseases Society of America*, *54*(10), 1427–36. http://doi.org/10.1093/cid/cis211

CHAPTER 6 – APPENDIX

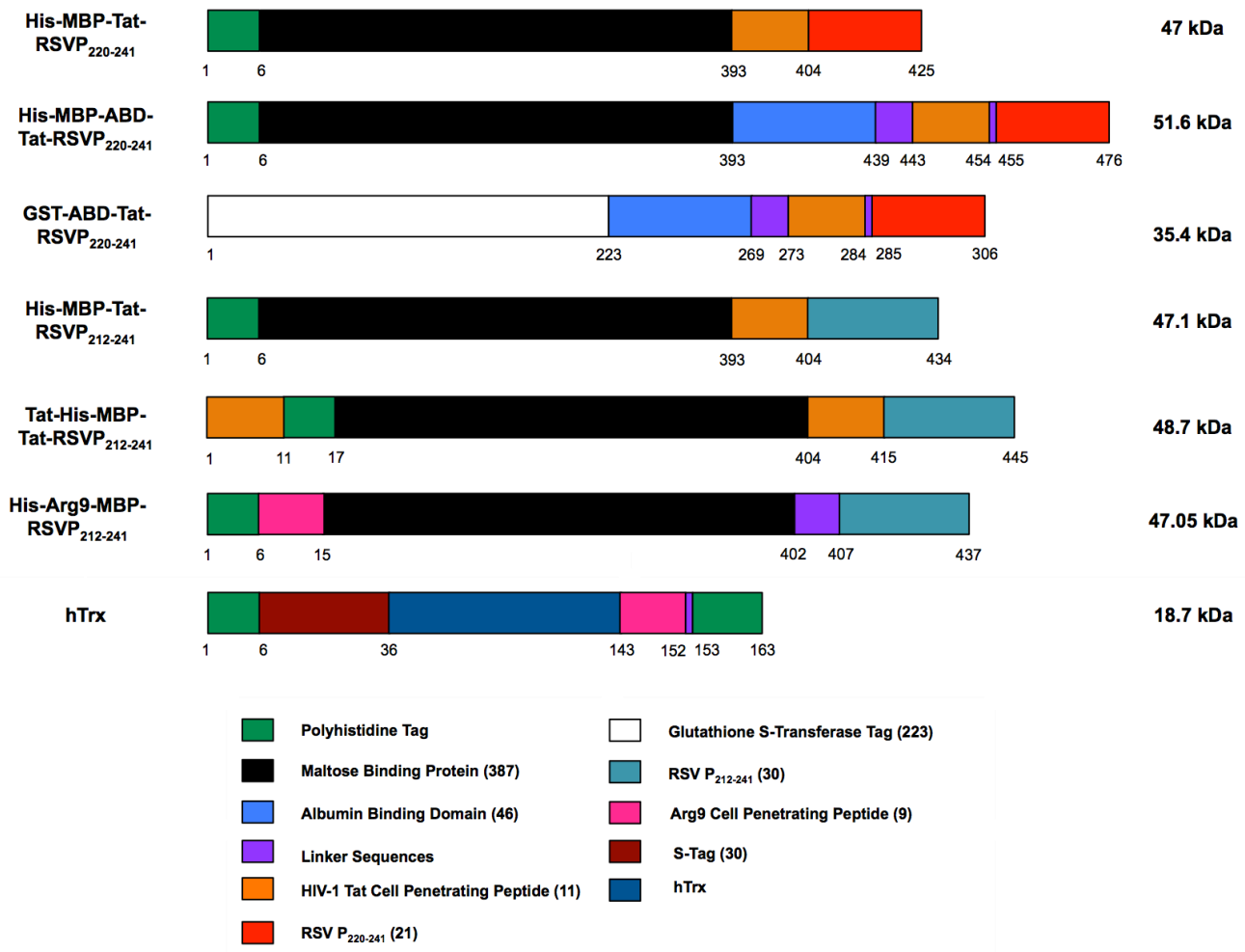

Figure 6.1. Schematic representation of the recombinant peptides used in this thesis. Boxcar diagram depiction of the recombinant peptides used in this thesis. The numbers below each protein domain indicate the cumulative length of amino acids for each peptide domain. Numbers in the brackets represent the amino acid length of a particular domain of the construct. The molecular weight of each construct was estimated using the online ExPASy Compute pI/MW tool.

Primer Set	Construct	Forward Primer (5' – 3')	Reverse Primer (5' – 3')
A	Tat-His-MBP-Tat-RSVP$_{212-241}$	TTG GCG GCG TTT TTT CCG ACC ATA CAT AAT CTA TGG TCC TTG TTG G	AAA AAA CGC CGC CAA CGT AGA CGG AAA ATC CAT CAC CAT CAC CAT C
B	His-Arg9-MBP-RSVP$_{212-241}$	CGC CGT CGT CGT CGC CGT CGC GAA GAA GGT AAA CTG GTA ATC T	GCG ACG ACG ACG GCG ACG ACG GTG ATG GTG ATG GTG ATG GA

Table 6.2. Primer Sets used in Inverse PCR. Each primer set was designed to include a 15 bp overlap at the 5' end of the forward and the reverse primer. Primer set A was used to insert a Tat CPP at the N-terminus of the His-tag in the His-MBP-Tat-RSVP$_{212-241}$ construct, whereas primer set B was used to insert an Arg9 CPP at the C-terminus of the His-tag in the pDEST-His-MBP vector.